In presenting the dissertation as a partial fulfillment of the requirements for an advanced degree from the Georgia Institute of Technology, I agree that the Library of the Institute shall make it available for inspection and circulation in accordance with its regulations governing materials of this type. I agree that permission to copy from, or to publish from, this dissertation may be granted by the professor under whose direction it was written, or, in his absence, by the Dean of the Graduate Division when such copying or publication is solely for scholarly purposes and does not involve potential financial gain. It is understood that any copying from, or publication of, this dissertation which involves potential financial gain will not be allowed without written permission.

3/17/65
b

COMPREHENSIVE STUDY OF THE TORSIONAL DEFORMATION OF ALUMINUM AND TWO ALUMINUM ALLOYS

A THESIS

Presented to

The Faculty of the Graduate Division

by

Steven Lawrence Haas

In Partial Fulfillment

of the Requirements for the Degree

Doctor of Philosophy

in the School of Mechanical Engineering

Georgia Institute of Technology

April, 1968

COMPREHENSIVE STUDY OF THE TORSIONAL DEFORMATION

OF ALUMINUM AND TWO ALUMINUM ALLOYS

Approved:

Chairman

Date approved by Chairman: 4/15/68

ACKNOWLEDGMENTS

I would like to express my sincere appreciation to Dr. John A. Bailey, who suggested this topic, and who served as my thesis advisor. I would also like to thank Dr. J. H. Murphy and Dr. R. H. Hochman for serving on the reading committee.

I wish to dedicate this work to my wife, Helen Joy, for the many sacrifices she has made, and for the love she provided throughout the course of my studies.

I thank God for blessing me with a wonderful wife and family, and for parents who have done so much to make all this possible.

This work was supported by the National Science Foundation, research grant GK-191.

TABLE OF CONTENTS

Page

ACKNOWLEDGEMENTS ii

LIST OF TABLES v

LIST OF ILLUSTRATIONS. vi

SUMMARY. x

Chapter

I. INTRODUCTION. 1

Object of the Investigation
Previous Methods of Testing
Scope of the Investigation

II. REVIEW OF LITERATURE. 5

Introduction
Low Temperature Tests
High Temperature Tests
Axial Deformation and Anisotropy in Torsion

III. DESIGN OF THE TORSION TESTING MACHINE 29

Initial Design Considerations
Description of the Machine
Instrumentation
Controls
Performance of the Torsion Testing Machine

IV. PROCEDURE 47

Materials
Specimen Characteristics
Testing Procedure
Calibration

V. EXPERIMENTAL DETERMINATION OF AXIAL CHANGE IN LENGTH. . . . 52

Introductory Comments
Observations of Change in Length
Effect of Constraint

Chapter Page

VI. AN ANALYTICAL INVESTIGATION OF ANISOTROPY IN TORSION USING HILL'S EQUATIONS 60

Initial Considerations
Analytical Development
Determination of the Principal Directions of Anisotropy
Computer Solution
Closure

VII. EFFECTS OF TEMPERATURE AND STRAIN RATE ON THE RESISTANCE TO DEFORMATION OF 1100-0, 2017-0, AND 6061-0 ALUMINUM ALLOYS 75

Discussion
Commercially Pure Aluminum 1100-0
Aluminum Alloy 2017-0
Aluminum Alloy 6061-0
Temperature Rise

VIII. CONCLUSIONS 94

Torsion Testing Machine
Anisotropy and Change in Length
Torsion Tests

IX. RECOMMENDATIONS 98

APPENDIX

A. TORSION TEST DATA 100

B. COMPUTER PROGRAM 136

BIBLIOGRAPHY 140

VITA 148

LIST OF TABLES

Table		Page
1.	Approximate Testing Speeds in RPM	32
2.	Chemical Composition Limits	49
3.	Annealing Procedures	50
4.	Axial Change in Length	56
5.	Values of the Strain Rate Sensitivity for 1100-0 Aluminum	82
6.	Comparison of Compression and Torsion Data at $\bar{\varepsilon}$ = 0.51 and $\dot{\bar{\varepsilon}}$ = 10 per Second	85
7.	Values of the Strain Rate Sensitivity for the 2017-0 Aluminum Alloy	88
8.	Values of the Strain Rate Sensitivity for 6061-0 Aluminum	91

LIST OF ILLUSTRATIONS

Figure		Page
1.	Rotation of the Anisotropic Axes.	25
2.	Schematic Representation of Testing Apparatus	31
3.	Test Assembly	34
4.	Bearing and Bearing Support Assembly.	37
5.	Bearing Housing	38
6.	Bearing Support	39
7.	Instrumentation for Measuring Change in Length.	41
8.	Control Panel Circuit Diagram	44
9.	Drive Train Assembly (Top) and Test Assembly (Bottom) . . .	46
10.	Dimensions of the Test Specimen	48
11.	Axial Change in Length (Inches) vs. Time (Seconds) as Taken from Recorded Data for 1100-0 Aluminum (at Room Temperature) at a Testing Speed of 1.46 RPM. . . .	54
12.	Axial Change in Length (Inches) vs. Time (Seconds) as Taken from Recorded Data for 2017-0 Aluminum (at Room Temperature) at a Testing Speed of 0.181 RPM . . .	57
13.	Axial Change in Length (Inches) vs. Time (Seconds) as Taken from Recorded Data for 6061-0 Aluminum (at Room Temperature) at a Testing Speed of 0.181 RPM . . .	58
14.	Incremental State of Strain	63
15.	Mohr's Circle Representing the Incremental State of Strain	64
16.	Comparison of the Empirical Change in Length Equation $\varepsilon = -0.07 \cos^3 2\phi$ with Experimental Data	68
17.	Shear Stress vs. Shear Strain for 1100-0 Aluminum at T = 22°C.	101

Figure		Page
18.	Shear Stress vs. Shear Strain for 1100-0 Aluminum at T = 22°C	102
19.	Shear Stress vs. Shear Strain for 1100-0 Aluminum at T = 22°C	103
20.	Shear Stress vs. Shear Strain for 1100-0 Aluminum at T = 200°C.	104
21.	Shear Stress vs. Shear Strain for 1100-0 Aluminum at T = 300°C.	105
22.	Shear Stress vs. Shear Strain for 1100-0 Aluminum at T = 400°C.	106
23.	Shear Stress vs. Shear Strain for 1100-0 Aluminum at T = 500°C.	107
24.	Shear Stress vs. Shear Strain for 1100-0 Aluminum at T = 550°C.	108
25.	Fracture Surfaces at a Testing Temperature of 500°C and Testing Speeds of Approximately 0.15 RPM (Upper Specimens) and 1500 RPM (Lower Specimens) for (a) 1100-0, (b) 2017-0, (c) 6061-0.	80
26.	Shear Stress vs. Strain Rate for 1100-0 Aluminum at γ = 1.0	109
27.	Shear Stress vs. Strain Rate for 1100-0 Aluminum at γ = 2.0	110
28.	Shear Stress vs. Strain Rate for 1100-0 Aluminum at γ = 3.0	111
29.	Relationship Between the Homologous Temperature and the Strain Rate Sensitivity	112
30.	Effect of Temperature on the Shearing Stress for 1100-0 Aluminum	113
31.	τ vs. ln 1/T for 1100-0 Aluminum at γ = 1.0	114
32.	τ vs. ln 1/T for 1100-0 Aluminum at γ = 2.0	115
33.	τ vs. ln 1/T for 1100-0 Aluminum at γ = 3.0	116
34.	Variation of C_1 with Strain Rate.	117

Figure		Page
35.	Variation of C_2 with Strain Rate.	118
36.	Shear Stress vs. Shear Strain for the 2017-0 Alloy at T = 350°C	119
37.	Shear Stress vs. Shear Strain for the 2017-0 Alloy at T = 400°C	120
38.	Shear Stress vs. Shear Strain for the 2017-0 Alloy at T = 450°C	121
39.	Shear Stress vs. Shear Strain for the 2017-0 Alloy at T = 500°C	122
40.	Shear Stress vs. Strain Rate for the 2017-0 Alloy at γ = 0.5	123
41.	Shear Stress vs. Strain Rate for the 2017-0 Alloy at γ = 1.0	124
42.	Shear Stress vs. Strain Rate for the 2017-0 Alloy at γ = 2.0	125
43.	Effect of Temperature on the Shearing Stress for 2017-0 . .	126
44.	Shear Stress vs. Shear Strain for the 6061-0 Alloy at T = 350°C	127
45.	Shear Stress vs. Shear Strain for the 6061-0 Alloy at T = 400°C	128
46.	Shear Stress vs. Shear Strain for the 6061-0 Alloy at T = 450°C	129
47.	Shear Stress vs. Shear Strain for the 6061-0 Alloy at T = 500°C	130
48.	Shear Stress vs. Strain Rate for the 6061-0 Alloy at γ = 1.0	131
49.	Shear Stress vs. Strain Rate for the 6061-0 Alloy at γ = 2.0	132
50.	Shear Stress vs. Strain Rate for the 6061-0 Alloy at γ = 3.0	133

Figure Page

51. Effect of Temperature on the Shearing Stress for 6061-0 Aluminum 134

52. Calculated Temperature Rise vs. Shear Stress for an 1100-0 Aluminum Specimen 135

SUMMARY

The present investigation was concerned with the determination of the effects of temperature and strain rate on the resistance to deformation of metals, and includes the development of a testing means to conveniently and accurately obtain this information.

After a careful study of available testing methods, torsion testing of hollow cylinders with reduced central gage length was selected in order to overcome the inherent disadvantages encountered in other testing methods. The materials used for the tests were commercially pure aluminum, 1100-0, and two aluminum alloys, 2017-0 and 6061-0.

The research consisted essentially of three stages. Initially, a torsion testing machine was designed and built, and its performance analysed. The machine consists of two main sections, the drive train assembly containing the motor and speed reduction units, and the test assembly, consisting primarily of the clutch, furnace and grip assembly, and the torque sensor. A linear bearing was specially designed to allow axial freedom while providing torsional constraint, and was successful in allowing the test specimen to naturally expand or contract in length, free of longitudinal stresses. Instrumentation was provided to allow continuous measurement of torque, strain, temperature and change in length of the specimens.

The second phase of the investigation was concerned with the extent of anisotropy and the subsequent change in length of the test

specimens. Experimental investigations indicated that all three materials experienced a change in length during torsion. The test specimens generally exhibited a tendency to increase their length while being twisted, although at high temperatures, an initial shortening was observed, followed by a gradual increase in length.

The experimental data from room temperature tests was used to determine an empirical equation which was then incorporated into an analytical study of the extent of anisotropy in torsion. Using the anisotropic plasticity theory of Hill, equations were developed which expressed the anisotropic parameters or the associated yield stresses along the principal anisotropic directions as a function of the through-thickness yield strength.

A comprehensive series of torsion tests were performed over a wide range of strain rates (approximately 0.015 to 150 per second) and temperatures (22°C to 550°C for the commercially pure aluminum, and 350°C to 500°C for the 2017-0 and 6061-0 aluminum alloys). Longitudinal stresses were eliminated by allowing natural change in length during twisting.

The effect of strain rate was found to be reasonably approximated by a power law, while the strain rate sensitivity was observed to increase with increasing temperature. The effects of temperature and strain rate on the shape of the stress strain curve could be explained by a consideration of the effects of work hardening, recovery, and recrystallization.

CHAPTER I

INTRODUCTION

Object of the Investigation

The changes that occur to the mechanical properties of metals subjected to large plastic deformations are not only of theoretical interest, but can be of much significance in the manufacturing industry. An accurate knowledge of the flow stress under changing conditions of strain, strain rate and temperature is obviously necessary in order to determine power requirements, the number of anneals, or even the manufacturing process itself. Clearly, the knowledge of how mechanical properties vary with strain, strain rate and temperature is vital for the manufacturing engineer in order to specify that process which will lead to the most economical means of manufacture.

The object of the present investigation was to develop a testing procedure to conveniently and accurately obtain data relating the effects of strain rate and temperature to flow stress of several selected materials at high strains.

Previous Methods of Testing

Many methods have been used in determining the resistance to deformation of materials, such as tension, axi-symmetric compression, plane strain compression and torsion with solid test pieces. However, these testing methods have several inherent disadvantages.

When testing in tension, it is difficult to obtain true stress-true strain data because of the necking of the specimen. Furthermore, the strain rate of extension is not constant when the test is conducted at constant velocity, which is provided by most tensile testing machines. The instantaneous strain rate in tension (or compression) is given by the equation

$$\dot{\varepsilon} = \frac{1}{h}\left(\frac{dh}{dt}\right) \tag{1}$$

where h is the instantaneous height of the specimen at any time t, and dh/dt is the testing speed. If the specimen is strained at a constant velocity (dh/dt = Const.) then as h increases, $\dot{\varepsilon}$ will decrease. If the strain rate is to be held constant, the velocity of extension must be adjusted so that the quantity (1/h)(dh/dt) remains constant during the test.

Strain rate tests in compression have been performed using a logarithmic cam to give a constant rate of straining during the test. The most common type of compression test is axi-symmetric compression, in which the specimen consists of a solid cylinder which is compressed between flat dies. In this type of test, however, friction exists between the specimen and the die faces which can cause the specimen to barrel, even with the most efficient lubricants. Overall reductions are necessarily limited to about 0.7, because of the increasing cross-sectional area of the specimen with reduction, requiring greater loads for further reduction. No measure of ductility may be obtained with very ductile materials.

Plane strain compression of a metal strip between indenting dies has also been used in determining strain rate and temperature effects. This type of testing is closely analogous to the metal rolling process, which is the primary interest of many investigators in this area. Yet, friction still exists between the specimen and the die faces, and will, of course, influence the test data. Corrections for friction are available but they are laborious to carry out. Additionally, total compressive strain is limited to about 2.3 because of the onset of lateral spread. Again, no measure of ductility may be obtained with very ductile materials.

Torsion with solid test pieces results in a variation of strain and strain rate as the radial distance increases from the center of the specimen. Additionally, the distribution of shearing stress in the plastic range is non-linear over the cross section. Methods have been derived for computing the stress in the plastic range with the aid of the torque twist diagram, but the results are only approximate.

Scope of the Investigation

A careful study of available testing methods has led to the conclusion that the torsion testing of hollow test pieces would overcome most of the disadvantages encountered in other testing methods. The stress throughout the thin wall may be considered essentially uniform, and any strengthening effect of the inner material present in solid specimens would thereby not affect the results. However, specimen geometry is of importance in order to avoid failure by buckling. Such instability is due in part to the tendency of metals to change their

length when subjected to large torsional strains. Due to the lack of a stabilizing inner core, hollow test pieces can be very sensitive in this respect. To date, little is known about this phenomenon, and it must certainly be further investigated before torsion testing of hollow cylinders can be widely applied.

The research consisted of essentially three phases:

1. A torsion testing machine was designed, constructed and its performance analysed. The machine was designed to be capable of testing over a wide range of temperatures and strain rates, and to simultaneously allow the natural change in length of the specimen during testing.

2. The change in length of the torsion specimens was investigated in detail. This phase of the research included both an analytical and experimental approach in order to obtain a better understanding of torsional deformation at large plastic strains, and the subsequent development of anisotropy within the torsion specimen.

3. A series of comprehensive torsion tests on commercially pure aluminum (1100-0) and two aluminum alloys (2017-0 and 6061-0) were performed over a wide range of temperatures and strain rates. Longitudinal stresses were eliminated by allowing natural changes in length to occur during twisting. The effects of temperature and strain rate on the mechanical properties of these metals were analysed in detail.

CHAPTER II

REVIEW OF LITERATURE

Introduction

The effects of temperature and strain rate on the flow stress of materials has been the subject of many investigations in the past. Much of this work, however, has been concerned with extremely low rates of strain, 10^{-6} sec^{-1} (creep), or very high strain rates, 10^{3} sec^{-1} (impact). Such data is of limited value in the metal-working industry, where the majority of the forming processes involve intermediate rates of deformation between these extremes. The following review will be primarily concerned with the discussion of previous investigations over the ranges of temperature and strain rate likely to be encountered in metal-working processes. In addition, since the present work incorporates the torsion test, a discussion of torsional deformation will be included which will cover the development of anisotropy and the subsequent axial changes in length of the torsional specimen.

Low Temperature Tests

Ludwik (1) was one of the most important of the early contributors in investigating strain rate effects. Using the tension test, he found that the ultimate stress of tin wires increased with the logarithm of the strain rate. According to the relationship proposed by Ludwik

$$\sigma = \sigma_o + A \ln \dot{\varepsilon} \qquad (2)$$

where σ is the stress for a given strain, and σ_o is the stress at unit strain rate for the strain. A similar relationship was proposed by Prandtl (2) using a mathematical model.

In general, much of the early work involved tensile testing of materials, such as that of Meyer (3), Weerts (4), Koeber and Storp (5) Morrison (6), Elam (7), Davies (8), and Clark and Datwyler (9), showed that the yield and ultimate strength and, in some cases, the elongation to fracture, increased with an increase in strain rate.

Honegger (10), using tensile impact tests on aluminum and copper, found both the tensile strength and the elongations at rupture larger than in the static tests. Ginns (11) utilized an elastic spring as a high-speed loading mechanism and obtained rates of strain in the order of 60 per second. Mann (12) has described a high velocity impact machine capable of producing high rates of strain. Steel and bronze were tested up to rates of 3840 per second, and a transition velocity was noted above which the impact energy would decrease with increasing strain rate.

More recently, Clark and Wood (13), Hammer and Cadle (14) and Abbe (15) investigated the tensile impact properties of some high-strength steels; however, only a single dynamic strain rate was considered, and a general relationship between stress and strain rate was not determined.

In recent years, the effect of strain rate on the resistance to deformation of materials has been discussed in terms of dislocation

theory. The dislocation mechanisms controlling deformation are known to depend on the strain, strain rate and temperature. At very high rates of strain, other properties of dislocations must be considered. For example, Gillis (16) proposed that the velocity of dislocations, and therefore deformation, is controlled by a drag force. The dislocation velocity may then be expressed as

$$V = V^{*} e^{-\left(\frac{D}{\sigma}\right)} \tag{3}$$

where V^{*} is some limiting velocity and D a drag parameter. If the strain rate is assumed proportional to the dislocation velocity, then

$$\dot{\varepsilon} = Be^{-\left(\frac{D}{\sigma}\right)} \tag{4}$$

An examination of this equation, along with several other theories concerning the mathematical relationship between stress, strain and strain rate has been discussed by Hoge (17), and evaluated in terms of experimental data.

Campbell (18) has discussed the existence of a strain rate effect on yielding in iron-carbon alloys based on the Cottrell-Bilby theory of yielding, involving the tearing away of a number of dislocations from their locking "atmospheres." Kendall and Davidson (19), utilizing the Cottrell-Bilby model, proposed a strain rate effect model which predicts a power law relationship for the yield stress as a function of strain rate.

$$\sigma_y\Big|_{T=\text{Const.}} \propto (\dot{\varepsilon})^{\frac{1}{\alpha+1}} \qquad (5)$$

where $\alpha = \frac{1}{nkT}$, n and k are constants, and T is the absolute temperature. Campbell (18) found that mild steel does exhibit a power law relationship, however, a minimum value of strain rate, varying with the material, was observed below which a power law does not apply.

An extensive series of room temperature tests investigating the strain rate dependence of the flow stress in some aluminum alloys was conducted by Holt, Babcock, Green, and Maiden (20). It was found that for the materials tested in the O-temper, the principal effect of alloying was to raise the rate insensitive component of the flow stress, while for two alloys in the T-6 temper (6061-T6 and 7075-T6), the rate sensitivity of flow stress was negligible.

High Temperature Tests

The preceding discussion has concentrated primarily on tests conducted at either room temperature or at temperatures generally lower than those utilized in hot metal-working processes. The research performed on strain rate effects at higher temperatures has, in most cases, been prompted by the desire to learn more about forces required for deformation in the various hot-working processes.

Itihara (21) conducted an extensive series of tests, considering the effect of both high and low temperatures on torsional impact testing, and compared static and impact data. His tests were on steel and iron, and conducted at temperatures ranging from -150°C to 1000°C.

Nadai and Manjoine (22,23), interested in the deformation forces inherent in both hot and cold rolling, conducted an extensive series of tensile tests to determine effects of temperature and strain rate on the mechanical properties of metals. Using both a high-speed (flywheel actuated) and a low-speed (power screw drive) tensile testing machine, they were able to demonstrate that the strain rate sensitivity of a metal may increase with increasing temperature, and that even at high temperatures the metals tested showed high ultimate strengths when deformed at high strain rates.

Clark and Russ (24), using the torsion test to analyse hot-working operations, found it to be of great value in providing a convenient means for the selection of optimum temperatures for various hot-working operations. Ihrig (25) performed similar tests analyzing the effects of various chemical elements on a wide variety of steels. Their work, however, utilized no central reduced portion of the specimen, and, as discussed by Bloom, Clarke and Jennings (26), the total number of turns of the specimen could be affected by the length of the hottest zone in the furnace and the temperature gradient existing across the specimen's length. However, the tests can still be considered to be of value because they afford an approximate measure of the ductility or workability at different temperatures.

Hughes (27) used hot torsion testing with specimens of reduced cross section to assess the hot-working properties of steels at temperatures from 950°C to 1400°C and speeds from 12 to 600 RPM. Measurements were made of longitudinal tensile stresses developed during the tests, which were found to be an important factor influencing failure.

The combined effect of strain rate and temperature has been considered by Zener and Hollomon (28), who suggested that the flow stress at a constant strain was related to both the strain rate and the temperature by the relation

$$\sigma = f(z) \tag{6}$$

Z is commonly referred to as the Zener-Hollomon parameter, where

$$Z = \dot{\varepsilon} e^{\frac{\Delta H}{RT}} \tag{7}$$

ΔH is an activation energy, expressed in calories per gram mole, R is the gas constant, and T is the absolute temperature. If the relationship holds, a plot of $\ln\dot{\varepsilon}$ against $\frac{1}{T}$ at a given value of stress and strain would result in a straight line. The parameter was based originally on experimental data for copper and mild steel. However, Bechtold (29) found the relation to hold true for tests on molybdenum while Trozera, Sherby, and Dorn (30) found it to hold for pure aluminum. The interpretation of the activation energies upon which the parameter depends is rather involved, and subsequent investigations have indicated that the parameter only holds for narrow ranges of strain rate and temperature, if at all.

Fields and Backofen (31) have found from torsion tests on a 2024-0 aluminum alloy that correlations of temperature and strain rate for fixed levels of flow stress, using the Zener Hollomon parameter, were obscured by strain aging during deformation.

MacGregor and Fisher (32) have developed a velocity modified temperature for representing, by means of a single variable, the combined effects of strain rate and temperature on the flow stress. The flow stress was considered a function of the strain and the velocity modified temperature

$$\sigma = f(T_m, \varepsilon) \tag{8}$$

where the velocity modified temperature T_m is expressed as

$$T_m = T(1 - k\ln \frac{\dot{\varepsilon}}{\dot{\varepsilon}_o}) \tag{9}$$

where T is the absolute testing temperature, $\dot{\varepsilon}$ is the constant true strain rate during the test, $\dot{\varepsilon}_o$ is the unit strain rate taken to be 10^{-3} per second, and k is a constant. Using this relation, it was proposed that the behavior of a series of tensile tests could be determined using only one variable instead of two.

It has been suggested that the relationship $\sigma = f(Z)$ represents a mechanical equation of state. However, it implies that the flow stress is a function of the instantaneous values of strain, strain rate and temperature, and is independent of prior deformation history. Investigations, such as those by Dorn, Goldberg, and Tietz (33), and Tietz and Dorn (34), on aluminum, copper, stainless steel, and low-carbon steel, have shown that deviations can indeed occur from the behavior as predicted by a mechanical equation of state. Therefore, as pointed out by Smith (35) in his discussion of stress-strain-time-

temperature relationships, experimental studies can in some instances support, and in other instances refute the validity of a mechanical equation of state. Smith further pointed out that the concept is not always valid, either in part or wholly, because of differences in structure associated with different histories. Such differences include also those on an atomic scale.

Lubahn (36) has derived an equation expressing the stress in terms of strain, strain rate, and temperature. He assumed the true stress-true strain curve to be a simple power law for large strains. The assumption was supported by tensile test data by Fusfeld (37) and Low and Garofalo (38), but was in poor agreement with the results of Dorn, et al. (39,40).

Alder and Phillips (41) have obtained compressive stress-strain curves for aluminum, copper and steel which could not be expressed by a power law with the exception of curves obtained on aluminum at room temperature. From their data, they found it unlikely that any single function could be found to express the relation between stress and strain for the metals they tested over the wide range of variables.

Sokolov (42,43,44,45) has investigated the effects of speed on the resistance to deformation of cylinders of a wide range of metals, including copper, nickel, and aluminum, between the strain rates of 10^{-3} to 10^{2} per second. He found that the power law

$$\sigma\Big|_{\varepsilon,T} = C\dot{\varepsilon}^{n} \tag{10}$$

where C is a constant and n is commonly referred to as the strain rate

sensitivity, provided a better interpretation of the effect of strain rate than the semi-logarithmic relation of Equation (2).

Work and Dolan (46) have discussed the importance of temperature and strain rate studies in relation to the aerospace industry, where aircraft and missiles, traveling at extreme speeds, are subject to elevated temperatures and sudden loading. In their torsion tests on a variety of metals, they found that increasing the strain rate caused an increase in strength, while an increase in temperature reduced the strength of the metals tested except in the blue-brittle temperature range for steel.

Fink, Lueg, and Burger (47) performed high-speed compression (drop-hammer) tests on a variety of steels, and determined yield stress-strain curves over the temperature range 700°C-1200°C. This type of testing is of limited use, however, since the strain rate will vary during compression.

By the use of a testing instrument, such as a cam plastometer, compression tests may be performed by utilizing an appropriate cam to maintain either a constant testing velocity or constant strain rate. Such testing machines have been described by Orowan (48), Bailey and Singer (49), and Hockett (50).

Loizou and Sims (51) investigated the variation of the yield stress of pure lead in uni-axial compression with temperature and strain rate, using a cam plastometer. From their data, they found it likely that the yield stress is not only dependent upon instantaneous values of temperature, strain, and strain rate, but also in a complex manner on the total time taken to deform the specimen from the annealed

condition, on the rate of deformation, and on the time required for recovery and recrystallization.

The compression tests of Alder and Phillips (41) utilized a cam plastometer designed by Orowan and Los. The compressive stress-strain curves for copper and steel at certain temperatures showed a drop in stress at higher strains, while aluminum at 350°C-550°C continued at approximately constant stress above a certain strain. With regard to strain rate effects, Alder and Phillips found that the power law, Equation (10), appeared to provide a slightly better interpretation of their data than the semi-logarithmic formula of Ludwik.

Investigating temperature effects, Alder and Phillips calculated the power index n, and plotted it as a function of the homologous temperature T_h, where

$$T_n = \frac{\text{Testing Temperature (°K)}}{\text{Melting Point Temperature (°K)}} \qquad (11)$$

They found that n is small and shows little change with T_h at values of T_h below 0.55, but increases approximately linearly at values above 0.55.

Sokolov (52) found from compression tests on a number of steels (50 per cent compression) that n was proportional to T_h, but contrary to the work of Alder and Phillips, he found the extrapolated curve passed through the origin.

Cook (53), using the same machine as Alder and Phillips, presented true flow stress vs. natural strain curves for a wide variety of steels

at 900°, 1000°, 1100°, and 1200°C and at constant natural strain rates of 1 $\frac{1}{2}$, 8, 40 and 100 per second. Cook observed that many of the curves exhibited a drop in flow stress at high strains, and attributed this to the predominance of thermal softening over strain hardening as the compressive strain increased. A brief account was given of a method which could be used to calculate loads and torques in hot rolling. In some cases, the semi-logarithmic relation of Ludwik, and in other cases the power law, adequately described the effect of strain rate on the flow stress, but in general, no simple relation was evident.

The effect of strain rate and temperature on the compressive flow stress of titanium and two titanium alloys was investigated by Griest, Sabroff and Frost (54). It was found that at hot-working temperatures, the flow stress was noticeably sensitive to strain rate.

Further work using compression testing has been carried out by Arnold and Parker (55). The resistance to deformation of aluminum and some aluminum alloys were determined using a cam plastometer. The cams used, however, were the constant velocity type. For certain alloys, a loss of strength was noted at high strains in certain ranges of temperature and strain rate.

Rossard and Blain (56), using the torsion test, have shown that for several ferrous metals the true stress-true strain curves agreed closely with similar curves obtained in tension. In some cases the Von-Mises criterion gave a good agreement between the stresses, while in other cases, the maximum shear criterion gave closer agreement. Rossard and Blain (57) also used the torsion test to reproduce the rolling schedules used in a reversing, continuous, and planetary mill

for three low carbon steels. They found similarities in the resulting microstructures between the torsion specimens and the products obtained from the mill.

Omerod and McG. Tegart (58) have utilized the torsion method of testing super pure aluminum. At higher temperatures, they found the torque-revolution curve to level off to a fairly stable value which appeared to be relatively independent of the number of revolutions to fracture. The values of n for various temperatures were found to be in reasonably close agreement with those obtained from the data of Alder and Phillips for compression of commercially pure aluminum. Similar values of n have been obtained by Fields and Backofen (31,59) from torsion of a 2024-0 aluminum alloy.

Hodierne (60) has shown that the stress-strain data derived from the torsion test is in no way inferior to data given by other tests. His results agree remarkably well with the tension data of Nadai and Manjoine (23) and the compression data of Alder and Phillips (41), and Loizou and Sims (51). However, the anisotropy developed during each of the different types of tests will play a large part in prohibiting exact correlation of data and must be considered when comparing such tests. Hodierne also noted that, in addition, the initial mechanical anisotropy need be considered.

Hardwick and McG. Tegart (61) investigated the high temperature deformation of aluminum, copper, and nickel in torsion. They correlated the behavior of a metal during deformation and concurrent restoration as being related to the competition between polygonization and recrystallization, and associated this behavior with the stacking fault energy of

the metal. During tests at temperatures of approximately $0.7T_m$ and strain rates of approximately 1 sec^{-1}, aluminum was found to show only polygonization; nickel showed polygonization and recrystallization as concurrent processes, while copper showed only recrystallization. Peaks in the torque-twist curves were explained as follows: With Aluminum, dislocation climb and restoration is rapid, and thus, only a small peak, if any is observed. In nickel, dislocation climb is slower, and the initial work hardening cannot be removed rapidly enough by polygonization, so enough strain energy is available to initiate recrystallization; the original polygonized grains are replaced by fine equiaxed ones. With copper, dislocation climb is slow so that polygonization is not a significant process, and recrystallization occurs when sufficient strain energy is available. Thus, marked peaks can occur in both the copper and nickel curves.

The research by Bailey (62,63), and Bailey and Singer (49,64,65) has shown that the plane strain compression test can be used successfully to study the effects of strain rate and temperature on the resistance to deformation of metals. The results of their tests, performed on a cam plastometer, indicated that at high strains, after a rapid initial rise in the stress-strain curve, a drop in stress occurred which generally tended to approach a stable value for aluminum, some aluminum alloys, and pure lead. The results show some differences with the work of Loizou and Sims (51), Alder and Phillips (41), Hardwick and McG. Tegart (61) and Hodierne (60). The shape of the stress strain curves could be explained from a qualitative consideration of the relative effects of work hardening, recovery, and recrystallization, which

could in turn be related to the stacking fault energies of the metals. The effect of strain rate could be explained by the power law, and values of n, the strain rate sensitivity exponent, agreed with those of Alder and Phillips, and Sokolov.

Reynolds and McG. Tegart (66) studied the deformation of some pure irons using high-speed torsion over the temperature range 700°-1250°C. The changes in the ductility of the irons tested were related to the microstructural changes during deformation. In the α-range, low ductility was associated with a stable substructure which prevented boundary migration and promoted intercrystalline fracture, while high ductility was associated with a recrystallized structure. At lower temperatures in the γ-range, ductilities of the three irons were low, but were found to increase rapidly with temperature above approximately 1100°C.

Robbins, Wagenaar, Shepard, and Sherby (67) have discussed torsion testing as a means of studying the influence of crystal structure, strain rate, temperature, and composition on the ductility and strength of iron base alloys at high temperatures. It was found that the use of the torsion test was especially suitable for permitting an interpretation of the contribution of concurrent straining to spheroidization.

The torsional ductility and strength of iron-carbon alloys at elevated temperature was investigated by Robbins, Shepard, and Sherby (68). The high purity alloys showed lower strength and higher ductilities than the commercial alloys when compared at the same carbon content. Increasing the carbon content increased the ductility and decreased the strength of iron in the austenite range throughout the

range of carbon contents studied.

Cook (69) has described a differential torsion-testing machine which could be considered analogous to the testing of thin-walled cylinders. Two specimens of slightly different size could be simultaneously tested, and the difference in the twisting moment measured. The shear stress could then be determined as a function of the difference in torques and the two radii.

In general, torsion testing for the purpose of investigating temperature and strain rate effects has been almost exclusively restricted to the testing of solid specimens. The inherent limitations of such tests have already been mentioned. It would then appear that the ideal specimen for the torsion test would be the hollow cylinder, however, with this type of specimen, buckling can occur under certain conditions of specimen geometry. Primarily because of this problem, it has not been used extensively in the past. Hodierne (60), however, has discussed the advantages of employing hollow test pieces in torsion tests, using short gage lengths to eliminate distortion and to insure uniform stresses in the test piece during high-speed deformation.

Specimen geometry for thin-walled test pieces has been discussed by Marin (70) and Richards (71). Marin suggested as a general guide to use a ratio of length of reduced section to diameter of about 0.5, and a diameter to wall thickness ratio of about 10. A tendency for failure by buckling may be present for larger ratios.

Axial Deformation and Anisotropy in Torsion

In 1909, and later in 1912, Poynting (72,73) reported his observations that when a torsional stress was applied to wires of steel and copper, they tended to elongate. Poynting's experiments were, however, kept within the elastic limits of the materials tested. Reiner (74) analytically examined the case of elastic torsion of a circular cylinder, and derived an equation which was confirmed by Poynting's observations.

Little attention was apparently given to Poynting's experiments until Swift (75) reported on length changes in metals during large plastic torsional strains. By use of a special gripping fixture which permitted axial freedom, the twist and extension of many cylindrical specimens were simultaneously measured. It was found that final axial elongation varied from about 1 per cent for a carbon steel, to over 11 per cent for a 70-30 brass.

If both ends of a torsional gripping fixture are constrained with respect to the axial direction, then a compressive stress will naturally result in a material that would otherwise have tended to lengthen. Swift has found that on test of solid specimens of 70-30 brass and austenitic stainless steel, the rate of axial strain was about 3 per cent of the rate of the shear strain over the greater part of the plastic range, and thus deduced that an axial compression of approximately 9 per cent of the principal shear stress is caused by suppressing the axial strain. Such a stress may be expected to introduce an error in the resulting shear stress-shear strain relationship.

It can be expected that the lesser strained inner core of the specimen would exert some restraint on the elongation of the outer layers. Comparative free torsion tests by Swift, between solid and hollow specimens, indicated that the core does indeed exert such a restraint.

From his results, Swift naturally suspected that the work-hardenability of a material played an important part in the process of elongation. On tests of lead, a non-workhardening material at room temperature, he found that large torsional strains actually caused an axial shortening of the specimen.

Several interesting effects occur when a cylinder, which has already been subject to cold work, is twisted. For example, Swift found that after applying some initial twist, and then reversing the sense of the torque, there is first a transient tendency to reverse the axial strain. Soon, however, this tendency is overcome, and the extension of the piece follows approximately the same rate of extension as before the reversal of twist. Also, for bars that were stretched in tension before being tested in torsion, initial shortening occurred followed by a stretching rate almost identical with that for the initially unstrained bar.

It appears that such behavior of metals under large torsional strains is due, at least to a certain extent, to the resulting anisotropy which is developed as a result of the torsional straining. Certainly, plastic deformation theories assuming isotropy become less applicable as the deformation continues. For example, Cook (76) has shown that the tensile yield stress in a direction transverse to that

of rolling may be as much as 10 per cent greater than that parallel to the rolling direction in a heavily cold-rolled brass.

The development of anisotropy in rolled metals has been studied in detail by many workers, including Svensson (77), Hazlett, Robinson and Dorn (78), Dorn (79), Klingler and Sachs (80), Wilson (81), and Grumbach and Pomey (82). The consideration of the preferred orientation of sheet metals is an excellent indication of how cold-working can cause considerable deviations from isotropy.

Hill (83,84) has proposed a theory which describes, on a macroscopic scale, the yielding and plastic flow of an anisotropic metal. By using the Von-Mises concept of a plastic potential, relations were formed between the stress and strain increment tensors. He has shown that his theory predicts the changes in length of a hollow cylinder, as earlier observed by Swift.

It will be valuable to review briefly Hill's anisotropic theory, as it will be used as the basis for further analytical development considering the extent of anisotropy developed in torsion.

Hill considered the yield criterion of the form

$$2f(\sigma_{ij}) \equiv F(\sigma_y-\sigma_z)^2 + G(\sigma_z-\sigma_x)^2 + H(\sigma_x-\sigma_y)^2 \qquad (12)$$

$$+ 2L\tau_{yz}^2 + 2M\tau_{zx}^2 + 2N\tau_{xy}^2 = 1$$

where F,G,H,L,M,N are six parameters indicating the current state of anisotropy. The axes of anisotropy were considered to be mutually orthogonal, while the Baushinger effect was assumed absent.

If X is the tensile yield stress in the x-direction of the principal anisotropic axis system, then, when only σ_x is applied

$$\frac{1}{X^2} = G + H \tag{13a}$$

and similarly,

$$\frac{1}{Y^2} = H + F \tag{13b}$$

$$\frac{1}{Z^2} = F + G \tag{13c}$$

If R, S, and T are the yield shear stresses with respect to the principal axes, then

$$2L = \frac{1}{R^2}$$

$$2M = \frac{1}{S^2} \tag{14}$$

$$2N = \frac{1}{T^2}$$

Therefore, the six yield stresses need be known in order to indicate the values of the anisotropic parameters. Using the relation

between the stress and strain increment tensors, Hill showed that

$$d\varepsilon_x = d\lambda[H(\sigma_x-\sigma_y) + G(\sigma_x-\sigma_z)]$$

$$d\varepsilon_y = d\lambda[F(\sigma_y-\sigma_z) + H(\sigma_y-\sigma_x)] \qquad (15)$$

$$d\varepsilon_z = d\lambda[G(\sigma_z-\sigma_x) + F(\sigma_z-\sigma_y)]$$

and that

$$d\gamma_{yz} = d\lambda L\tau_{yz}$$

$$d\gamma_{zx} = d\lambda M\tau_{zx} \qquad (16)$$

$$d\gamma_{xy} = d\lambda N\tau_{xy}$$

where $d\lambda$ is a positive scalar factor of proportionality.

Hill has applied this theory to explain analytically the length changes observed by Swift. The torsion specimen used in the analysis was assumed to be an initially isotropic thin-walled cylinder, gripped at the ends in such a way that there is no axial constraint. The extended surface of the thin-walled tube as drawn in Figure 1 was used to illustrate the development of anisotropy.

The initial direction of greatest compression for any shear strain γ can be shown to lie on OC, which bisects angle AON, where the lines AO and BO, respectively, represent a line which is first compressed

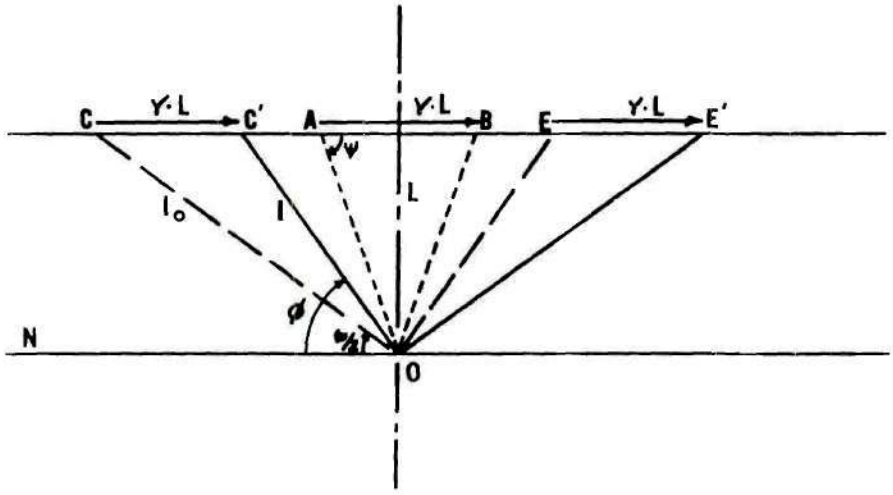

Figure 1. Rotation of the Anisotropic Axes

and then extended an equal amount due to the shear strain γ.

After applying any shear strain γ, OC is compressed to the position OC', and this can be shown to represent the maximum compressive strain. It can be shown that the initial and final directions of greatest extension are similarly found to lie in the directions of OE and OE', respectively. The directions OC' and OE' are then defined as the principal axes of anisotropy, and can be shown to be perpendicular to each other.

Assuming the tube to be initially isotropic, the angle ϕ will increase from $\pi/4$ to $\pi/2$. Therefore, the rotation of the anisotropic axes is $(\phi - 45^{\circ})$. The rotation is confined to the x-y plane about the z-axis which is directed outward in the radial direction.

The stresses along the principal anisotropic axes may be represented in terms of the principal shear stress τ, and the angle ϕ. Substitution of these values into Equation (12) gives

$$\tau = [2N + (F+G+4H-2N)\mathrm{Sin}^2 2\phi]^{-\frac{1}{2}} \tag{17}$$

Also,

$$\begin{aligned} d\varepsilon_x &= -\tau d\lambda(G+2H)\mathrm{Sin}2\phi \\ d\varepsilon_y &= \tau d\lambda(F+2H)\mathrm{Sin}2\phi \\ d\varepsilon_z &= \tau d\lambda(G-F)\mathrm{Sin}2\phi \\ d\varepsilon_{xy} &= \frac{d\gamma_{xy}}{2} = \tau d\lambda N\mathrm{Cos}2\phi \end{aligned} \tag{18}$$

Using the strain transformation equations, the axial strain increment and the shear strain increment were shown to be

$$d\varepsilon = [(N-G-2H)\mathrm{Sin}^2\phi - (N-F-2H)\mathrm{Cos}^2\phi]\mathrm{Sin}2\phi\tau d\lambda \qquad (19)$$

$$d\gamma = [2N + (F+G+4H-2N)\mathrm{Sin}^2 2\phi]\tau d\lambda \qquad (20)$$

Equations (19) and (20) were the fundamental equations proposed by Hill to predict analytically the change in length. Their quotient expresses the rate of elongation. The limiting feature of these equations is that their use is dependent upon the evaluation of the parameters F,G,H, and N.

Hu (75), using Hill's basic theory, considered plane stress and plane strain problems, and discussed the influence of anisotropy on the interpretation of conventional biaxial tension, tension, and tension, torsion tests. He found that the development of anisotropy could explain irregularities in test data.

The axial change in length has been found to be dependent upon temperature. Morozumi, in measuring the resultant axial stresses in steels, found that when a twisting deformation is applied at a temperature lower than the recrystallization temperature, the axial length of the specimen extends with progressive twisting, and finally fractures. At a temperature higher than the recrystallization temperature, an extension occurs in the initial stage of twisting and then tends to contract as the shear strains increase. Thus, the contraction in axial length necessarily leads to the appearance of a tensile stress if the

gripping ends are constrained. Hughes (27) also measured such tensile stresses during high temperature tests on steels, and found them to vary with temperature and strain rate.

Thomsen, Yang, and Kobayashi (86) have discussed instability in torsion of thin-wall cylinders, and the possibility of necking in the plastic range. Using the assumption that the criterion for necking is given by $dT/d\bar{\varepsilon} = 0$, where T is the torque and $\bar{\varepsilon}$ is the effective stress, they evaluated this differential to obtain

$$\frac{dT}{d\bar{\varepsilon}} = \frac{2\pi r^2 t}{\sqrt{3}} \frac{d\bar{\sigma}}{d\bar{\varepsilon}} = \frac{2\pi r^2 t}{\sqrt{3}} mC(\bar{\varepsilon})^{m-1} \qquad (21)$$

However, the expression in Equation (21) cannot be zero unless m is zero, where m is the work-hardening exponent. Thus, for a work-hardening metal, necking should not occur. They pointed out that it would be of interest to perform a high-speed, high-temperature torsion test on a metal which may, under those conditions, have a negative value of m. Such a test would provide additional support for the theory should necking be observed.

CHAPTER III

DESIGN OF THE TORSION TESTING MACHINE

Initial Design Considerations

The first phase of the investigation was the design, construction, and evaluation of a torsion-testing machine to determine accurately the effects of temperature and strain rate on the mechanical properties of materials. The initial design requirements were as follows:

1. The testing speeds should be in the range of 1500 RPM to 0.0015 RPM in steps no greater than 5:1.

2. Clutch engagement times should be rapid enough to provide an approximately constant rate of deformation throughout the total test period.

3. The machine should be capable of withstanding torsional loads of 2000 inch pounds.

4. The machine should be equipped with a furnace capable of maintaining constant temperatures up to 600°C. The furnace should be of such a design as to allow rapid installation and removal of test specimens.

5. A special mechanism should be provided to allow natural change in length during torsion. The machine must also be able to accommodate a standard-type gripping fixture if the change in specimen length is not desired.

6. Instrumentation to provide simultaneous measurements of torque, temperature, strain and change of specimen gage length must be provided.

Description of the Machine

A total of 12 feasible drive units were designed and analysed with particular reference to their behavior under dynamic conditions. The overall unit finally selected as the optimum design is shown schematically in Figure 2. It consists of two main sections, the drive train assembly containing the motor and speed reduction units, and the test assembly, consisting primarily of the clutch, furnace, grip assembly, and the torque sensor.

Drive Train Assembly

The prime mover is an electric motor built to order by the General Electric Company, capable of providing 100 inch pounds of torque at speeds of 1800 RPM and 450 RPM. The output shaft of the motor is connected through a system of gears to either of two high efficiency Winsmith planetary speed reducers with reduction ratios of 51:1 and 1238:1, respectively. The intermediate gear system connecting the motor output shaft to the reducers can be adjusted to provide reduction ratios of 1:1, 2:1, 3:1, and 5:1 by replacement of the gear pairs.

The planetary gear reducers may be operated either separately or in series, thus providing a speed range of approximately 0.0015 RPM to 35 RPM. For speeds in the higher ranges, the power requirements are such that a flywheel becomes necessary. In this case, the motor is connected directly to a flywheel mounted on the clutch input shaft by means of a timing belt drive.

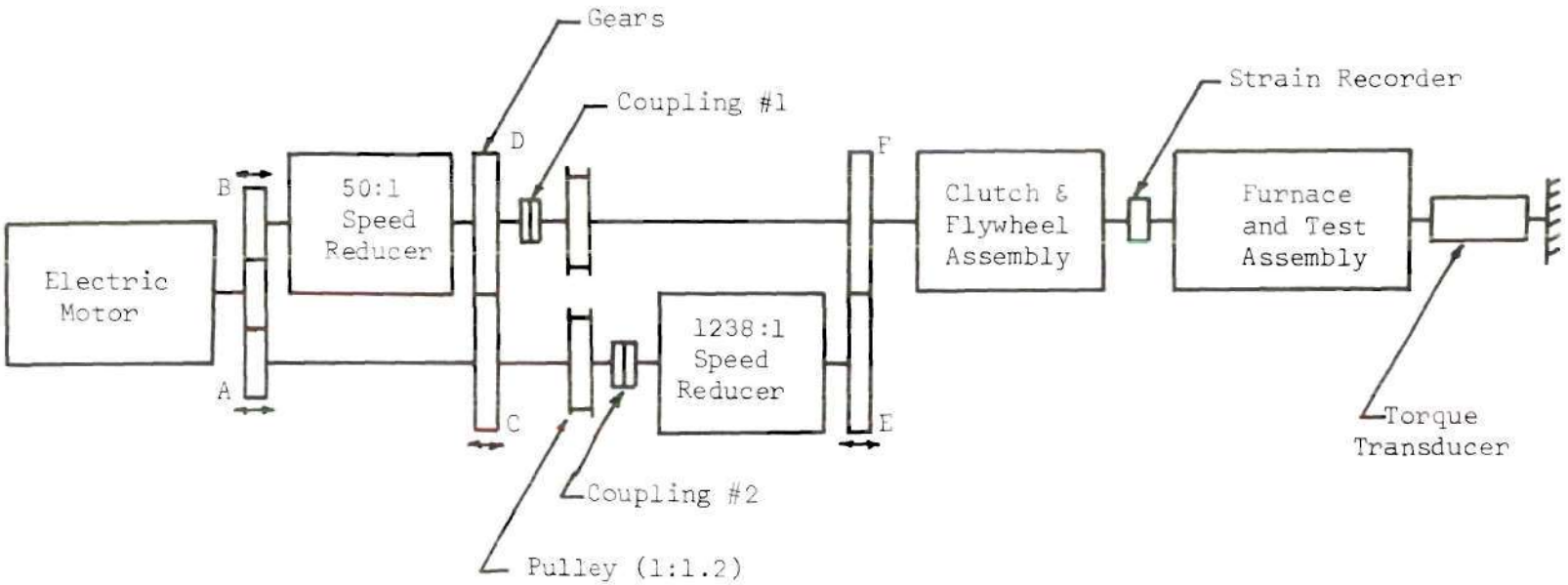

Figure 2. Schematic Representation of Testing Apparatus

The testing speed may thus be selected by proper arrangement of the drive train. For example, if a testing speed of 35 RPM is desired, a 1:1 gear pair would be selected to connect the motor to the 51:1 planetary reduction unit. Referring to Figure 2, gears A, C, and E would be disengaged, with the motor speed set at 1800 RPM; the power then flows from the motor, through the intermediate gears and planetary reducer, to the clutch. If the slowest testing speed of approximately 0.0015 RPM is desired, a 5:1 intermediate gear reduction would be chosen, with gear A disengaged, coupling number 1 disconnected, and gears C and D, and E and F, meshed, and the motor set at 450 RPM. For a direct drive at the higher speeds, gear B would be disengaged along with gears C and E. Both couplings are disconnected, and the timing belt installed, allowing direct power transmission to the clutch and flywheel. Table 1 lists the possible testing speeds which may be utilized.

Table 1. Approximate Testing Speeds in RPM

1500	75	4.4	0.36	0.015
750	35	2.9	0.29	0.0095
500	18	1.8	0.18	0.0071
375	12	1.5	0.12	0.0057
300	8.8	0.73	0.073	0.0036
188	7.0	0.48	0.029	0.0014
125				

Test Assembly

The overall design of the test assembly is illustrated in Figure 3. Torque is transmitted from the drive train and is applied to the forward end of the test specimen upon activation of the clutch. A strain gage reaction torque sensor holds the other side of the specimen stationary, while providing an indication of the applied torque. The specimen is held on the reaction side by a linear bearing, specifically designed to allow axial freedom while providing torsional constraint. A description of the major items in the test assembly and their functions will now be given.

Air Clutch

A Force Control Model 5 pneumatic disc clutch is used to transmit torque from the drive train to the specimen. An internal brake assembly is provided to insure no rotation of the clutch output shaft when the clutch is disengaged. The clutch is actuated by compressed air at 80 psi,passing through a Schrader three-way solenoid pilot-operated air valve. A small surge tank is placed adjacent to the clutch and air valve to insure a rapid supply of air upon engagement of the clutch. Dry filtered air, regulated at 80 psi is supplied to the surge tank from an air compressor.

Furnace and Specimen Mounting Assembly

The furnace consists of two units which horizontally slide together forming a cylindrical heating zone enclosing the specimen and grip assembly. Each unit contains a Lindberg Model 50211 semi-cylindrical heating element mounted in ceramic insulating brick. A chromelalumel thermocouple is permanently mounted inside the furnace,

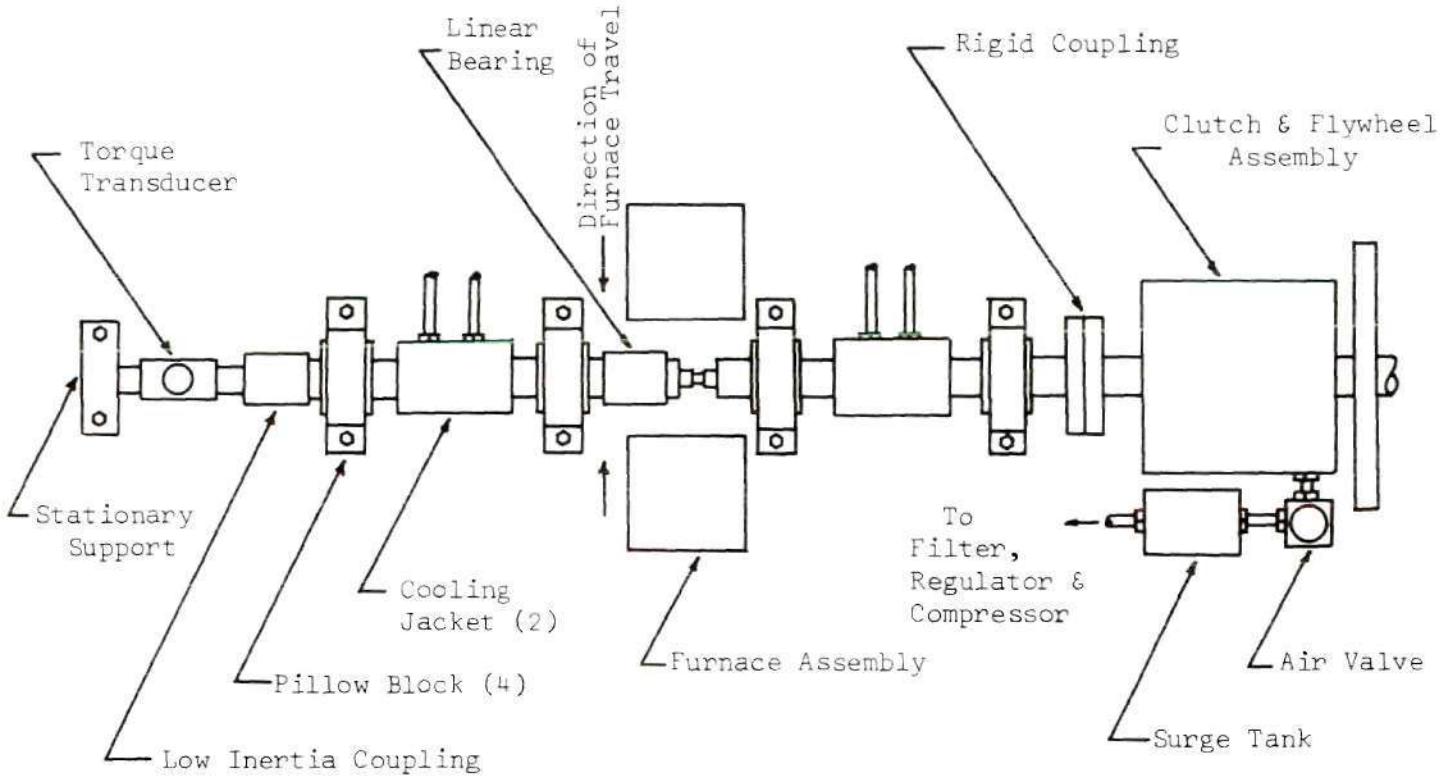

Figure 3. Test Assembly

its extension wires being connected to a Lindberg Model 59344 controller to provide automatic regulation of the air temperature within the furnace. Enough clearance is provided between the furnace grips and the ceramic insulation to allow a chromel-alumel thermocouple mounted in the specimen to pass out of the furnace to a Leeds and Northrup Speedomax H recording potenticmeter.

An important feature of the furnace design is its short length. This enables the supporting pillow blocks on each side to be close to the specimen grips, providing a greater degree of axial rigidity.

The specimen is securely held in each grip by three set screws spaced 120° apart. The grip on the rotating side is connected to the clutch output shaft through $1\frac{1}{4}$ inch stainless steel shafting, while the grip on the reaction side is located within the linear bearing, which in turn is connected to the torque sensor through similar stainless steel shafting. Both shafts are adequately cooled with water jackets mounted and sealed to the shafts, so that they can rotate without any leakage of the coolant.

Linear Bearing

Perhaps the most significant feature of the overall design is the incorporation of a specially-designed mechanism to allow natural changes in length of the specimen during twisting. Many different factors were taken into consideration in the design of this bearing; factors such as axial rigidity to eliminate distortion and torsional rigidity to avoid excessive backlash were of considerable importance, and since the unit was to be adjacent to the specimen, it would have to be able to withstand high temperatures.

The assembly drawing of Figure 4 shows the design of linear bearing. The assembly is seen to consist of two main units, the bearing housing and the bearing support, shown in Figures 5 and 6, respectively.

The bearing housing was machined from type 304 stainless steel which has excellent high temperature properties including relatively low thermal conductivity. Three holes were bored longitudinally through the rear of the housing; each accommodate two Thomson linear ball bushings. The ball bushings are free to slide on shafting mounted in the bearing support unit. These shafts act as an inner bearing race, and were made from 1060 steel, case hardened and ground in order to insure continued serviceability under high loads. The bearing could accommodate torsional loads of 150 inch pounds. For greater loads, correspondingly larger bearings would be required.

The forward portion of the bearing housing accommodates a specimen grip for the reaction side, and is capable of withstanding high temperature during tests. The rear section of the bearing housing, which remains outside of the furnace, is cooled by a surrounding coil of copper tubing with small holes on the inner surface to allow compressed air to impinge upon the exposed surface of the bearing.

The entire bearing assembly is connected to the torque sensor by the main shaft. Connection of the bearing assembly to the main shaft is illustrated in Figure 4.

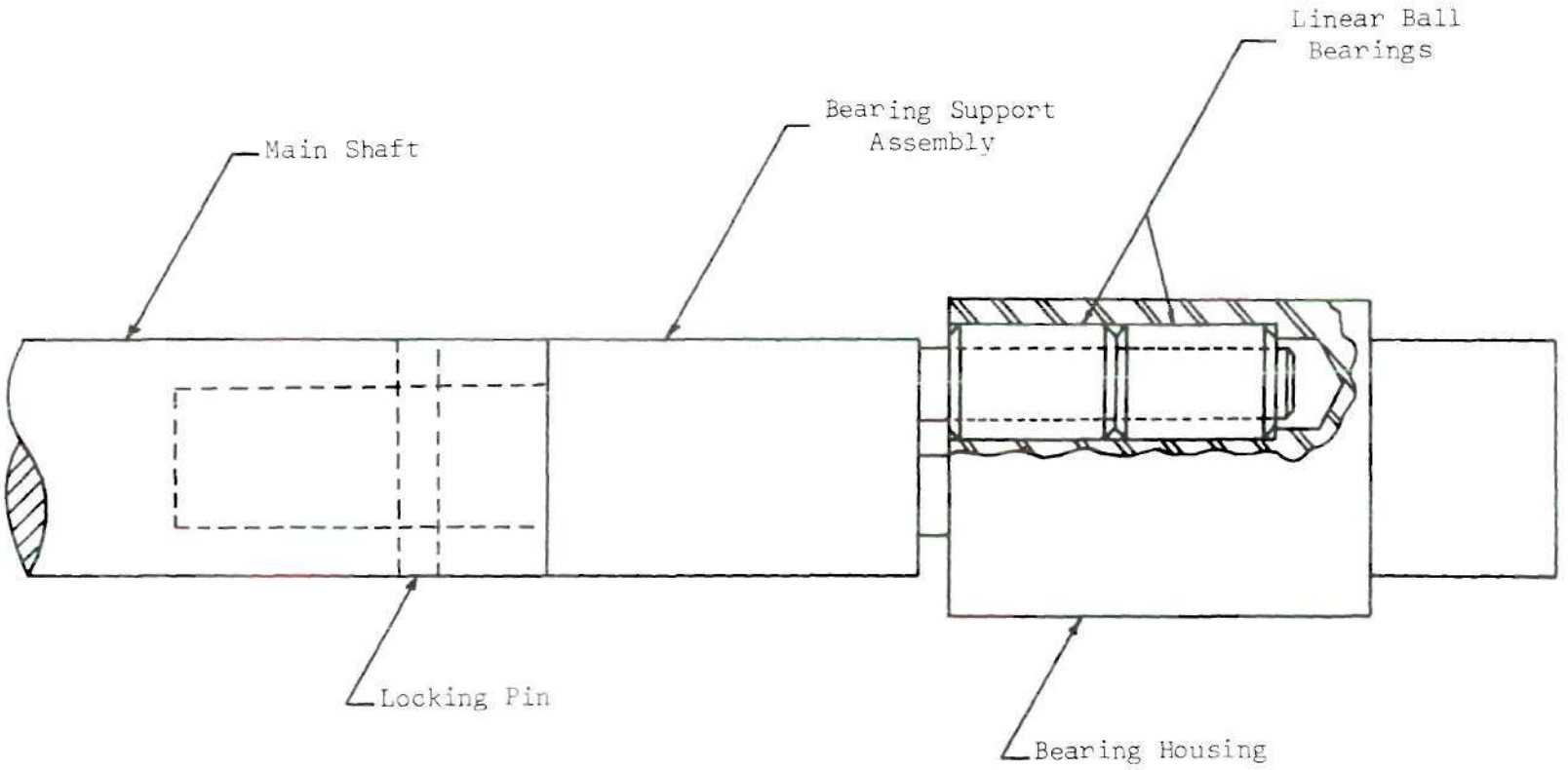

Figure 4. Bearing and Bearing Support Assembly

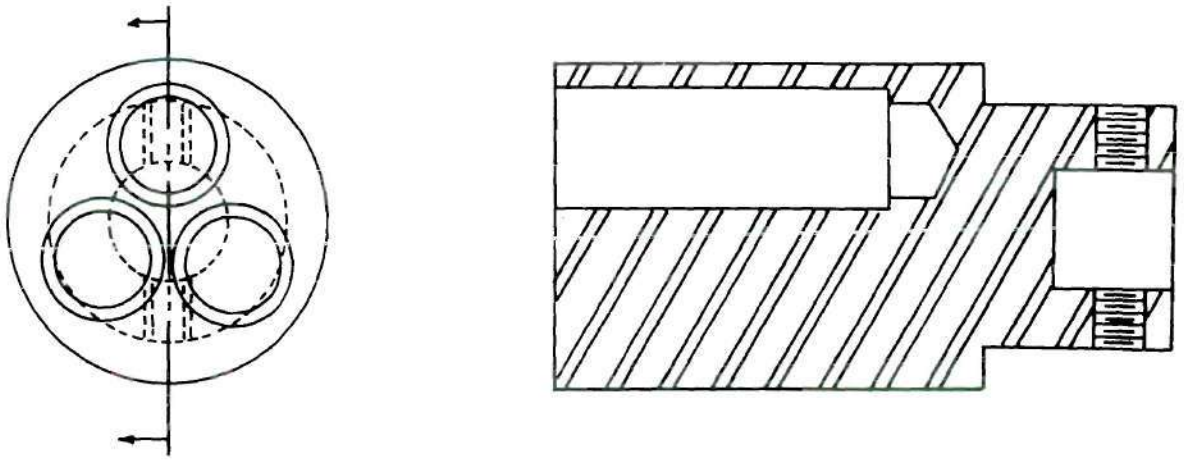

Figure 5. Bearing Housing

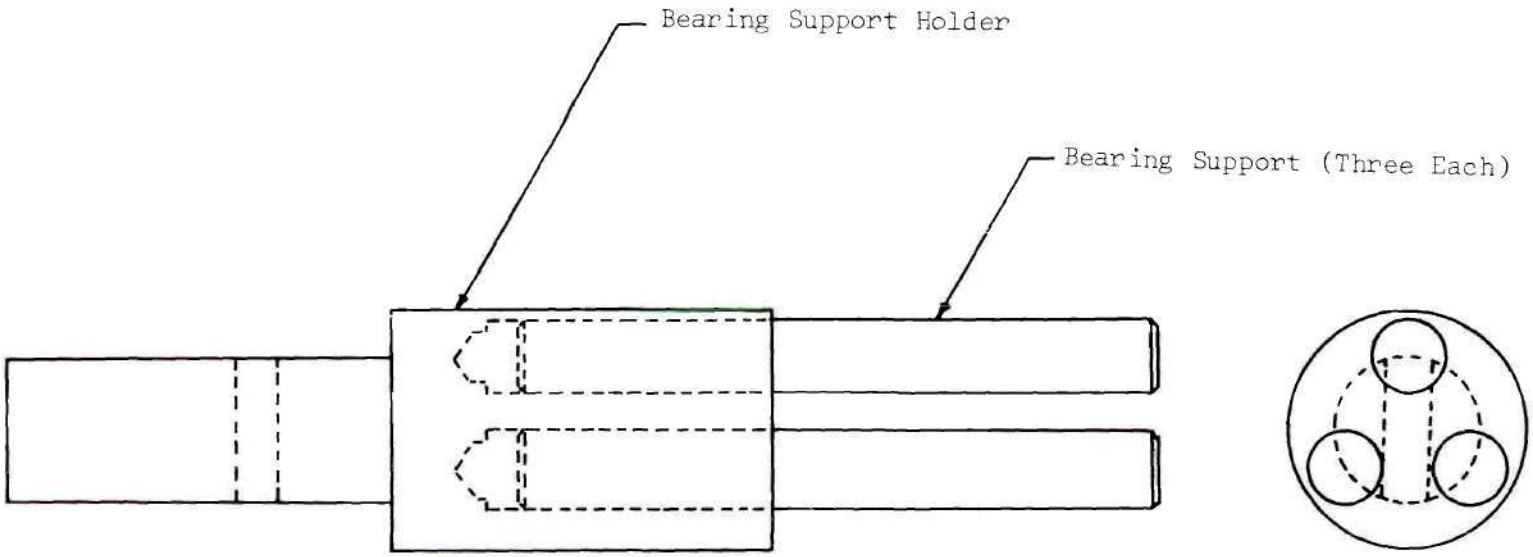

Figure 6. Bearing Support

Reaction Torque Sensor

The torque is measured using a Lebow strain gage reaction torque sensor with a capacity if 200 inch pounds, linearity being within 0.1 per cent of rated capacity. The rigid coupling connecting the torque sensor to the main shaft was designed specifically to have a low polar moment of inertia in order to reduce dynamic effects during high-speed testing. The other end of the torque sensor is rigidly mounted to the frame, thereby stabilizing the reaction or stationary side of the specimen.

Strain and Strain Rate Measurement

The angular displacement of the specimen is determined by means of a ten-turn rotary potentiometer connected to the clutch output shaft through an intermediate gear reduction system. A slip clutch, mounted on the potentiometer shaft prevented overriding. The testing speed is determined from the time rate of change of the angular displacement. Determination of strain and strain rate is readily obtained from Equations (51) and (52).

Change in Length Measurement

The axial change in length is equal to the displacement of the linear bearing. Measurement is by means of a linear differential transformer. The transformer core is supported by two ball bushings, as can be seen in Figure 7. A spring-loaded follower arm is attached to the core extension, and rests against the rear face of the linear bearing. The follower thus displaces the transformer core an amount equal to the displacement of the linear bearing, the movement of the bearing being continuously detected by the generated output signal of the transformer.

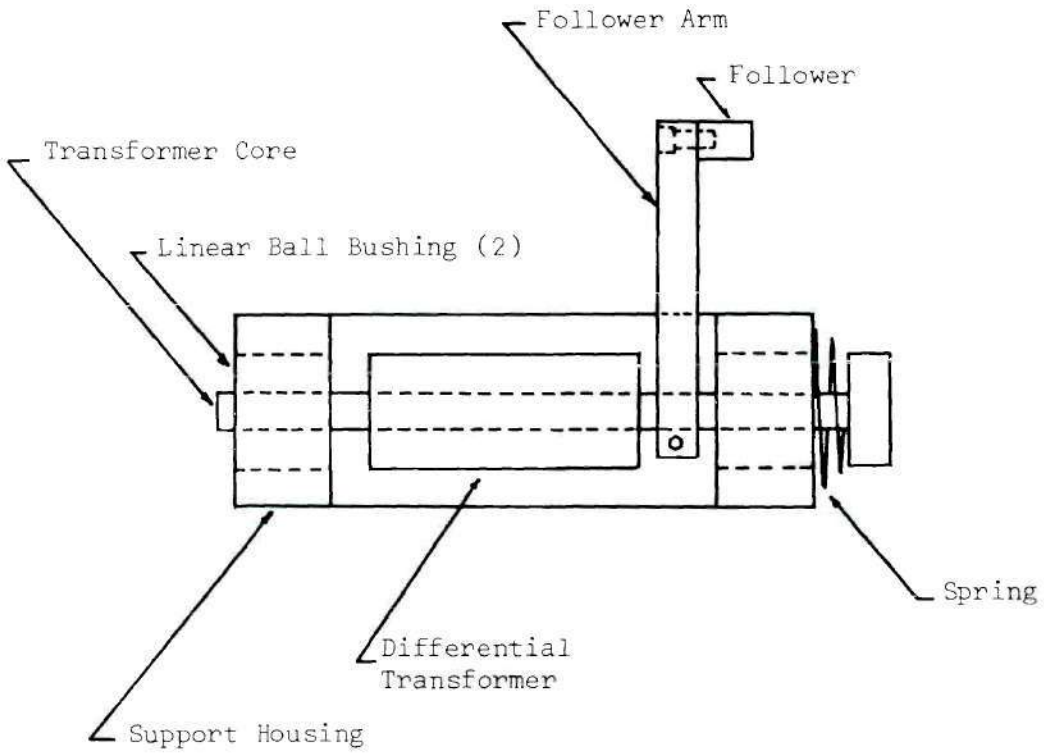

Figure 7. Instrumentation for Measuring Change in Length

Instrumentation

The specimen temperature was continuously measured with a Leeds and Northrup Speedomax H recording potentiometer. Signals received from the chromel-alumel thermocouple mounted in the specimen were amplified and continuously recorded on the strip chart. Data obtained from the chart was converted from millivolts to temperature using a standard conversion table for chromel-alumel thermocouples.

Furnace temperature was controlled by a Lindberg "Hevi-Duty" controller, type 59344. The controller utilized a chromel-alumel thermocouple permanently mounted within the furnace.

At all but the fastest testing speed of 1500 RPM, two Sanborn two-channel recording systems, model 296, with Sanborn carrier pre-amplifiers, model 350-1100B, were used to record values of the torque, rotary displacement, and linear displacement. These units provided a transducer excitation voltage of approximately five volts at an excitation frequency of 2400 cycles. Data was recorded by hot wire writing arms on heat sensitive Sanborn Permapaper chart. The recorders provided a four-speed chart drive, with chart speeds of 1, 5, 20, and 100 millimeters per second. A marker arm with an internal one-second timer produced timing marks on the right margin of the chart for calibration of sweep rate.

At the fastest testing speed, the Sanborn units were used to furnish the power supply and amplify the output voltage from the transducers, but the output signals were displayed on a Tektronix Type 564 storage oscilloscope. With this instrument, a single-sweep trace could be stored on the screen; a camera was not required unless a permanent

record was desired, in which case a photograph was made using a Polaroid camera with 3000 speed film. The oscilloscope utilized a Type 3A72 dual trace amplifier which provided simultaneous viewing of the torque and the angular displacement. Axial change in length was not measured during the high-speed tests. A Type 3B3 time base was used which allowed an adjustable delayed sweep and external triggering. The oscilloscope was automatically triggered upon actuation of the clutch, with a sweep delay set at 20 milliseconds to allow for actuation time of the clutch air valve.

Controls

A control panel was installed at the test section to allow for ease of operation. The controls consist of a master switch, a clutch control switch permitting either jogging or continuous operation, and two calibration switches to shunt the proper calibration resistor across either the 200 inch pound torque sensor or an alternate 2000 inch pound transducer. The oscilloscope trigger voltage is actuated by a voltage drop across a 2700 ohm resistor in the control panel wiring circuit when the clutch control switch is turned on. The electrical circuit diagram of the control panel is shown in Figure 8.

Performance of the Torsion Testing Machine

The operation of the torsion-testing machine was found to be entirely satisfactory. After at least 200 hours of operation, no maintenance problems occurred in any of the system components.

No drop in speed was noticeable during the high speed tests. The response time of the clutch, with the particular installation of

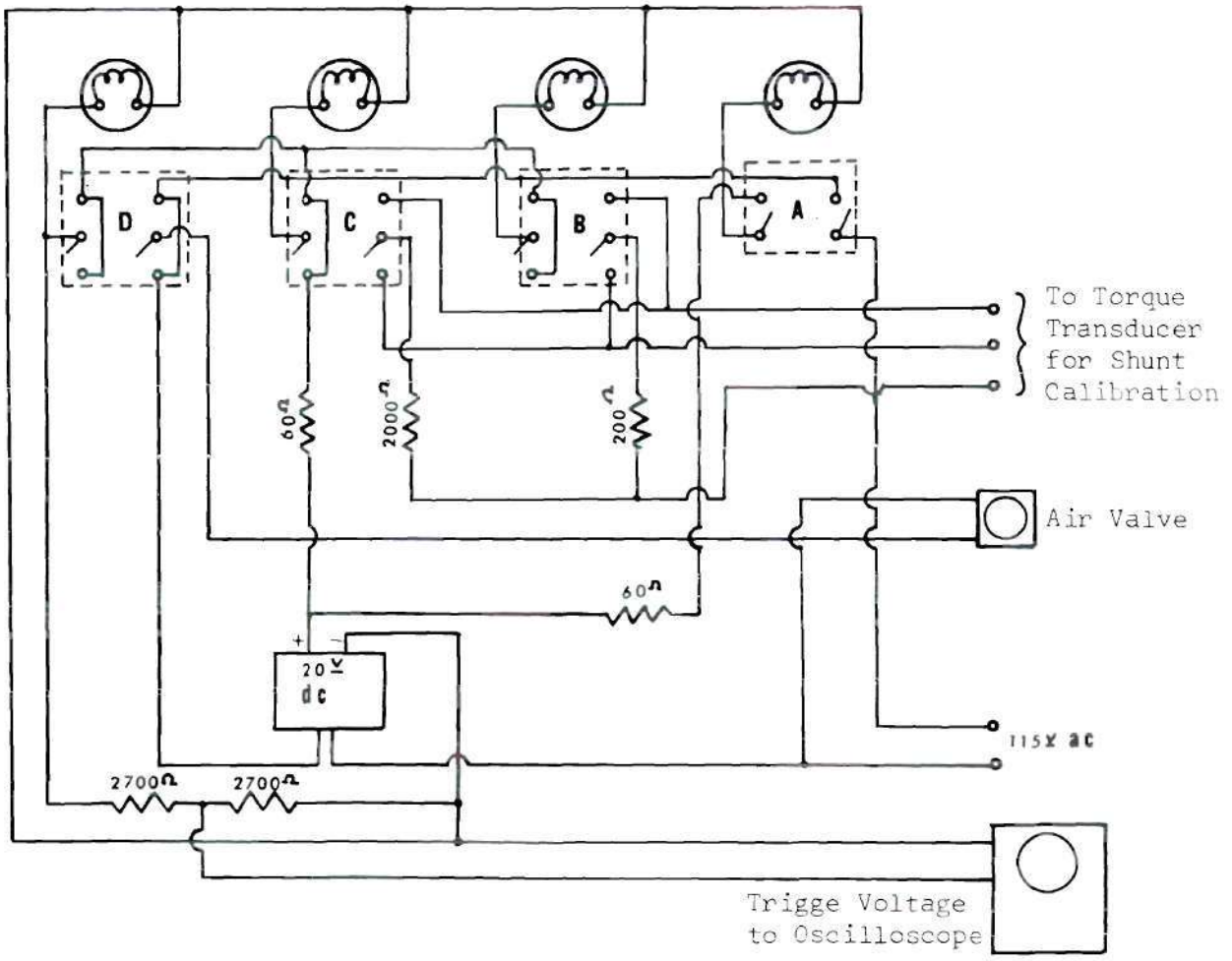

Figure 8. Control Panel Circuit Diagram

air valve and surge tank, was found to be approximately 20 milliseconds.

The extreme care taken in the construction and alignment of the test section appeared more than justified, as no irregular distortion of the test specimens was observed. The test grips were still accurately aligned after the entire series of tests had been run.

Performance of the linear bearing was impressive. Even at high torques, operation of the bearing was smooth, regardless of the test temperature.

During the tests at elevated temperatures, there was no visible means of determining the onset of fracture, since the furnace completely enclosed the specimen. The incorporation of a means of observation would indeed be highly desirable for future work.

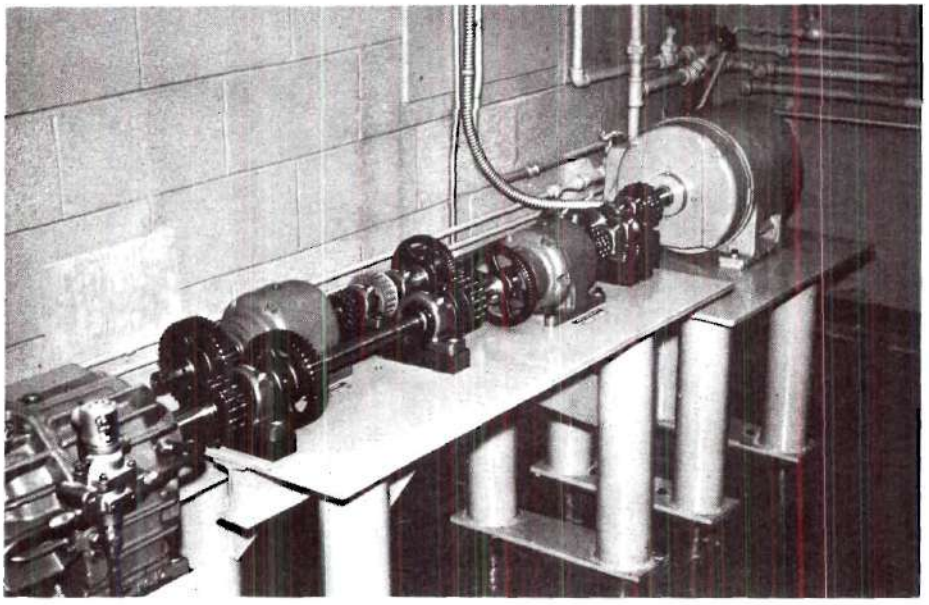

Figure 9. Drive Train Assembly (Top) and Test Assembly (Bottom)

CHAPTER IV

PROCEDURE

Materials

The materials used in the tests were commercially pure aluminum 1100-0, and two aluminum alloys, 2017-0 and 6061-0, the approximate compositions being given in Table 2. The commercially pure aluminum was originally obtained in the F-temper, the 2017 alloy in the T-451 temper, and the 6061 alloy in the T-651 temper. All materials were annealed to the 0-temper according to standard procedures (87,89) as given in Table 3.

Specimen Characteristics

The dimensions of the test specimens are shown in Figure 10. All specimens were machined on a lathe from one-half inch diameter cold-rolled rod. A gage length of 0.125" was specified, although variations from this dimension were permitted because of difficulties in exact repetition of the nominal value. This presented no difficulty in conversion of data, since all important specimen dimensions were measured using a Leitz toolmakers microscope.

Measurement of the specimens was performed after the annealing process. A small hole was then drilled adjacent to the gage length, but in the thicker portion of the specimen, to accommodate the thermocouple used for obtaining exact specimen temperatures.

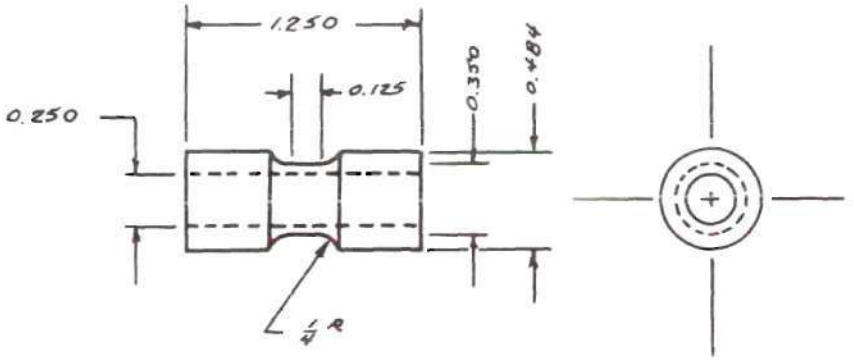

Figure 10. Dimensions of the Test Specimen

Table 2. Chemical Composition Limits

Alloy Number	Silicon	Iron	Copper	Manganese	Magnesium	Chromium	Zinc	Titanium	Others		Aluminum
									Each	Total	Min.
1100	1.0 S_i+Fe		0.20	0.05			0.10		0.05	0.15	99.0
2017	0.8	1.0	3.5-4.5	0.40-1.0	0.20-0.8	0.10	0.25		0.05	0.15	Remainder
6061	0.4-0.8	0.7	0.15-0.4	0.15	0.8-1.2	0.15-0.35	0.25	0.15	0.05	0.15	Remainder

Table 3. Annealing Procedures

Alloy	Temperature	Time	Cooling
1100	650°F	1 Hour	Not Critical (Air)
2017	775°F	2 Hours	50°F/hr. to 500°F then Air Cool
6061	775°F	2 Hours	50°F/hr. to 500°F then Air Cool

Testing Procedure

The torsion-testing machine was set at the desired testing speed according to procedures outlined in the previous chapter. The specimen was then inserted into the specimen grips and fastened in place. The chromel-alumel thermocouple was then inserted with a press fit into the non-rotating side of the specimen, while its extension wires were connected to the Leeds and Northrup Speedomax H recording potentiometer. The change in length mechanism was then positioned in place before closing the furnace, and the rotary potentiometer adjusted to the correct position.

Following sufficient warmup time for instrumentation, the machine was placed in operation by performing the following steps: Dry filtered air was supplied to the clutch surge tank and regulated at 80 psi. Water and air cooling units were turned on before selecting the desired temperature with the Lindberg controller. After the specimen reached the desired temperature, the motor was turned on. Testing was accomplished upon activation of the air clutch.

Calibration

The Lebow torque transducer was calibrated by two independent means. A known resistance was shunted across two of its terminals to simulate a load of 125 inch pounds. To verify the calibration at lower values of the torque, a cantilever arrangement with dead weight attachment was used. Both methods were found to yield identical results.

The differential transformer was calibrated by a micrometer arrangement which also allowed an accurate determination of the null point of the transformer. Calibration was performed over a range of travel of 0.050". Accuracy of calibration was within 0.001".

The rotary potentiometer was calibrated by simply rotating the clutch output shaft a known number of revolutions.

The Leeds and Northrup Speedometer H recording potentiometer was calibrated with a Leeds and Northrup 8686 Millivolt Potentiometer, using ice baths to eliminate thermal emf's generated at the junctions of the thermocouple extension wires and the calibrating potentiometer junctions.

CHAPTER V

EXPERIMENTAL DETERMINATION OF AXIAL CHANGE IN LENGTH

Introductory Comments

With the incorporation of the linear bearing as described in Chapter III, torsion tests may be performed free of secondary stresses that can occur with fixed specimen grips. The elimination of these stresses should tend to reduce irregular distortion, especially in the case of compressive stresses caused by large increases in length at high strains.

During preliminary tests on solid aluminum specimens with relatively long gage lengths ($L/d \approx 6$), the change in length was suppressed, and compressive stresses became so great as to actually cause the specimens to buckle. With hollow specimens, which are known to distort much more readily than solid specimens, the tendency for buckling can be even greater, should axial constraint be imposed. The absence or presence of this constraint can thus have a decided effect on the outcome of the torsion test. It was therefore felt that not only should axial freedom be provided, but also that the changes in length occurring during the tests be measured. In this way, a better understanding of torsional deformation would be obtained, and, if necessary, data could be corrected for changes in specimen geometry during the test.

Observations of Change in Length

The change in length data for the commercially pure aluminum was determined at nominal strain rates of 0.015, 0.15, 1.5, and 15 per second, in the temperature range of 22°C to 550°C. Similar data for the 2017-0 and 6061-0 aluminum alloys were taken at nominal strain rates of 0.015, 1.5, and 15 per second, in the temperature range of 350°C to 500°C.

Tests on the commercially pure aluminum indicated that an overall increase in length occurred over the entire range of temperatures and testing speeds. At temperatures above 400°C, an initial decrease in length was noted, generally amounting to less than 0.001", followed by a gradual increase in length. At high temperatures and very large strains, the specimen stopped lengthening and began to shorten again. Since this occurred at very large strains, it was possible that this was due to some natural distortion of the hollow tube, rather than to a property of the material. At lower temperatures, fracture occurred at lower strains, and the subsequent decrease in length was not observed.

A typical change in length curve for the 1100-0 alloy is shown in Figure 11. The initial increase in length is seen to be very small at first, followed by an increased rate of extension which gradually levels off until fracture occurs rather abruptly as indicated by the sharp change in slope.

The change in length behavior of the 2017-0 and 6061-0 aluminum alloys were generally quite similar to the commercially pure aluminum. The initial shortening at high temperature, however, was much more pronounced in these alloys, especially at the slowest testing speed.

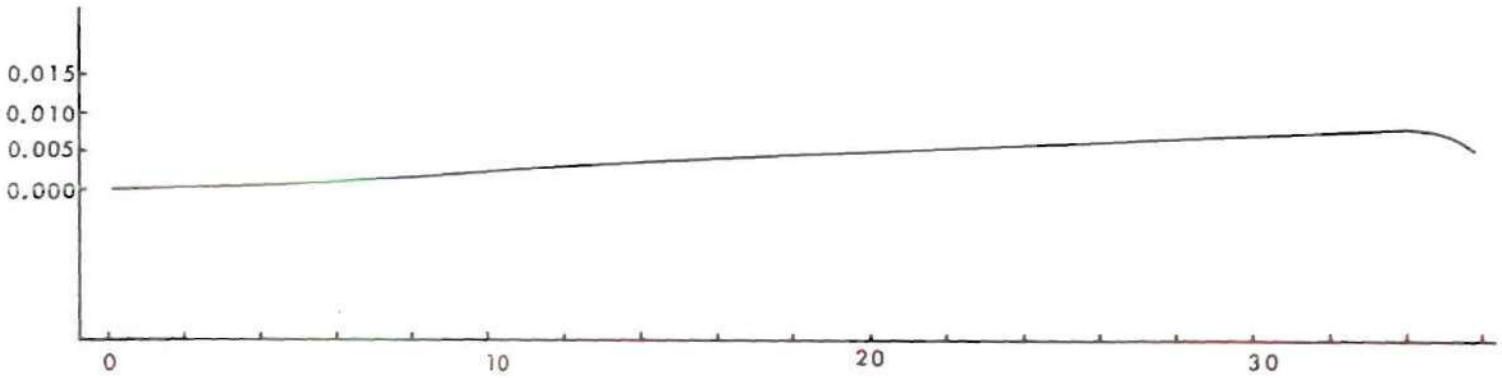

Figure 11. Axial Change in Length (Inches) vs. Time (Seconds) as Taken from Recorded Data for 1100-0 Aluminum (at Room Temperature) at a Testing Speed of 1.46 RPM

This behavior is illustrated in Figures 12 and 13 for tests over the entire temperature range. It can be seen that both alloys behave quite similarly. The initial shortening of the alloys was not noticeable at 350°C, but at 400°C a small amount of shortening was observed, and was found to increase with increasing temperature to a value of about 0.010" at 500°C. Increasing the testing speed generally decreased the amount of initial shortening. Typical change in length data are given in Table 4 at testing speeds providing nominal strain rates of 1.5 and 15 per second.

At a given strain, the increase in length was observed to generally decrease with increasing temperature. Although no pronounced effect of strain rate was noted, elongations at a given strain appeared to be slightly larger at the higher testing speeds. It is interesting to note that in the case of the 2017-0 and 6061-0 aluminum alloys, the rate of lengthening (after initial contraction ceased) appeared to increase with increasing temperature, as may be seen in Figures 12 and 13, respectively.

The change in length of metals under torsional strain is believed to be caused primarily by the resulting anisotropy. In the following chapter, the mathematical theory of anisotropic plasticity (after Hill) will be used as a basis for further analytical investigation of anistropy in torsion.

Table 4. Axial Change in Length

Data in Thousandths of an Inch

T°C	$\dot{\gamma}$ = 1.5 sec^{-1}			$\dot{\gamma}$ = 15 sec^{-1}		
	γ=1	γ=3	γ=5	γ=1	γ=3	γ=5
1100-0 Aluminum						
22°	0	3	6	0.5	5	9
200°	1	4.5	6	0.5	6	9
300°	0	1	3	0.5	2	5
400°	-0.5	1.5	3	0.5	2.5	3
500°	-0.5	3	3.5	0	2	2.5
550°	0	2	2.5	0.5	2	2.5
2017-0 Aluminum						
350°	0	2	5	0.5	3	6
400°	0	2	3.5	0.5	4	5
450°	0	2	3	0	1	3
500°	-1	-2	-1	0	1	-1
6061-0 Aluminum						
350°	0.5	3	5	0	3	5.5
400°	0	1	3.5	0.5	2.5	4
450°	0	1.5	2.5	0	1	3
500	-2	0	2.5	0	1.5	2

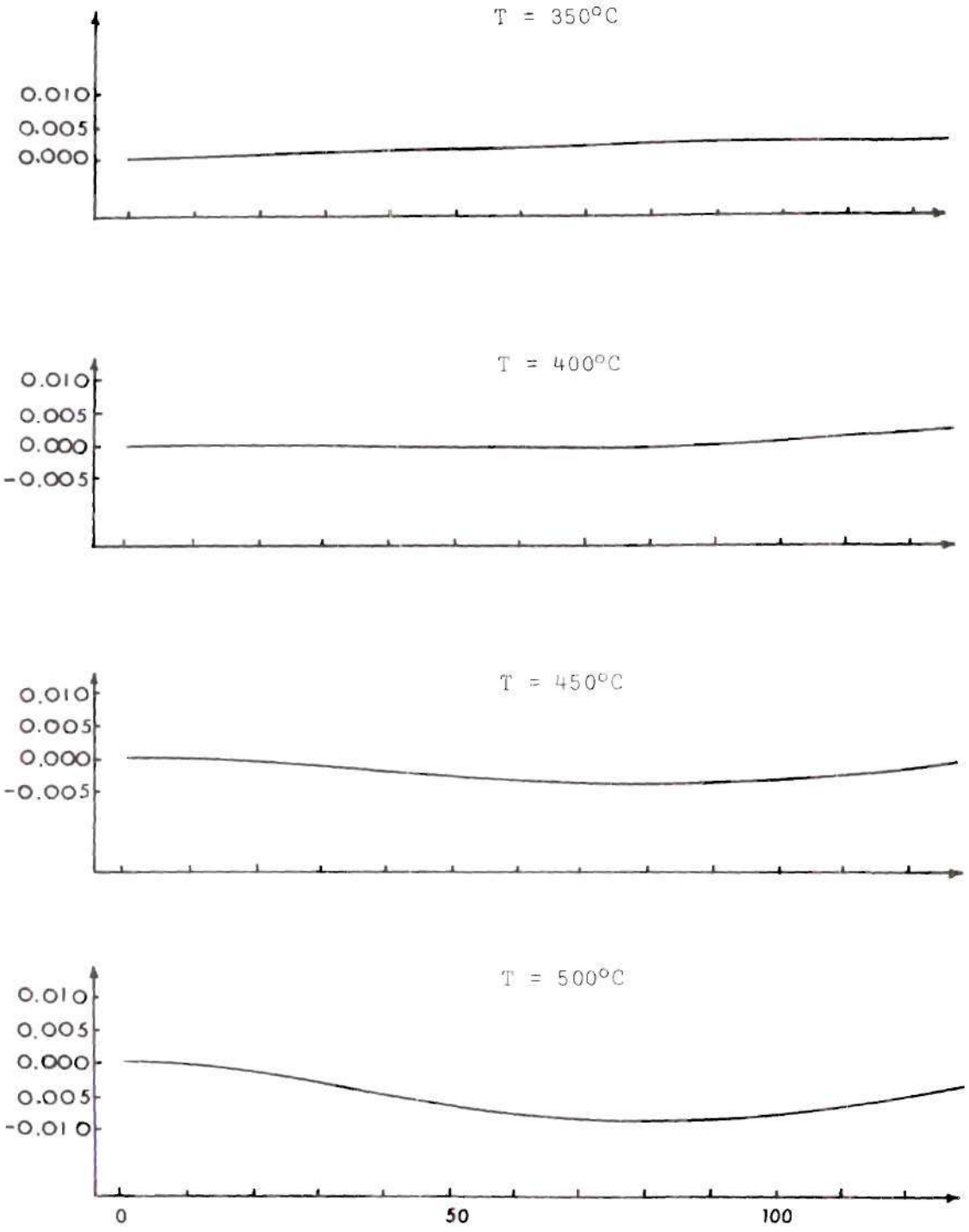

Figure 12. Axial Change in Length (Inches) vs. Time (Seconds) as Taken from Recorded Data for 2017-0 Aluminum at a Testing Speed of 0.181 RPM

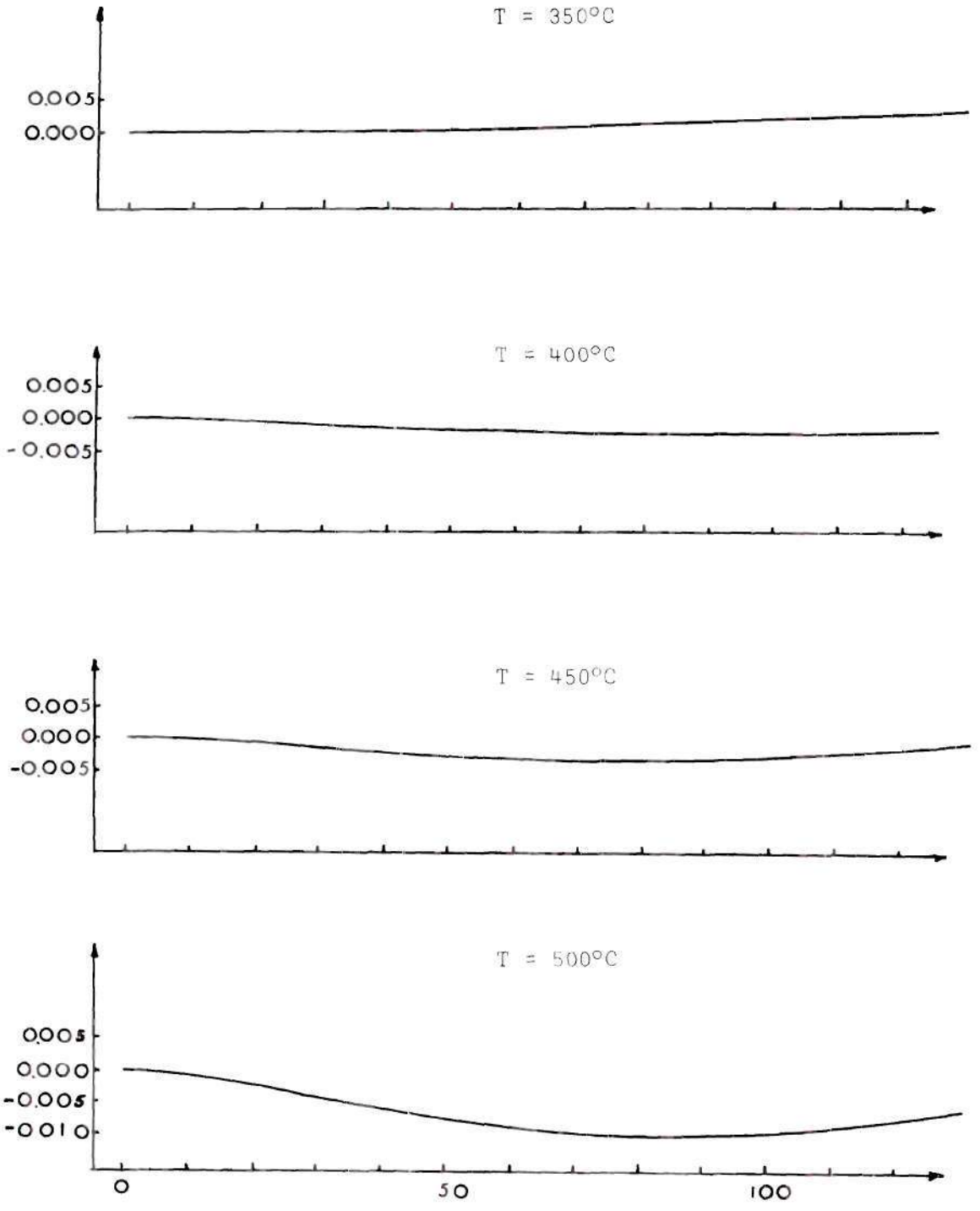

Figure 13. Axial Change in Length (Inches) vs. Time (Seconds) as Taken from Recorded Data for 6061-0 Aluminum at a Testing Speed of 0.181 RPM

Effect of Constraint

It was decided to compare the stress-strain data for specimens twisted with and without axial freedom to determine the effect of axial stresses on the shear stress of the material. Three tests under each condition were performed at a testing speed of approximately 4 RPM at room temperature.

The mean ultimate shearing stress, based on original dimensions, for the tests with axial freedom was found to be 14,800 psi, while the specimens subjected to axial constraint had a mean ultimate shearing stress of 15,300 psi; a difference of approximately 3 per cent. Repeatability was found to be within 0.5 per cent from the mean for the tests with axial freedom, and 1.5 per cent for the constrained tests.

Two conflicting tendencies may be considered primarily to cause the difference in shearing stress. During the test, high compressive stresses develop due to the constraint, and tend to lower the torque required for deformation. However, it was noted that the torque in this constrained condition was actually higher than in the free case. This apparent abnormality can be explained by the fact that the compressive stresses are of sufficient magnitude to cause plastic deformation and an increase in the cross-sectional area of the specimen. This effect is, of course, accentuated at high strains. Apparently, this increase in torque is more than sufficient to overcome the drop caused by the compressive stress.

CHAPTER VI

AN ANALYTICAL INVESTIGATION OF ANISOTROPY IN TORSION USING HILL'S EQUATIONS

Initial Considerations

The object of this analysis was to further investigate the behavior of the anistropic parameters used by Hill (83,84) in his theory concerning the anisotropy and subsequent change in length of plastically deformed thin-walled cylinders in torsion. The axial change in length, as determined in the previous chapter for a hollow aluminum cylinder, will be used in conjunction with Hill's anisotropy equations in order to develop an analytical method of further evaluating the anisotropic parameters. A determination of the character of these parameters would certainly be most valuable, for their variation clearly indicates the extent of anisotropy in torsion, and can lead to a better understanding of torsional deformation.

The extent of anisotropy in cold-rolled metals is certainly not obvious. For example, in some heavily-rolled metals, the tensile yield stress, measured in a direction transverse to that of rolling, is actually greater than that parallel to the rolling direction, and yet there is essentially no strain in the transverse direction. In the case of cold-rolled metals in which the anisotropy is pronounced, the anisotropic parameters may readily be determined using methods discussed by Hill and others. These methods consist essentially of

uniaxial tension tests along the principal directions of anisotropy. The yield stresses (or strain ratios) can then be used to determine the value of these parameters. Such tests are certainly feasible with a cold-rolled sheet in which the anisotropic axes remain fixed; in the case of a hollow cylinder, however, a similar experimental determination of these parameters appears unlikely because the axes rotate.

Analytical Development

For a thin-walled cylinder in torsion, the change in axial strain with respect to the shearing strain was shown by Hill (23,84) to be

$$\frac{d\varepsilon}{d\gamma} = \frac{[(N-G-2H)\mathrm{Sin}^2\phi - (N-F-2H)\mathrm{Cos}^2\phi]\mathrm{Sin}2\phi}{2N + (F+G+4H-2N)\mathrm{Sin}^2 2\phi} \qquad (22)$$

where $d\varepsilon$ is the incremental axial strain, and ϕ represents the orientation of the anisotropic axes, as previously discussed in Chapter II. Certain pertinent observations have been made by Hill regarding the behavior of this equation. For example, the denominator is always positive, and is equal to $1/\tau^2$ by Equation (17). Under the initial condition of zero strain, the cylinder is isotropic and F = G, while for small values of γ, $\frac{d\varepsilon}{d\gamma}$ can be seen to have the sign F - G since $\mathrm{Sin}^2\phi$ is close in value to $\mathrm{Cos}^2\phi$. At large strains, ϕ approaches 90° and the cosine term is negligible; $\frac{d\varepsilon}{d\gamma}$ will therefore be positive providing $N > G + 2H$.

From Equations (17) and (20), the following relation is obtained

$$d\gamma = \frac{1}{\tau^2}\tau d\lambda = \frac{d\lambda}{\tau}$$

therefore,

$$d\lambda = \tau d\gamma \tag{23}$$

Substituting the value of $d\lambda$ from Equation (23) into Equations (18), the relationships

$$d\varepsilon_x = -\tau^2(G+2H)\mathrm{Sin}2\phi d\gamma$$

$$d\varepsilon_y = \tau^2(F+2H)\mathrm{Sin}2\phi d\gamma \tag{24}$$

$$d\varepsilon_{xy} = \frac{d\gamma_{xy}}{2} = \tau^2 N\mathrm{Cos}2\phi d\gamma$$

are obtained.

The incremental state of strain of an element on the surface of the cylinder is represented in Figure 14. Figure 14a represents an element oriented along the major axes of the cylinder, while Figure 14b represents an element along the principal anisotropic axes, which have rotated some angle (ϕ-45°) due to the shear strain γ; $d\varepsilon$ represents the incremental axial strain, with a resulting incremental transverse strain of $\left(-\frac{d\varepsilon}{2}\right)$.

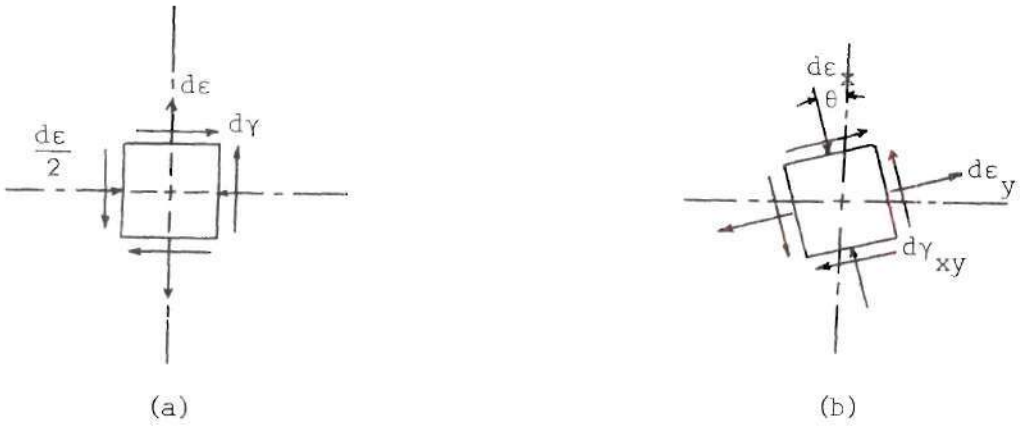

Figure 14. Incremental State of Strain

This state of strain can be graphically represented by the Mohr's strain circle of Figure 15. In this case, the Mohr's circle is representative of only incremental strains applied after the anisotropic axes have rotated to some position ϕ. Thus, for the element of Figure 14 rotated to some angle θ ($\theta=90^\circ-\phi$), line 0'0' of Figure 15 rotates 2θ.

If it is assumed that the incremental axial strain is some function of the shear strain, that is

$$\varepsilon = f(\gamma)$$

then

$$d\varepsilon = df(\gamma) = f'(\gamma)d\gamma \qquad (25)$$

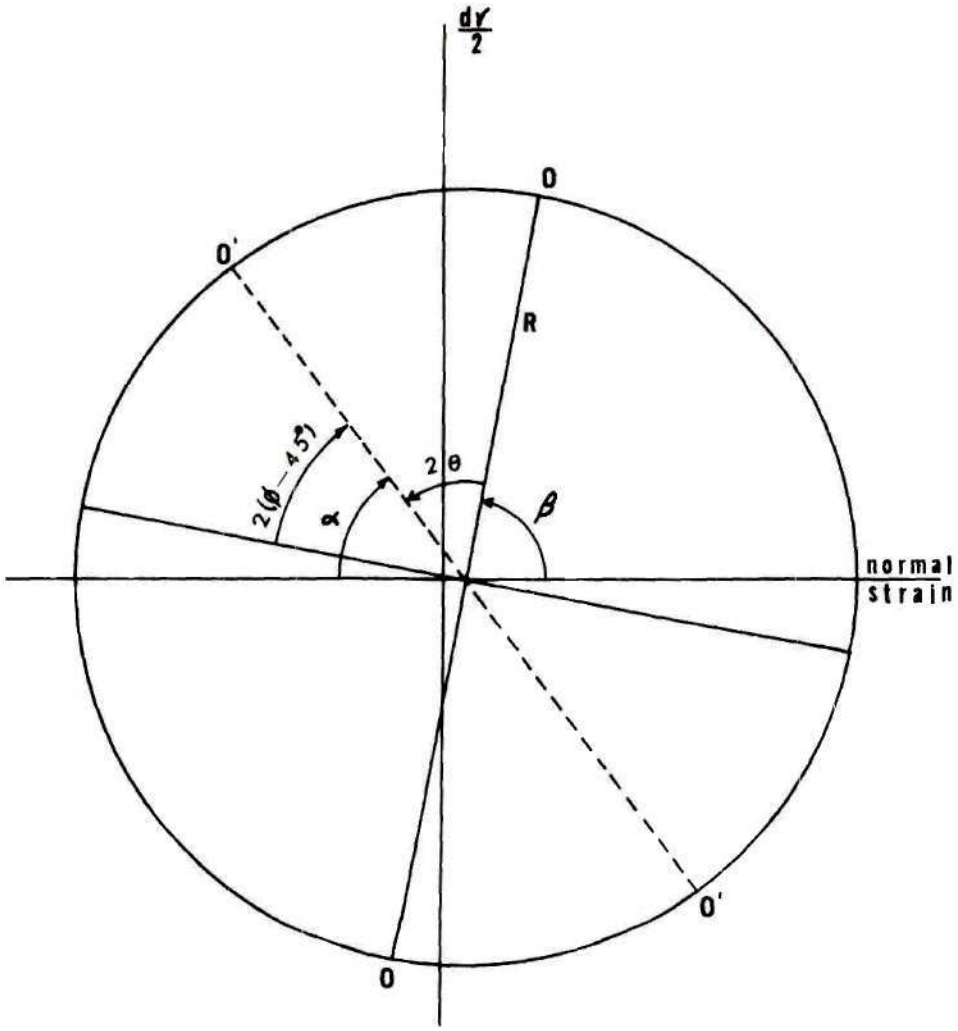

Figure 15. Mohr's Circle Representing the Incremental State of Strain

The angle β (Figure 15) is given by

$$\beta = \text{Cot}^{-1}\left(\frac{3/4\ d\varepsilon}{d\gamma/2}\right) = \text{Cot}^{-1}\left(\frac{3}{2}\ \frac{d\varepsilon}{d\gamma}\right) \qquad (26)$$

$$= \tan^{-1}\left(\frac{2}{3f'(\gamma)}\right)$$

and from the Mohr's circle:

$$d\varepsilon_x = -R\text{Cos}\alpha + \frac{df(\gamma)}{4}$$

$$d\varepsilon_y = R\text{Cos}\alpha + \frac{df(\gamma)}{4} \qquad (27)$$

$$d\varepsilon_{xy} = R\text{Sin}\alpha$$

where R is the radius of the Mohr's circle, that is,

$$R = \frac{d\gamma}{2\text{Sin}\beta} \qquad (28)$$

Substituting Equation (28) into Equations (27) gives

$$d\varepsilon_x = -\frac{\text{Cos}\alpha}{2\text{Sin}\beta}\,d\gamma + \frac{f'(\gamma)}{4}\,d\gamma$$

$$d\varepsilon_y = \frac{\text{Cos}\alpha}{2\text{Sin}\beta}\,d\gamma + \frac{f'(\gamma)}{4}\,d\gamma \qquad (29)$$

$$d\varepsilon_{xy} = \frac{\text{Sin}\alpha}{2\text{Sin}\beta}\,d\gamma$$

where

$$\alpha = 180^\circ - (\beta+90^\circ) + 2(\phi-45^\circ) \tag{30}$$

$$= 2\phi - \beta$$

From Equations (24) and (29), the anisotropic parameters may be equated to the incremental strains obtained from the assumed function of Equation (25). Hence,

$$-\tau^2(G+2H)\sin 2\phi\, d\gamma = -\frac{\cos\alpha}{2\sin\beta}\, d\gamma + \frac{f'(\gamma)}{4}\, d\gamma$$

$$\tau^2(F+2H)\sin 2\phi\, d\gamma = \frac{\cos\alpha}{2\sin\beta}\, d\gamma + \frac{f'(\gamma)}{4}\, d\gamma \tag{31}$$

and

$$\tau^2 N\cos 2\phi\, d\gamma = -\frac{\sin\alpha}{2\sin\beta}\, d\gamma$$

also,

$$\cos\alpha = \cos(2\phi-\beta) = \cos 2\phi\cos\beta + \sin 2\phi\sin\beta$$

and (32)

$$\sin\alpha = \sin(2\phi-\beta) = \sin 2\phi\cos\beta - \cos 2\phi\sin\beta$$

The values of (G+2H), (F+2H), and N may now be determined from Equations (31) and (32).

$$G + 2H = \frac{1}{2\tau^2}\left[1+\text{Cot}2\phi\text{Cot}\beta - \frac{f'(\gamma)}{2\text{Sin}2\phi}\right]$$

$$F + 2H = \frac{1}{2\tau^2}\left[1+\text{Cot}2\phi\text{Cot}\beta + \frac{f'(\gamma)}{2\text{Sin}2\phi}\right] \qquad (33)$$

$$N = \frac{1}{2\tau^2}\left[1 - \tan 2\phi\text{Cot}\beta\right]$$

It remains a matter of finding a suitable function $f(\gamma)$ in order to evaluate the above parameters. This function can be determined empirically from experimental data. By observation of Equation (22), it can be seen that

$$\left.\frac{d\varepsilon}{d\gamma}\right|_{\phi=45^\circ,90^\circ} = 0$$

To meet this criteria, the following function will be assumed:

$$\varepsilon = f(\gamma) = K\text{Cos}^3 2\phi \qquad 45^\circ \leq \phi < 90^\circ \qquad (34)$$

where K is a constant. Using a value of K = -0.07, Equation (34) is seen from Figure 16 to very closely describe the experimental results determined under room temperature conditions. It follows from Equation (34) that

$$f'(\gamma) = -6K\text{Cos}^2 2\phi\text{Sin}2\phi \frac{d\phi}{d\gamma} \qquad (35)$$

where ϕ is a known function of γ. The value of β from Equation (26)

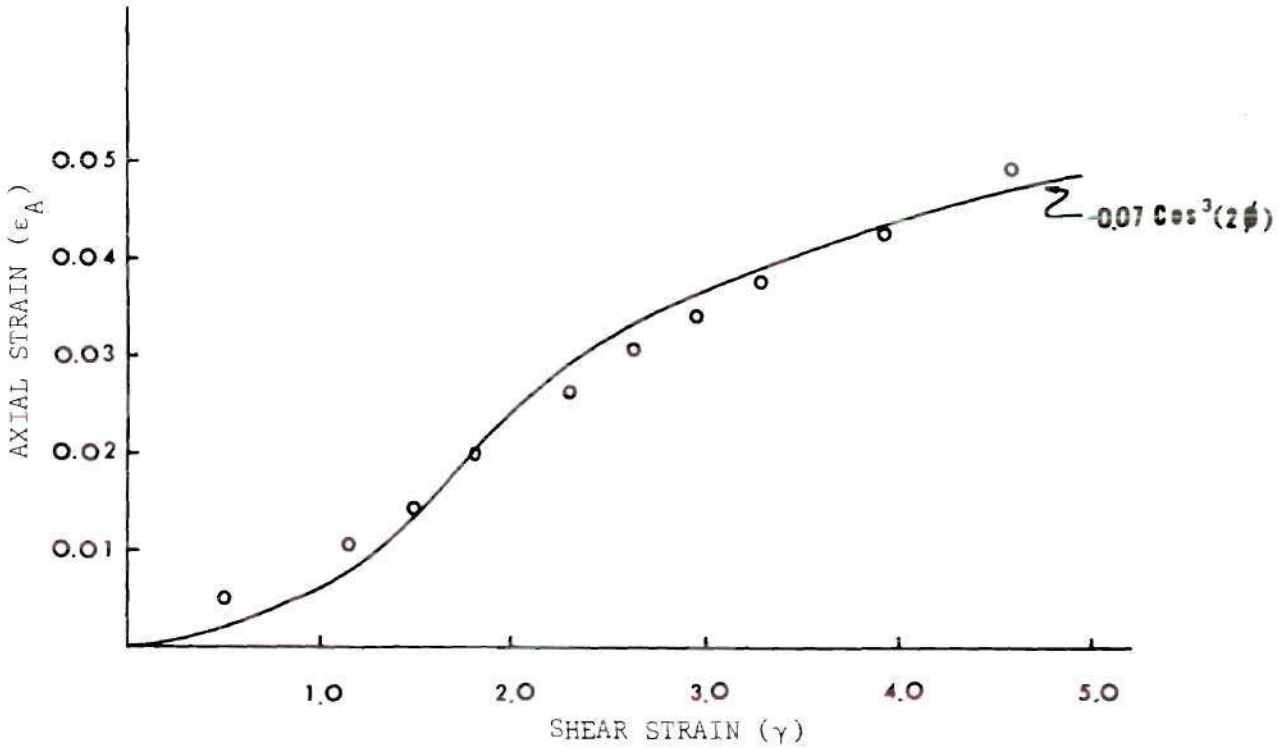

Figure 16. Comparison of the Empirical Change in Length Equation $\epsilon = -0.07\ \mathrm{Cos}^3 2\phi$ with Experimental Data

may now be written as

$$\beta = \tan^{-1}\left(\frac{2}{3f'(\gamma)}\right) = \tan^{-1}\left[\frac{-1}{9K\cos^2 2\phi \sin 2\phi \frac{d\phi}{d\gamma}}\right] \tag{36}$$

and therefore

$$G + 2H = \frac{1}{2\tau^2}\left[1+\cot 2\phi \cot\beta + 3K\cos^2 2\phi \frac{d\phi}{d\gamma}\right]$$

$$F + 2H = \frac{1}{2\tau^2}\left[1+\cot 2\phi \cot\beta - 3K\cos^2 2\phi \frac{d\phi}{d\gamma}\right] \tag{37}$$

$$N = \frac{1}{2\tau^2}\left[1-\tan 2\phi \cot\beta\right]$$

From Equations (37) the value of N may be determined, along with the values of (G+2H) and (F+2H), using the value of the shearing stress τ, which may be obtained from the torsion test data.

As previously mentioned, the yield stresses S_x and S_y along the X and Y anisotropic axes on the surface of the cylinder are not likely to be directly determined by experimental means; however, the yield stress S_z through the wall thickness (along the radial Z axis) could be determined with relatively little difficulty, such as by a compressive test of a cutout portion of the cylinder. Using the values of (F+2H) and (G+2H), the yield stresses S_x and S_y may now be solved in terms of S_z. From Equations (13) it can be shown that

$$G + 2H = \frac{3}{2S_x^2} + \frac{1}{2S_y^2} - \frac{1}{2S_z^2} \tag{38}$$

$$F + 2H = \frac{1}{2S_x^2} + \frac{3}{2S_y^2} - \frac{1}{2S_z^2} \tag{39}$$

solving Equations (38) and (39) simultaneously gives

$$S_y^2 = \frac{4}{3(F+2H) - (G+2H) + \frac{1}{S_z^2}} \tag{40}$$

$$S_x^2 = \frac{4}{3(G+2H) - (F+2H) + \frac{1}{S_z^2}} \tag{41}$$

The yield stress in shear along the principal anisotropic axes is readily determined from Equation (14).

Determination of the Principal Directions of Anisotropy

The rotation of the anisotropic axes readily follows from Hill's discussion of anisotropy in torsion. Referring to Figure 1

$$\tan \psi = \frac{L}{\gamma L/2} = \frac{2}{\gamma}$$

therefore,

$$\psi = \tan^{-1}\left(\frac{2}{\gamma}\right) \tag{42}$$

Also,

$$\mathrm{Sin}\phi = \frac{L}{\ell} \tag{43}$$

Using the law of cosines,

$$\ell^2 = \ell_o^2 + (\gamma L)^2 - 2\ell_o\gamma \cdot L\mathrm{Cos}\,\frac{\psi}{2} \tag{44}$$

$$\left(\frac{\ell}{\ell_o}\right)^2 = 1 + \left(\frac{\gamma L}{\ell_o}\right)^2 - \frac{2\gamma L}{\ell_o}\,\mathrm{Cos}\,\frac{\psi}{2}$$

$$= 1 + \left(\gamma \mathrm{Sin}\,\frac{\psi}{2}\right)^2 - 2\gamma \mathrm{Sin}\,\frac{\psi}{2}\,\mathrm{Cos}\,\frac{\psi}{2}$$

Since $\tan(90^\circ-\psi) = \frac{\gamma L}{2L} = \frac{\gamma}{2} = \mathrm{Cot}\psi$

$$\gamma = 2\mathrm{Cot}\psi \tag{45}$$

Substituting the value of γ from Equation (45) into Equation (44) and rearranging

$$\ell = \ell_o\left[1 + (2\mathrm{Cot}\psi \mathrm{Sin}\,\frac{\psi}{2})^2 - 2\mathrm{Cos}\psi\right]^{\frac{1}{2}} \tag{46}$$

The value of the angle ϕ, indicating the position of the anisotropic axes may now be determined from Equations (43) and (46).

$$\phi = \text{Sin}^{-1}\left[\frac{L}{\ell_o[1 + (2\text{Cot}\psi\text{Sin}\frac{\psi}{2})^2 - 2\text{Cos}\psi]^{1/2}}\right] \qquad (47)$$

$$= \text{Sin}^{-1}\left[\frac{\ell_o \text{Sin}\frac{\psi}{2}}{\ell_o[1 + (2\text{Cot}\psi\text{Sin}\frac{\psi}{2})^2 - 2\text{Cos}\psi]^{1/2}}\right]$$

$$= \text{Sin}^{-1}\left[\frac{\text{Sin}\frac{\psi}{2}}{[1 + (2\text{Cot}\psi\text{Sin}\frac{\psi}{2})^2 - 2\text{Cos}\psi]^{1/2}}\right]$$

Using Equation (42), ϕ may be expressed as a direct function of the shear strain γ.

$$\phi = \text{Sin}^{-1}\left[\frac{\text{Sin}\left\{\frac{\tan^{-1}\left(\frac{2}{\gamma}\right)}{2}\right\}}{\left\{1 + \left[2\text{Cot}\left(\tan^{-1}\frac{2}{\gamma}\right)\text{Sin}\left(\frac{\tan^{-1}\frac{2}{\gamma}}{2}\right)\right]^2 - 2\text{Cos}\left(\tan^{-1}\frac{2}{\gamma}\right)\right\}^{\frac{1}{2}}}\right]$$

The derivative of ϕ with respect to γ may now be determined for use in Equations (37).

$$\frac{d\phi}{d\gamma} = \frac{d\psi}{d\gamma} \cdot \frac{d\phi}{d\psi} = -\frac{2}{\gamma^2 + 4} \cdot \left[1 - \frac{\sin^2(\psi/2)}{1 + \left[\frac{2\sin\left(\frac{\psi}{2}\right)}{\tan\psi}\right]^2 - 2\cos\psi}\right]^{-1} \cdot \tag{49}$$

$$\frac{\frac{1}{2}\{1 + \left(\frac{2\sin\frac{\psi}{2}}{\tan\psi}\right)^2 - 2\cos\psi\}^{\frac{1}{2}} \cos\frac{\psi}{2}}{\{1 + \left(\frac{2\sin\frac{\psi}{2}}{\tan\psi}\right)^2 - 2\cos\psi\}} \cdot$$

$$- \left[\frac{\frac{1}{2}\sin\frac{\psi}{2}\{1 + \left(\frac{2\sin\frac{\psi}{2}}{\tan\psi}\right)^2 - 2\cos\psi\}^{-\frac{1}{2}}}{\{1 + \left(\frac{2\sin\frac{\psi}{2}}{\tan\psi}\right)^2 - 2\cos\psi\}} \cdot \right.$$

$$\left. \frac{\{\left(\frac{4\sin\frac{\psi}{2}}{\tan\psi}\right)\left(\frac{\tan\psi\cos\frac{\psi}{2} - 2\sin\frac{\psi}{2}\sec^2\psi}{\tan^2\psi}\right) + 2\sin\psi\}}{\{1 + \left(\frac{2\sin\frac{\psi}{2}}{\tan\psi}\right)^2 - 2\cos\psi\}}\right]$$

Computer Solution

Equations (37), (48) and (49) have been programmed on a Burroughs 5500 digital computer. Values of ϕ, $\frac{d\phi}{d\gamma}$, and the anisotropic parameters (F+2H), (G+2H), and N expressed in terms of $1/2\ \tau^2$ have been determined for shear strains in increments of 0.1 up to 10.0. The program and data printout are included in the Appendix.

Closure

The extent of the present investigation was limited to an analytical discussion of the extent of anisotropy in torsion. With the derivation of Equations (37) it has been shown that the anisotropic parameters may be determined readily by an experimental investigation of the through-thickness yield strength. Further work utilizing the previous results is therefore highly recommended in order that a precise determination of these parameters may be made.

With the determination of the anisotropic parameters, the yield criterion, as given in Equation (12) may be completely defined. Additionally, the yield stresses along the principal anisotropic directions may be determined using Equations (40) and (41).

The parameters themselves clearly serve as an index to the extent of anisotropy in a material. In this respect, a comparison of the anisotropic parameters of various materials should prove significant.

CHAPTER VII

EFFECTS OF TEMPERATURE AND STRAIN RATE ON THE RESISTANCE TO DEFORMATION OF 1100-0, 2017-0, AND 6061-0 ALUMINUM ALLOYS

Discussion

The previous considerations concerning the design of the torsion-testing machine and the analytical and experimental studies of torsional deformation now lead directly to the determination of the effects of strain, strain rate and temperature on the resistance to deformation of materials. The materials used in the present work were commercially pure aluminum (1100-0), and two aluminum alloys, (2017-0 and 6061-0), the chemical composition being given in Table 2. The materials were machined into the shape of hollow cylinders having a reduced central gage length, the dimensions of which have been given in Chapter IV.

All tests were performed allowing the specimens to naturally change their length during torsional deformation. Thus, no longitudinal stresses, either tensile or compressive, were developed during the tests. The axial change in length and the resulting changes to specimen geometry were generally found to be small over the range of strain considered, and it was therefore felt justifiable not to correct the data for this effect.

The shearing stress τ imposed on the specimens during the tests was calculated using the relation

$$T = \int_{o}^{2\pi} \int_{r_i}^{r_o} \tau r^2 dr d\theta$$

$$= \frac{2}{3} \pi\tau(r_o^3 - r_i^3)$$

or,

$$\tau = \frac{3T}{2\pi(r_o^3 - r_i^3)} \tag{50}$$

where T is the measured torque, and r_o and r_i are respectively the outer and inner radii of the specimen. The shear strain γ and the rate of shear strain $\dot{\gamma}$ are readily determined using the mean radius r_m and the gage length L.

$$\gamma = \frac{r_m}{L} \theta \tag{51}$$

$$\dot{\gamma} = \frac{r_m}{L} \dot{\theta} \tag{52}$$

where θ is the angular displacement in radians, and $\dot{\theta}$ is the angular velocity or testing speed in radians per second.

Commercially Pure Aluminum 1100-0

Tests were performed at nominal strain rates of 0.015, 0.15, 1.50, 15.0, and 150.0 per second, exact values being given for each test. The testing temperatures for each of the five testing speeds were 22°C, 200°C, 300°C, 400°C, 500°C, and 550°C.

The effect of strain rate on the shear stress at room temperature was found to be small, especially at the larger strains, and only slight variations were noted for values of the ultimate stress. The shear stress-shear strain (τ vs. γ) curves were found to be of similar shape for all tests at this temperature throughout the entire range of strain rates. Figure 17 shows typical τ vs. γ curves at strain rates of 0.02 and 14.2 per second. The continuously increasing stress indicated that work-hardening progressed until just before fracture. Figures 18 and 19 show the τ vs. γ curves at room temperature for strain rates of 0.16 and 2.01 per second, respectively, plotted a log-log scale. The material can be seen to obey the power law of Equation (53) for shearing strains generally greater than 0.8.

$$\tau\Big|_{\substack{\dot{\gamma} \\ T=22^{\circ}C}} = C\gamma^{m} \tag{53}$$

The value of m, commonly referred to as the work-hardening exponent, was found to be approximately 0.15.

Figures 20 through 24 show the effect of strain rate on the τ vs. γ curves for temperatures of 200°C to 550°C, respectively. The curves are drawn up to a shearing strain of 5.0. At larger strains, the stress generally becomes less dependent upon the strain, and, to some extent, dependent upon the mode of torsional deformation or distortion. As the specimen extends its length, the cross-sectional area is slightly reduced, and the curves at these temperatures exhibit a slightly negative slope as the strain becomes larger, due in part to

the reduction of cross-sectional area and thermal softening.

As the strain rate increases, the τ vs. γ curves may show small peaks, especially in the temperature range between 300°C and 500°C. The width of these peaks is seen to increase with increasing strain rate, and are most noticeable at these higher rates of strain.

The peaks can be considered to be the result of the interaction between the tendencies for work hardening and thermal softening. At the lower temperatures, work hardening is predominant, for the amount of thermal energy present is too small to introduce significantly softening effects brought about by recovery and recrystallization. At the higher temperatures, however, recovery and recrystallization become significant processes, and take place at a much greater rate than at lower temperatures. Polygonization is one of the most important recovery processes that can take place in aluminum and can usually occur rapidly enough to reduce the size of the peak in the stress-strain curves. The stacking faults in pure aluminum are believed to be very narrow with a correspondingly high energy. During deformation at elevated temperatures dislocation climb and rearrangement is rapid with the formation of low angle or subgrain boundaries leading to a reduction in lattice strain energy. Although the grade of aluminum in the present work contains impurities which undoubtedly alter the stacking fault energy, the effect on the deformation process is thought to be minor. The extent to which competition exists between recrystallization and polygonization as restoring processes can be determined by metallurgical examination, similar to the work of Hardwick and McG. Tegart (61) for super pure aluminum.

At 550°C, the τ vs. γ curves exhibited relatively no indication of peaks, even at the highest strain rate. This is a clear indication of the speed at which thermal softening is occurring, and polygonization can be presumed to account for this rapid rate of restoration.

In the torsion test, the revolutions to failure can be used as an indication of the ductility of a metal, providing the effects of temperature, strain rate, and specimen geometry are considered. However, in the tests on the commercially pure aluminum, no sharp break in the stress-strain curves were noted during tests at the higher temperatures, thereby not allowing an accurate determination of the fracture strain. It seemed that a crack initiated at the surface and gradually spread around and across the section of the test specimen over several revolutions.

From the photograph of Figure 25(a), the fracture surfaces of the specimens tested at 500°C at the fastest and slowest testing speeds are shown. No significant differences are noticeable. Both specimens show evidence of necking, the diameter at fracture being about the same in both cases. It is significant to note that axial symmetry was obviously still maintained throughout the hollow cylinders, even at these large strains. It will be most interesting to later compare these observations with those of the other two alloys tested, where although symmetry was still maintained, marked differences were noted in both fracture appearance and ductility.

The variation in ductility may be related to structural changes, similar to the work of Hardwick and McG. Tegart (61) and Reynolds and

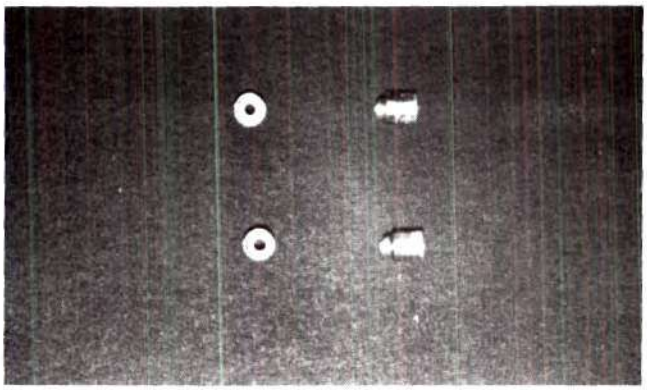

(a)

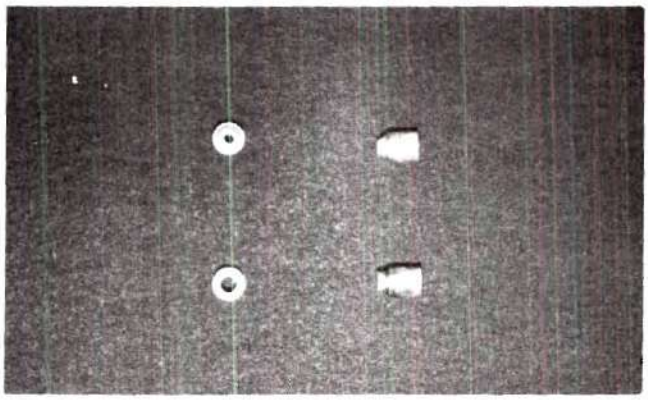

(b)

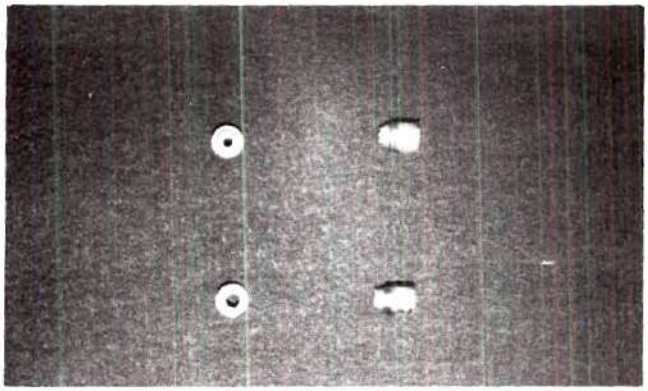

(c)

Figure 25. Fracture Surfaces at a Testing Temperature of 500°C and Testing Speeds of Approximately 0.15 RPM (Upper Specimens) and 1500 RPM (Lower Specimens) for (a) 1100-0, (b) 2017-0, (c) 6061-0

McG. Tegart (66). For example, at low temperatures, heavily deformed grains would be noted with no indication of polygonization or recrystallization. At higher temperatures, the strained grains are replaced by new grains or sub-grains, enabling further deformation to occur with the continuous removal of work hardening by thermal softening.

The effect of the strain rate $\dot{\gamma}$ at constant values of strain and temperature was found to be reasonably approximated by a power law of the form

$$\tau\Big|_{\gamma,\tau} = \tau_o \dot{\gamma}^n \qquad (54)$$

where the exponent n is commonly referred to as the strain rate sensitivity and τ_o is a constant equal to the shear stress at unit strain rate. Figures 26 to 28 illustrate the τ vs. $\dot{\gamma}$ data plotted on a log-log scale for shearing strains of 1.0, 2.0, and 3.0, respectively. It can be seen that the curves are reasonably approximated as straight lines enabling the determination of n and τ_o over the range of temperatures and strains considered. Table 5 lists the variation of n with temperature for five constant values of shear strain.

The values of n were found to increase with temperature, demonstrating the temperature dependence of the strain rate sensitivity. As the strain rate is raised, the process of thermal softening has increasingly less time to cause a reduction of the internal strain energy, and its ability to reduce the amount of applied stress necessary for further deformation is lowered. At the lower temperatures, where restoration effects are small, the metal can be expected to be less

sensitive to the rate of deformation since the time dependent effects of thermal softening are slight.

Table 5. Values of the Strain Rate Sensitivity For 1100-0 Aluminum

Temperature		Strain Rate Sensitivity				
°C	T_h	γ=0.2	γ=0.5	γ=1.0	γ=2.0	γ=3.0
22	0.322	.02	.018	0.020	0.021	0.022
200	0.516	.035	.04	0.047	0.052	0.053
300	0.626	.06	.068	0.072	0.072	0.079
400	0.735	.095	.095	0.097	0.102	0.105
500	0.844	0.13	.125	0.127	0.140	0.153
550	0.898	0.18	.17	0.181	0.182	0.207

The values of n generally exhibited a small increase with the shearing strain. The variation with strain was found to be somewhat larger as the temperature increased.

The variation of n with the homologous temperature T_h is shown in Figure 29 for shear strains of 0.2, 0.5, 1.0, 2.0, and 3.0. The strain rate sensitivity is seen to vary non-linearly, its value increasing with the homologous temperature. The extrapolated curve approaches zero as T_h approaches zero. Although the values of n were found to be generally similar to the compression test data of Alder and Phillips (41), the n vs. T_h curve is seen to exhibit some differences with their graph which interpolates the data into two intersecting straight lines.

Although no distinct transition point was noted from Figure 29, n is seen to rise sharply at the higher temperatures, where the effects of recovery and recrystallization play an increasingly larger role over work hardening.

The effect of the temperature on the shear stress is clearly shown in Figure 30 for constant strain rates of 0.1, 1.0, 10, and 100 per second and at a constant strain of 2.0. Data points were obtained from the curves of Figure 27. For the temperature range 200°C < T < 550°C, and range of strains $\gamma > 1.0$, the shear stress was found to be very closely approximated to the temperature by an equation of the form

$$\frac{1}{T} = Ce^{C_o \tau \Big|_{\gamma,\dot{\gamma}}} \tag{55}$$

or,

$$\tau\Big|_{\gamma,\dot{\gamma}} = C_1 \ln \frac{1}{T} + C_2 \tag{56}$$

where C_1 and C_2 are constants for a given strain and strain rate. This relationship was recognized from the semi-logarithmic graphs of Figures 31-33, where the data points very closely described straight lines. The relationship was found not to hold as closely for strains of 0.2 and 0.5.

Further investigation revealed that both C_1 and C_2 are functions of the strain rate $\dot{\gamma}$, and may be expressed by the exponential equation

$$C_1\Big|_\gamma = A_1\dot{\gamma}^{s_1} \tag{57}$$

$$C_2\Big|_\gamma = A_2\dot{\gamma}^{s_2} \tag{58}$$

where A_1, A_2, s_1, and s_2 are constants for a given strain, and the values of temperature, strain, and strain rate are within the limits covered in this discussion. The values of s_1, s_2, A_1 and A_2 at strains of 1.0, 2.0, and 3.0 may be determined from the log-log plots of C_1 and C_2 vs. $\dot{\gamma}$ in Figures 34 and 35, respectively.

The restriction of constant strain rate may now be removed from Equation (56) by substituting the values for C_1 and C_2. Equation (56) then becomes

$$\tau\Big|_\gamma = A_1\dot{\gamma}^{s_1}\ln\frac{1}{T} + A_2\dot{\gamma}^{s_2} \tag{59}$$

It is quite possible that s_1, s_2, A_1, and A_2 could be expressed as a function of the shear strain. If so, substitution of these values into Equation (59) would result in an expression for the shear stress in terms of the strain, strain rate, and temperature which would be most interesting in view of the previous discussion of the mechanical equation of state. However, for an accurate determination of these constants, many more tests would be needed to insure the validity of an accurate functional relation.

The results of the present work were compared with the compression test data of Alder and Phillips (41) for commercially pure aluminum. Effective stress, strain, and strain rate was obtained from the shear data by multiplying by $\sqrt{3}$, $1/\sqrt{3}$, and $1/\sqrt{3}$, respectively. Table 6 shows a relatively good agreement between the torsion and compression data for an effective strain of 0.5 and an effective strain rate of 10 per second.

Table 6. Comparison of Compression and Torsion Data at $\dot{\bar{\varepsilon}}$=0.51 and $\dot{\bar{\varepsilon}}$=10 per Second

Temperature °C	Interpolated Data of Alder and Phillips	Present Work
20	21,500	19,700
200	15,000	13,800
300	10,950	9,900
400	7,300	7,000
500	4,600	4,300
550	3,500	2,950

Aluminum Alloy 2017-0

Torsion tests were performed on the 2017-0 alloy at nominal strain rates of 0.015, 1.5, 15, and 150 per second, exact values being given for each test. The test temperatures for each of the four testing speeds were 350°C, 400°C, 450°C, and 500°C.

Figures 36-39 show the effect of strain rate on the τ vs. γ curves throughout the temperature range, the curves being drawn up to a shear strain of five. Again, peaks are apparent in the initial portion of the curves, seemingly more pronounced than with the commercially pure aluminum.

Since the addition of impurity elements will generally tend to lower the stacking fault energy, the climb of dislocations can be assumed to be more restricted in the 2017-0 alloy than in the 1100-0 alloy. Polygonization will be suppressed and sufficient strain energy can accumulate to cause recrystallization with a subsequent sharp drop in flow stress. It is of interest to note the unusually pronounced negative slope in the τ vs. γ curve at 350°C with a rate of deformation of 181 per second. Although a negative slope would be expected from the considerations of the previous paragraph, it is apparent that there is some temperature rise occurring during the test. Because of the very rapid rate of deformation, the specimen can be assumed to be adiabatic throughout the duration of the test. Clearly, the temperature rise increases with increasing strain, and causes some additional thermal softening which contributes to the drop in stress observed. An evaluation of the temperature rise occurring during high-speed tests is discussed at the conclusion of the chapter.

At temperatures of 450°C and 500°C, the τ vs. γ curves are not as flat as would be expected from the tests at the two lower temperatures. Actually, this is most likely due to the tendency for the test specimens to initially shorten at these higher temperatures, as discussed in the preceding chapter. The shortening causes a slightly increase in

the cross-sectional area (assuming constant volume) thereby increasing the torque required for further deformation. As the shear strain increases, the specimen will stop shortening and begin to lengthen, causing a slight drop in the torque in addition to the effects of thermal softening.

At the slow deformation rates, the point of fracture, as indicated by an abrupt drop in the stress-strain curve, could not be positively detected. At the higher rates of strain, however, the point of fracture was more easily located. In their torsion tests of 2024-0 aluminum alloy, Fields and Backofen (59) found that the fracture strain in torsion at elevated temperatures could not be precisely defined, since shallow surface cracks were found to appear at strains lower than that at which the sharp drop in the torque curve occurred with the complete separation of the specimen.

At a nominal strain rate of 15 per second, values of the revolutions to fracture for testing temperatures of 350°C, 400°C and 450°C were found to vary only slightly, being in the order of approximately 2.7 revolutions. At 500°C, however, the ductility decreased sharply, and fracture occurred at approximately 0.88 revolutions. The ductility also decreased abruptly when testing speed was increased to 1500 RPM ($\dot{\gamma} \approx 150$ per second). In this case, fracture occurred at approximately 0.9 revolutions at 400°C and 0.54 revolutions at 500°C.

Examination of the fracture surfaces indicated interesting comparisons between tests at the slowest and fastest rates of strain. Specimens twisted at a test temperature of 500°C are shown in the photograph of Figure 25(b). It can be seen that at the slowest strain

rate, large extension and subsequent necking is indicated (it is interesting to note that with this extreme deformation, axial symmetry was still maintained). The fracture surfaces at the highest testing speed surprisingly enough are seen to exhibit essentially no distortion. In this case, the ductility has been greatly reduced, resulting in fracture at much lower strains, and thereby allowing less time for distortion to occur.

Figures 40-42 show the effect of strain rate on the shearing stress for typical strains of 0.5, 1.0, and 2.0, respectively. For all strains investigated, from 0.2 to 3.0, the data could be interpolated into two intersecting straight lines, the point of intersection being at a strain rate of approximately 15 per second. Somewhat similar results were observed by Bailey (62) for tests in plane strain compression of an aluminum 4.1 per cent copper alloy. The values of n for strains of 0.2 to 3.0 ($\dot{\gamma} < 15 sec^{-1}$) are given in Table 7.

Table 7. Values of the Strain Rate Sensitivity for 2017-0 Aluminum Alloy

Temperature °C	Strain Rate Sensitivity				
	γ=0.2	γ=0.5	γ=1.0	γ=2.0	γ=3.0
350	0.09	0.11	0.11	0.11	0.11
400	0.12	0.12	0.12	0.12	0.13
450	0.16	0.16	0.15	0.15	0.16
500	0.20	0.19	0.18	0.17	0.19

These values can be seen to compare closely with those for the commercially pure aluminum.

The effect of temperature on the shear stress is shown in Figure 43 at a strain of 2.0, the data being obtained from the curves of Figure 42. An attempt was made to utilize the semi-logarithmic relationship of Equation (56) so that the shear stress could be expressed as a function of the temperature; however, it was found that the relationship did not hold as closely as for the commercially pure aluminum.

Aluminum Alloy 6061-0

Experiments were performed over the same range of testing speeds and temperatures for the 6061-0 alloy as with the 2017-0 aluminum alloy. The effect of the strain rate on the τ vs. γ curves is shown in Figures 44-47. At the fastest testing speeds, peaks in the initial portions of the curves were readily noted at each of the testing temperatures, while at the slower rates of strain, the peaks were much less pronounced. The arguments given previously regarding polygonization and restoration effects again apply, and need not be repeated.

At temperatures of 450°C and 500°C, the curves at the slowest testing speed are not as flat as would be expected. It is recalled that similar observations were noted with the 2017-0 alloy. Axial shortening again occurred at the beginning of the tests, and thus the cross-sectional area increased slightly, causing a small increase in the torque. As the shear strain increased, the specimens stopped shortening and began to lengthen, causing a slight drop in the torque

in addition to the effects of thermal softening.

Determination of revolutions to fracture at the slowest rate of strain was not possible, as no abrupt change in the stress-strain curve was generally noted. Evidence of fracture was noticeable, however, at the higher rates of strain. At a nominal strain rate of 15 per second, the number of revolutions to fracture was found to increase with increasing test temperatures. For example, at 350°C, fracture occurred at approximately 2.7 revolutions, in contrast to 5.8 revolutions at 500°C. When the testing speed was raised to provide nominal strain rates of 150 per second, the fracture strain was significantly reduced, revolutions to fracture being 1.45 at 350°C, and 2.9 at 450°C. Determination of fracture at 500°C was difficult to determine, but was in the range of 2.8 to 3.1 revolutions.

The fracture surfaces twisted at 500°C are shown in Figure 25(c) and represent fracture at the lowest and highest testing speeds. The slow speed test again showed a large extension and subsequent necking of the specimen, while symmetry was still maintained about the longitudinal axis. In contrast, the fracture surfaces of the specimen deformed at the fastest testing speed of 1500 RPM indicated essentially no distortion. In this case, as with the 2017-0 alloy, ductility had been reduced at these rapid testing speeds, and so fracture occurred at lower strains, allowing relatively less time for distortion to occur.

The effect of the strain rate on the shear stress is shown in Figures 48-50 for shearing strains of 1.0, 2.0, and 3.0, respectively. The data was found to agree reasonably well with the power law, although not as closely as with the commercially pure aluminum. At strains less

than 1.0, only limited agreement was obtained. The values of the strain rate sensitivity are given in Table 8. These values can be seen to compare closely with the values of n for the 1100-0 and 2017-0 alloys.

The effect of the temperature upon the shearing stress is shown in Figure 51 for a shear strain of 2.0. An attempt was made to relate the shearing stress to the temperature by the semi-logarithmic relationship of Equation (56), however, a close agreement with this equation was not obtained.

Table 8. Values of the Strain Rate Sensitivity

For 6061-0 Aluminum

Temperature °C	Strain Rate Sensitivity		
	γ=1.0	γ=2.0	γ=3.0
350	0.10	0.11	0.11
400	0.12	0.12	0.12
450	0.13	0.13	0.13
500	0.14	0.14	0.15

Temperature Rise

A temperature rise can be expected to occur in any metal subjected to rapid rates of deformation. In the previous tests, this was most noticeable during the room temperature tests of the commercially pure aluminum at a testing speed of 1500 RPM, where an overall drop in torque was noted when the testing speed was increased from 125 RPM to 1500 RPM.

The lower values of torque clearly indicated that a temperature rise had occurred within the specimen. Since the duration of the test was only 0.060 seconds, adiabatic heating, at least to a large extent, may be assumed to have occurred.

If all the heat generated during this time is assumed to be confined to the test section, the temperature rise may be calculated using the expression

$$\Delta T = \frac{1}{12Jc\rho} \int \bar{\sigma} d\bar{\varepsilon} \tag{60}$$

where $\bar{\sigma}$ = effective stress #/in.^{2}

$\bar{\varepsilon}$ = effective strain.

c = specific heat BTU/#°F.

ρ = density #/in.^{3}

J = mechanical equivalent of heat ft#/BTU

The integral term represents the work done per unit volume of the material. In torsion, this equation may be written as

$$\Delta T = \frac{1}{12Jc\rho} \int \tau d\gamma \tag{61}$$

The adiabatic temperature rise was computed from Equation (61) using the stress-strain data obtained from the room temperature test on the 1100-0 alloy. Figure 52 shows this theoretical temperature rise as a function of the shear strain.

The rise in temperature can be expected to be much less pronounced as the testing speed is decreased, since more time is available for operation of the various heat transfer mechanisms. Indeed, significant indications of temperature rise were not noted at speeds below 1500 RPM. Since temperature rise is relatively small at low strains, its effect on the stress-strain curve of tests performed at higher temperatures is reduced, since these curves exhibit maximum stress at low values of strain.

It is of interest to note that with the thin-walled cylinder, the temperature rise throughout the wall thickness or cross-sectional area can be assumed fairly uniform. In contrast, the tests on solid cylinders will exhibit a temperature gradient, since the temperature rise will be greatest at the surface of the specimen, where strains are largest.

CHAPTER VIII

CONCLUSIONS

The effects of temperature and strain rate on the resistance to deformation of commercially pure aluminum, 1100-0 and two aluminum alloys, 2017-0 and 6061-0, have been studied using a specially-designed torsion testing machine capable of performing torsion tests free of longitudinal stresses. As a result of this work, the following conclusions can be drawn regarding the three major phases of the investigation:

Torsion Testing Machine

An extensive series of torsion tests have indicated that the performance of the testing apparatus was entirely satisfactory. Conclusions regarding the operation of the machine may be summarized as follows:

1. Testing speeds of the apparatus were in the range 1500 RPM to 0.0015 RPM, while testing temperatures were in the range room temperature to 600°C.

2. The utilization of the linear bearing was successful in allowing the test specimen to freely expand or contract in length, free of longitudinal stresses.

3. The instrumentation was such that temperatures, speeds, torques and change in length of specimens could be recorded continuously.

Anisotropy and Change in Length

The change in length of specimens was determined from the displacement of the linear bearing during the test. The experimental data, in addition to indicating the change in length, was used to determine an empirical equation which was then incorporated in an analytical study of the extent of anisotropy in torsion. The following conclusions were drawn concerning this phase of the investigation:

1. All three materials tested experienced a change in length during torsion.

2. At temperatures of 400°C and above, an initial decrease in length, followed by a gradual increase in length, was observed. The initial shortening was most prevalent in the 2017-0 and 6061-0 alloys, ranging as much as 0.009" to 0.010" at 500°C.

3. At a given strain, the increase in length was observed to generally decrease with increasing temperature and decreasing speed.

4. An analytical investigation of torsion showed that the anisotropic parameters or the associated yield stresses along the principal anisotropic directions could be expressed as a function of the through-thickness yield stress.

5. Values of F+2H, G+2H, and N, expressed in terms of $1/2\tau^2$ were determined from the equations derived in Chapter VI, and provided an indication of the extent of anisotropy. Computations were performed with increasing shear strain. Computations were performed using a Burroughs 5500 digital computer. Values were calculated for shear strains in increments of 0.1 to 10.0.

Torsion Tests

A comprehensive series of torsion tests were performed over a wide range of strain rates and temperatures, using hollow cylindrical specimens. Longitudinal stresses were eliminated by allowing the natural change in length to occur during twisting. The effects of temperature and strain rate on the resistance to deformation of these metals were analysed in detail. The conclusions discussed in Chapter VII may be summarized as follows:

1. The torsion testing apparatus was found to be an accurate and convenient means of determining temperature and strain rate effects.

2. Even at high strains, test specimens showed no evidence of irregular distortion. It is interesting to note, however, that at the higher testing temperatures and slower testing speeds, necking was observed.

3. The effect of strain rate at constant values of strain and temperature was found to be reasonably approximated by a power law.

4. The effect of temperature and strain rate at a given strain on the shearing stress of commercially pure aluminum could be described by Equation (59) for the temperature range $200^{\circ}C < T < 550^{\circ}C$. No function was found to describe these effects for the other two alloys tested.

5. The effects of temperature and strain rate on the shape of the stress-strain curve could be explained by a consideration of the effects of work hardening, recovery, and recrystallization. The size of the peaks in the initial portion of the stress-strain curves could

be related to the rate at which polygonization could occur, and the resulting interaction between the restoration effects of polygonization and recrystallization.

CHAPTER IX

RECOMMENDATIONS

The present investigation has indicated that the torsion test is well suited for determining the effects of temperature and strain rate on the resistance to deformation of metals. It is therefore logical that the work should be continued, and its scope extended. The following recommendations are made concerning possible areas of future investigation:

1. A metallographic examination of the specimens deformed under various test conditions would provide an accurate means of determining the effects of work hardening, recovery, polygonization and recrystallization, to include an examination of the peaks in the initial portion of the stress strain curves. The design of a rapid quench mechanism would be highly desirable for this purpose.

2. The incorporation of a furnace that would allow observation of the specimen while being twisted would greatly aid in determining the beginning of fracture.

3. The analytical work presented in Chapter VI may be supplemented by an experimental investigation of the through-thickness yield stress of the cylinder, which would then allow the specific determination of the anisotropic character of the material.

4. It would be interesting to compare change in length data of solid cylinders with that of the hollow cylinders. Additionally,

further tests on other materials, along with an investigation of the resulting anisotropy, should provide interesting comparisons.

5. A wider range of tests is required to determine whether Equation (59) could be extended to include a strain term. In this respect, it would be appropriate to investigate the validity of this equation for super purity aluminum.

6. An X-ray examination might be utilized to relate analytical and experimental change in length studies with the development of preferred orientation.

7. Other materials, both ferrous and non-ferrous, should be examined.

APPENDIX A

TORSION TEST DATA

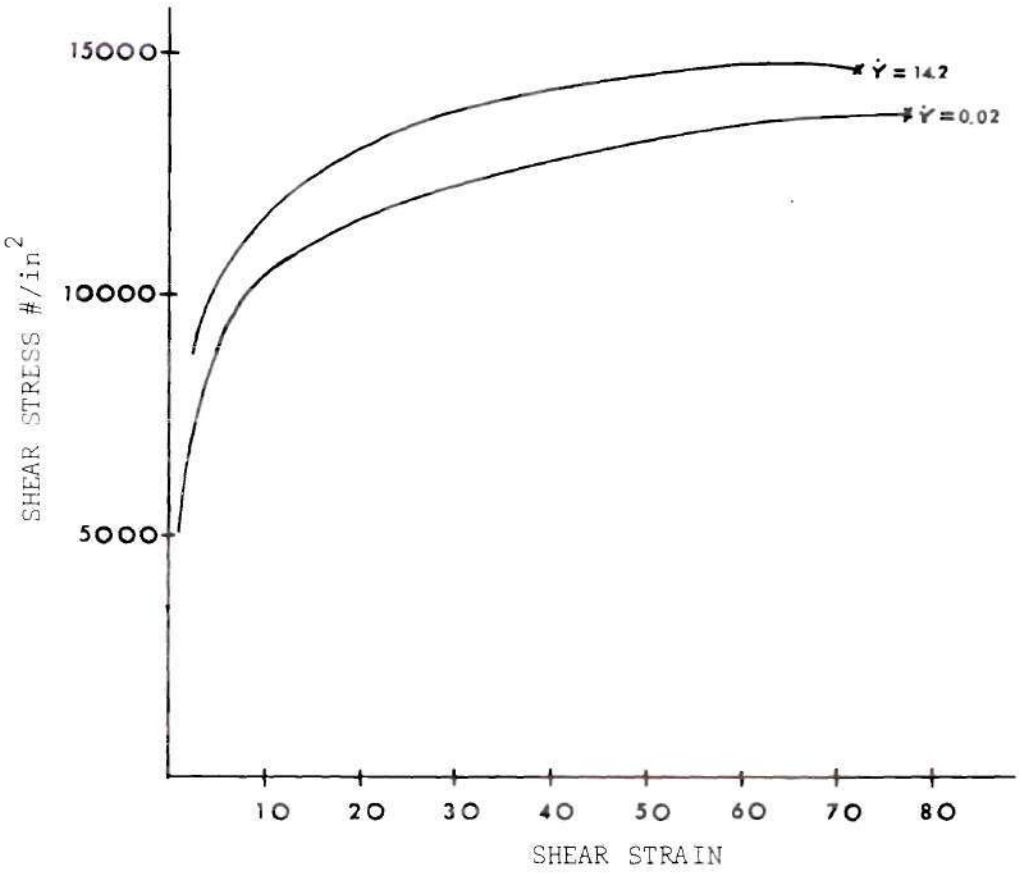

Figure 17. Shear Stress vs. Shear Strain for 1100-0 Aluminum at T = 22°C

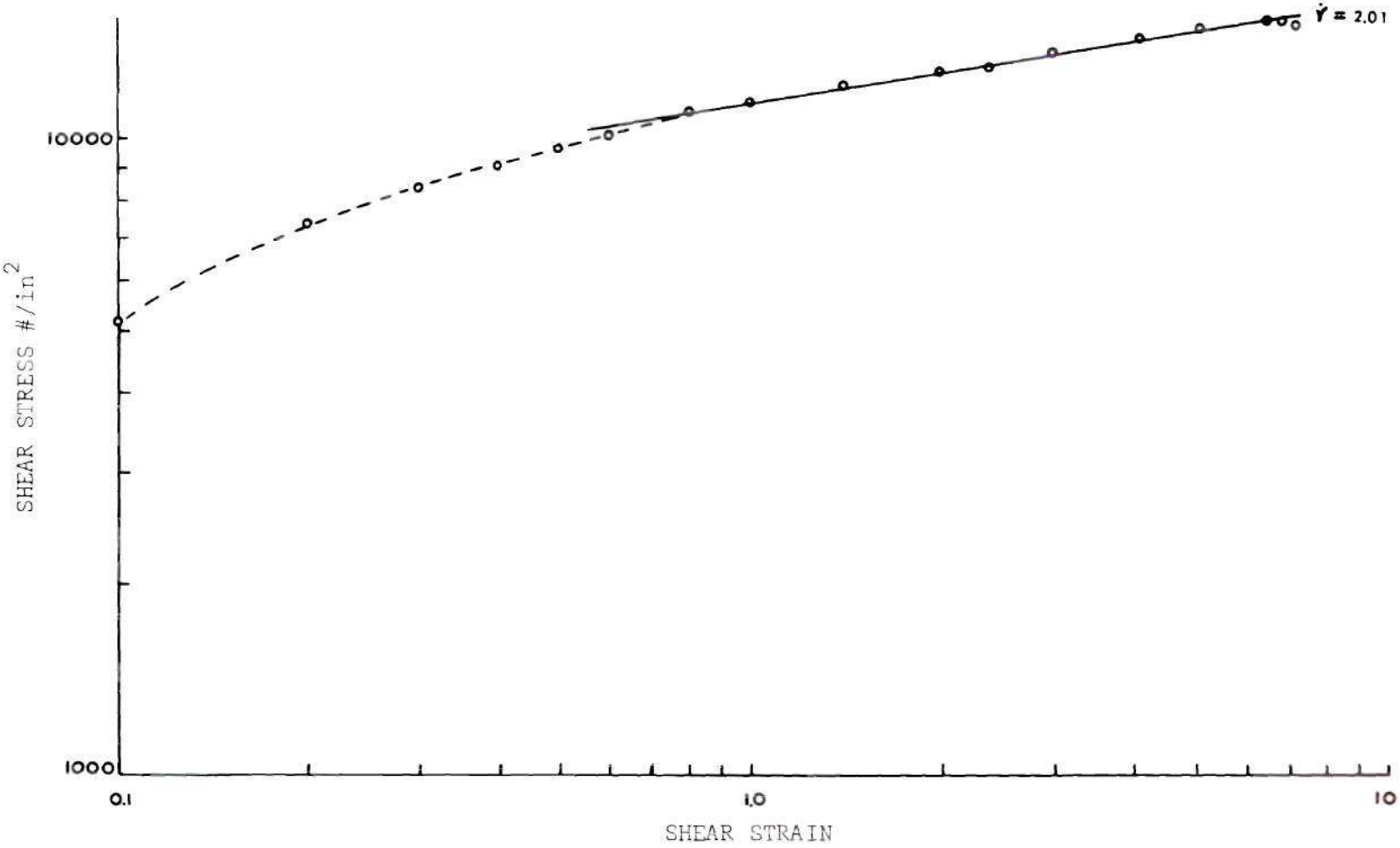

Figure 18. Shear Stress vs. Shear Strain for 1100-0 Aluminum at T = 22°C

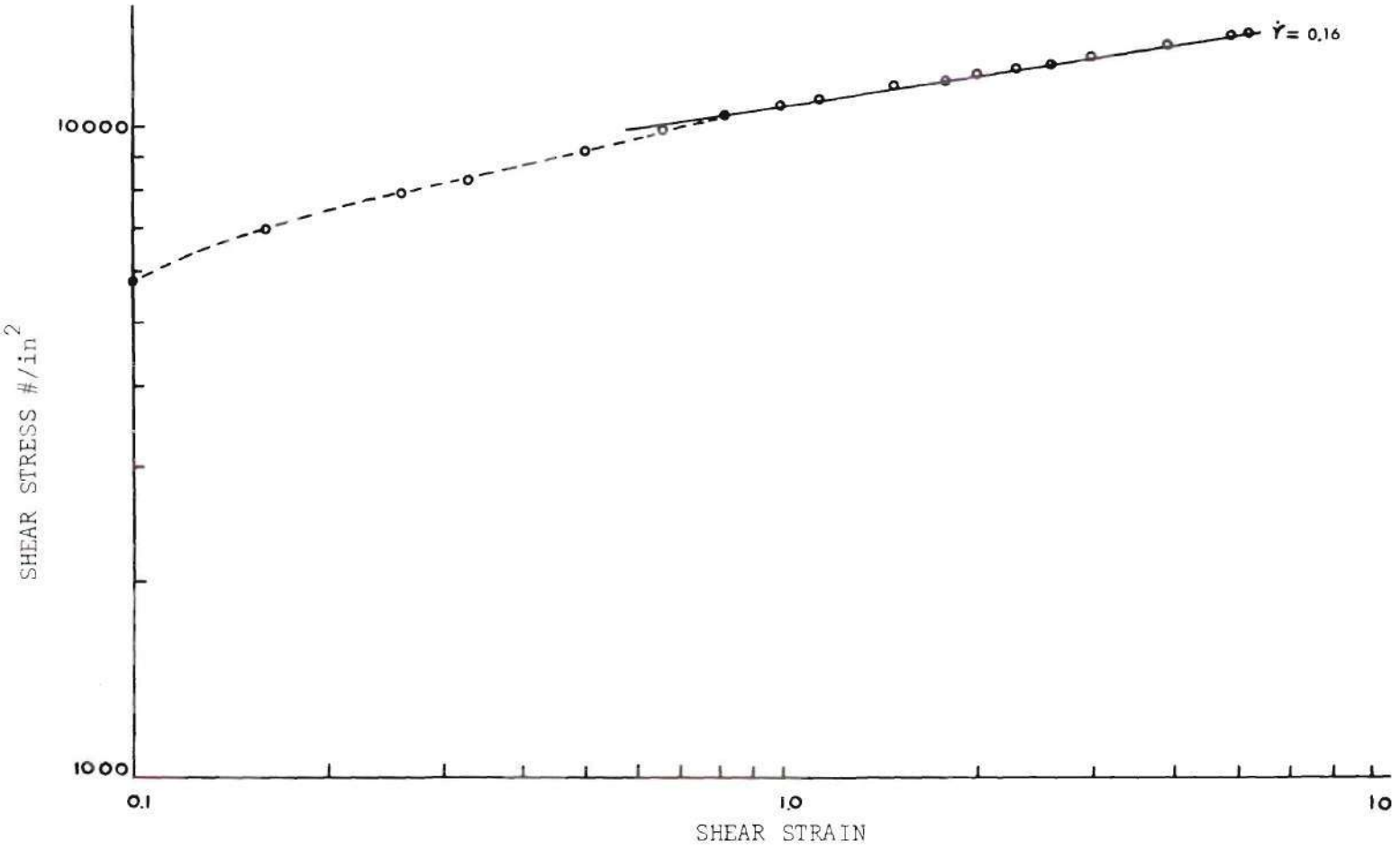

Figure 19. Shear Stress vs. Shear Strain for 1100-0 Aluminum at T = 22°C

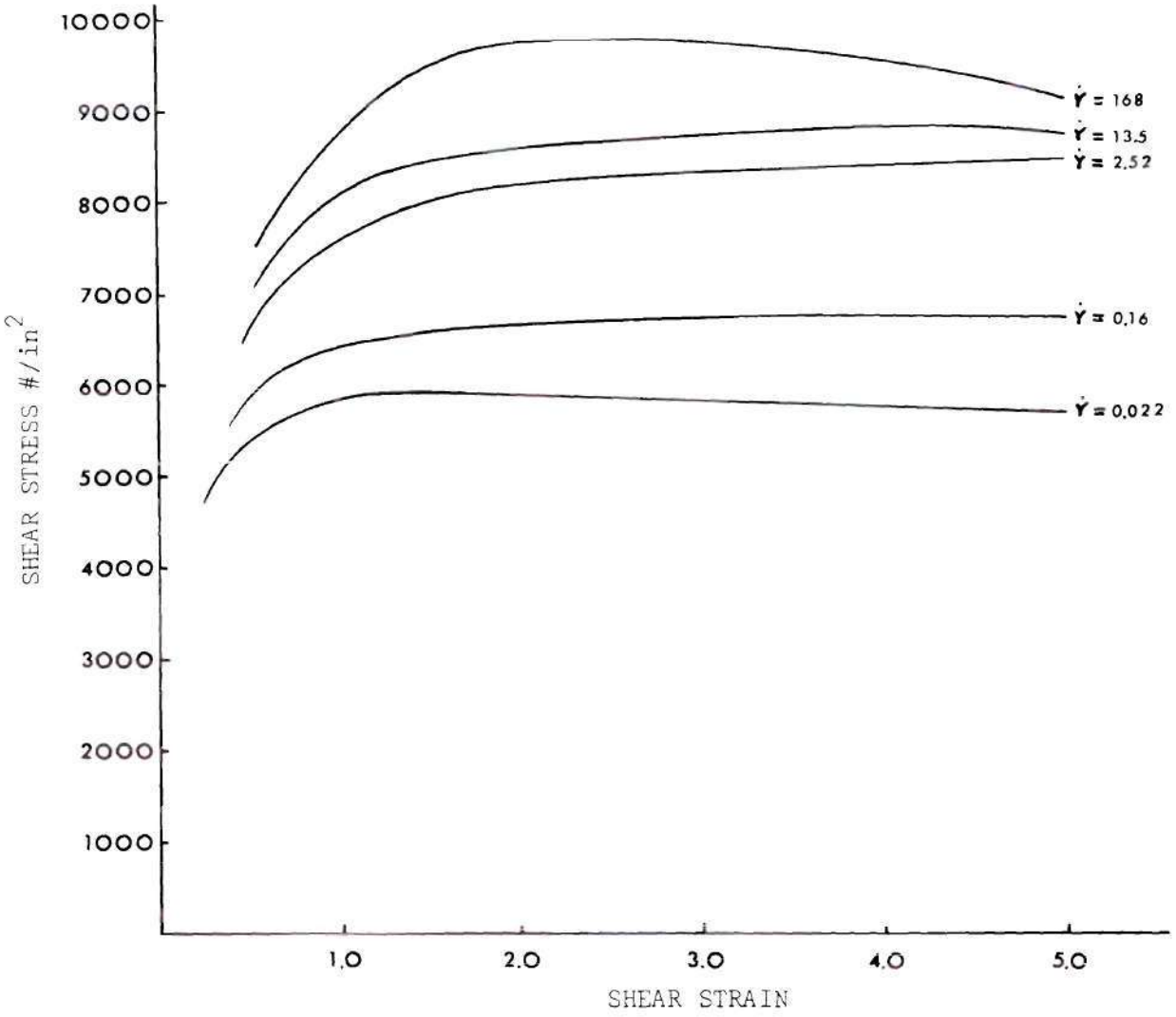

Figure 20. Shear Stress vs. Shear Strain for 1100-0 Aluminum at T = 200°C

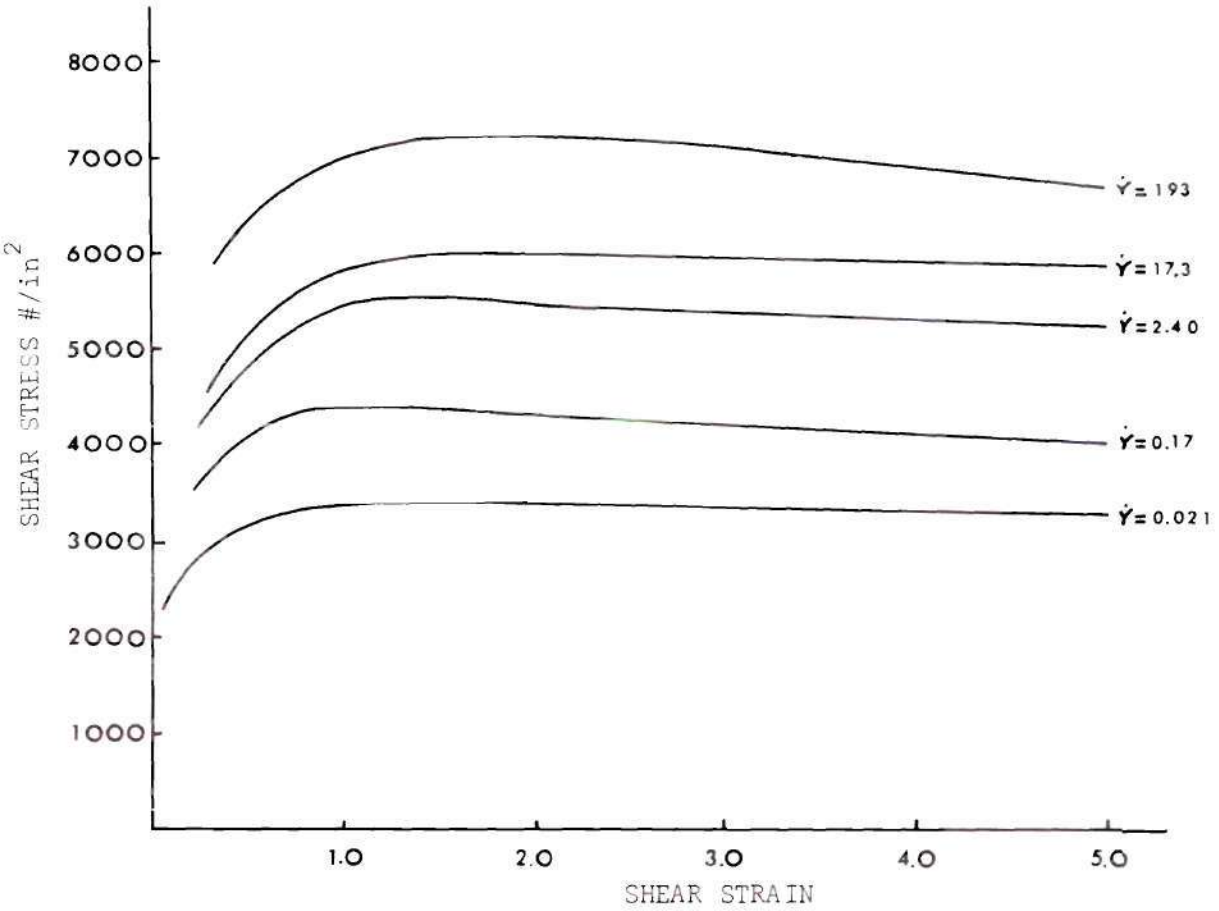

Figure 21. Shear Stress vs. Shear Strain for 1100-0 Aluminum at T = 300°C

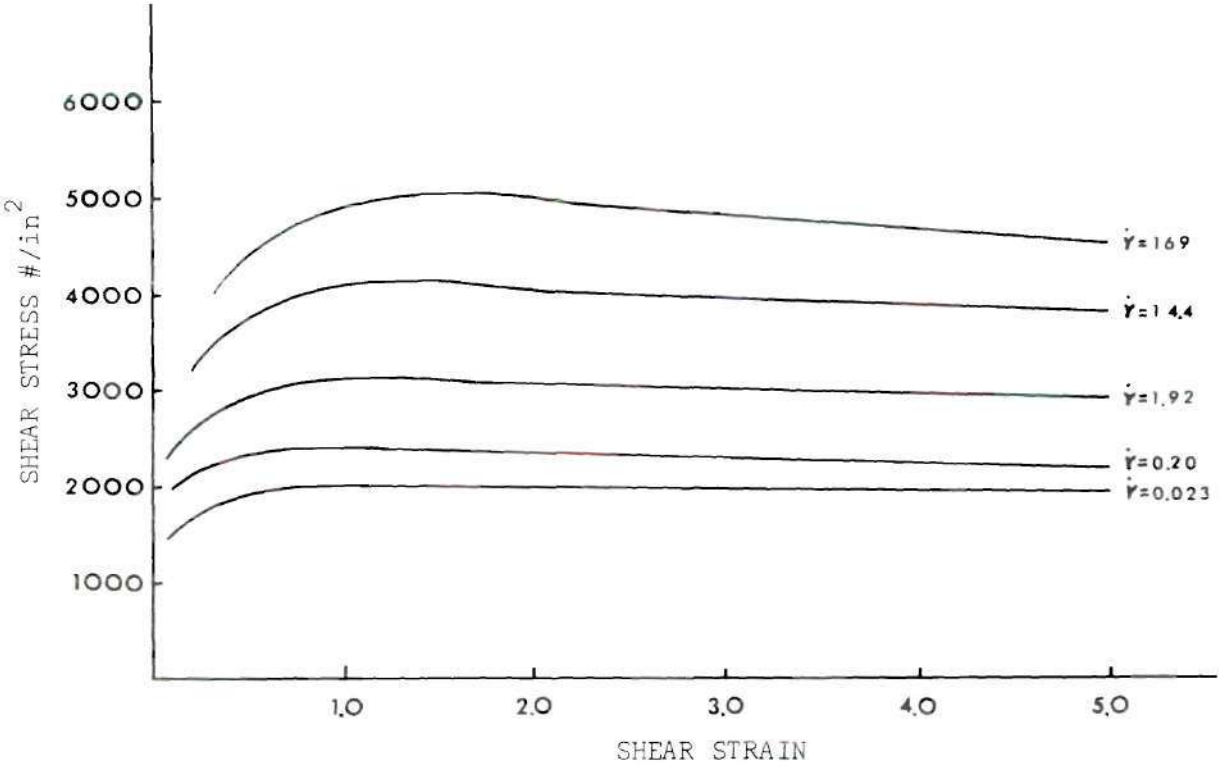

Figure 22. Shear Stress vs. Shear Strain for 1100-0 Aluminum at T = 400°C

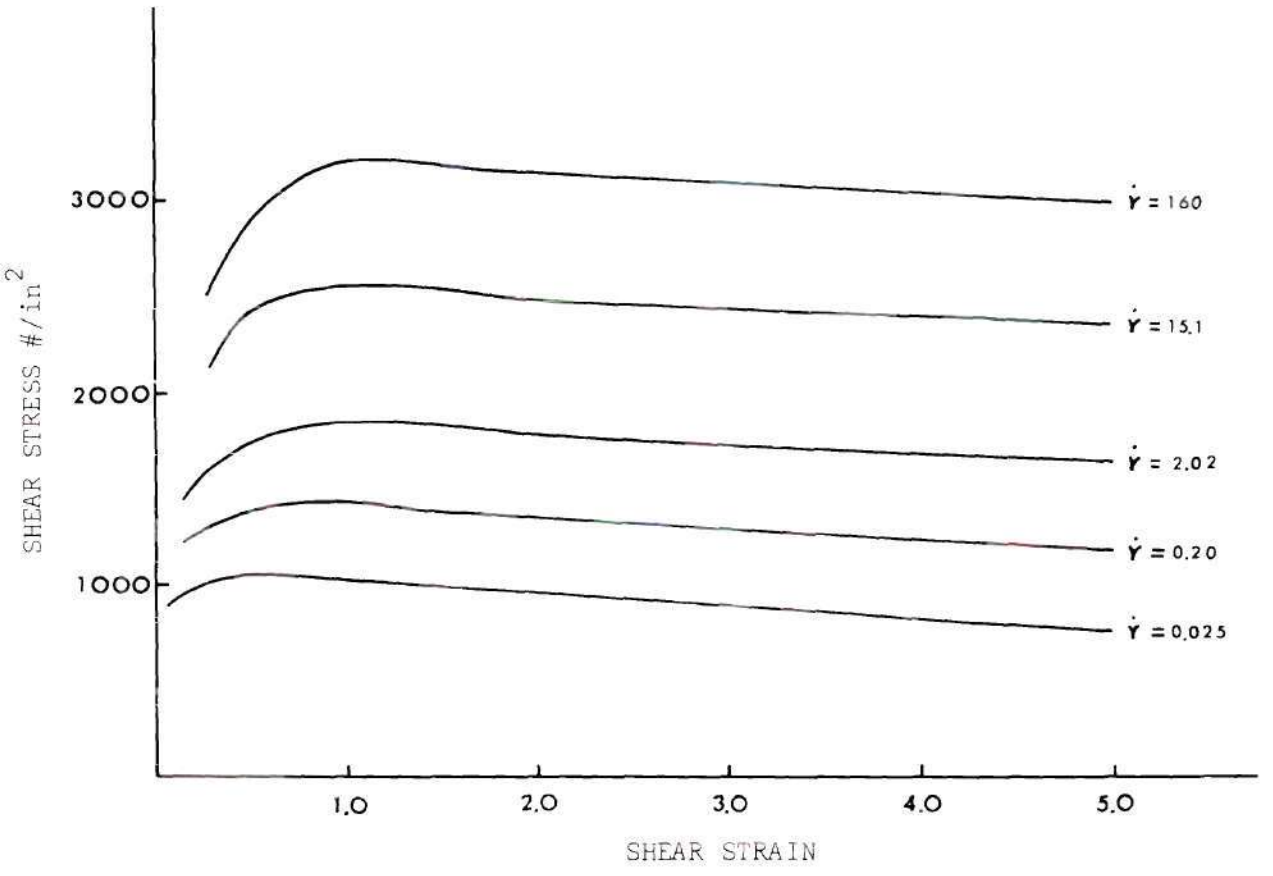

Figure 23. Shear Stress vs. Shear Strain for 1100-0 Aluminum at T = 500°C

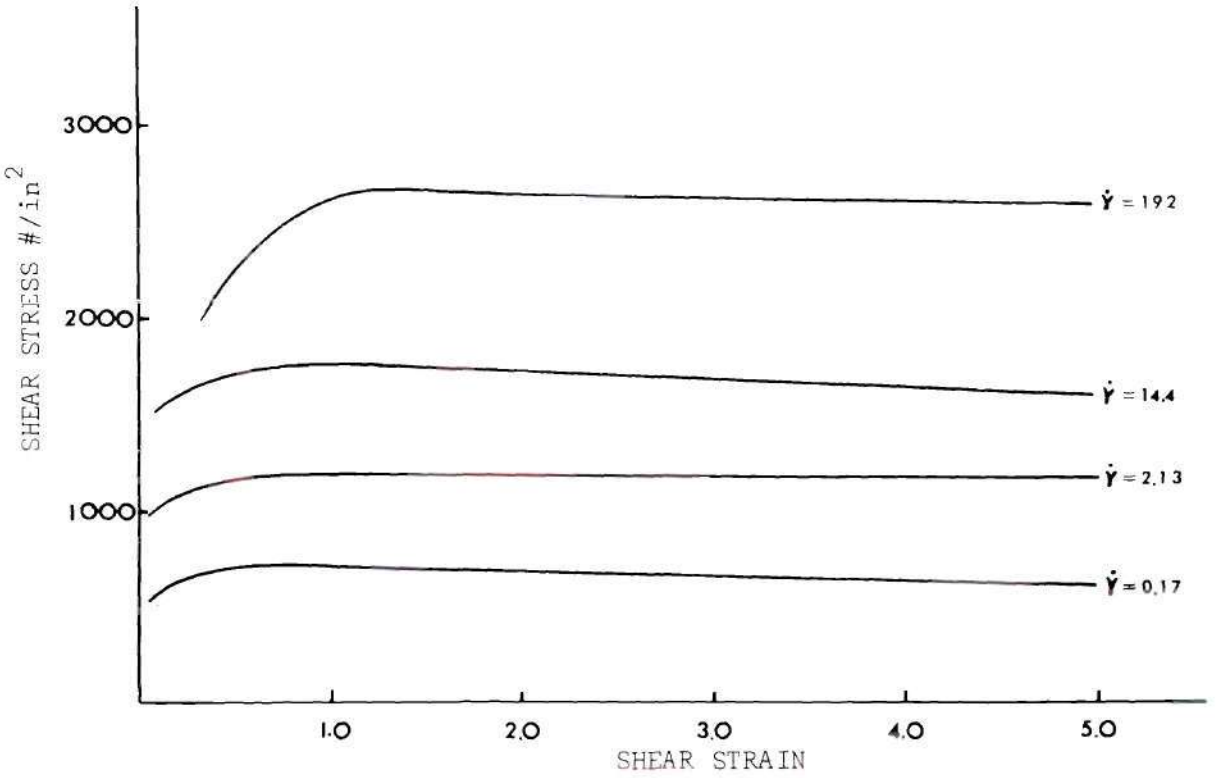

Figure 24. Shear Stress vs. Shear Strain for 1100-0 Aluminum at T = 550°C

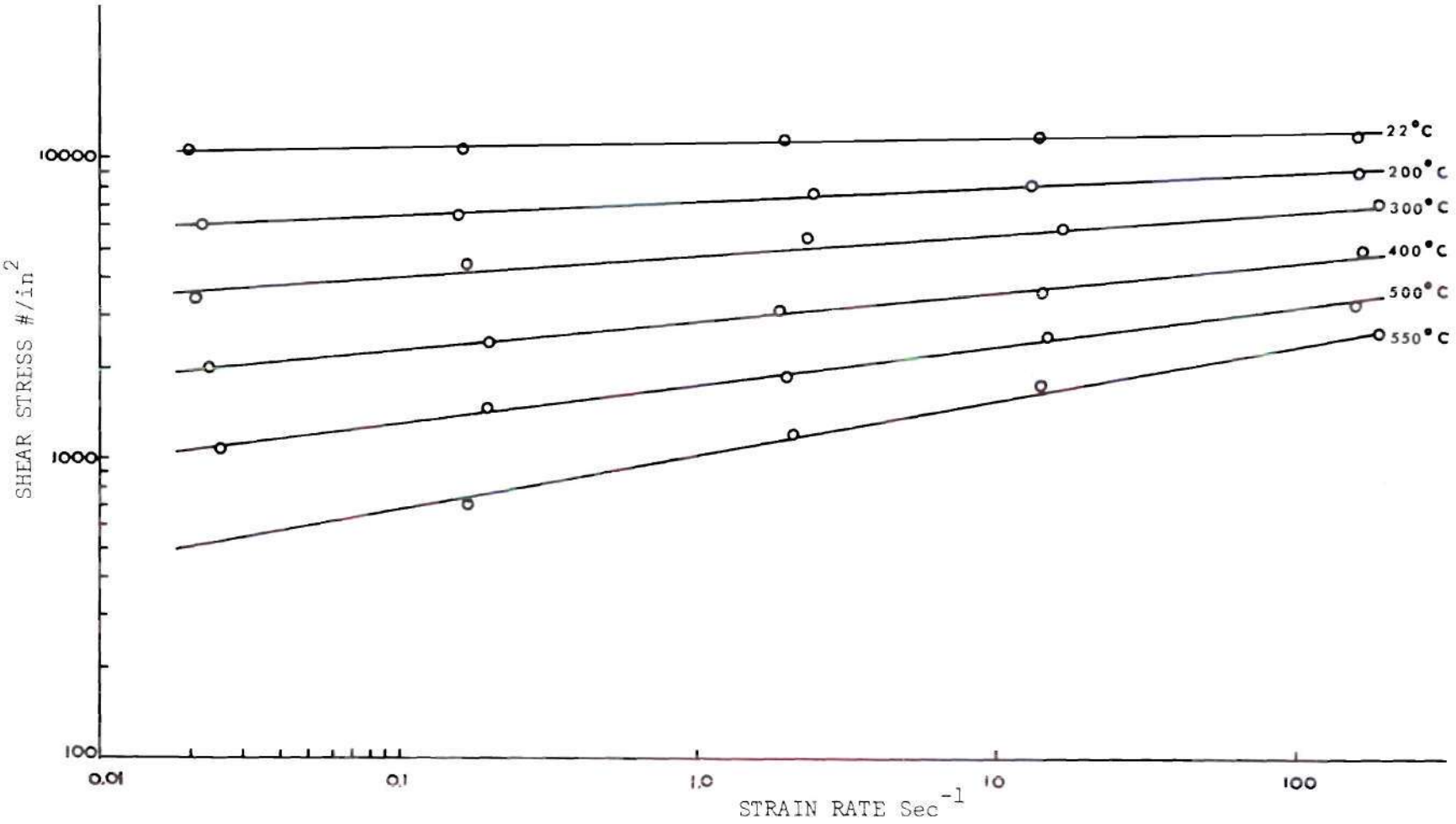

Figure 26. Shear Stress vs. Strain Rate for 1100-0 Aluminum at γ = 1.0

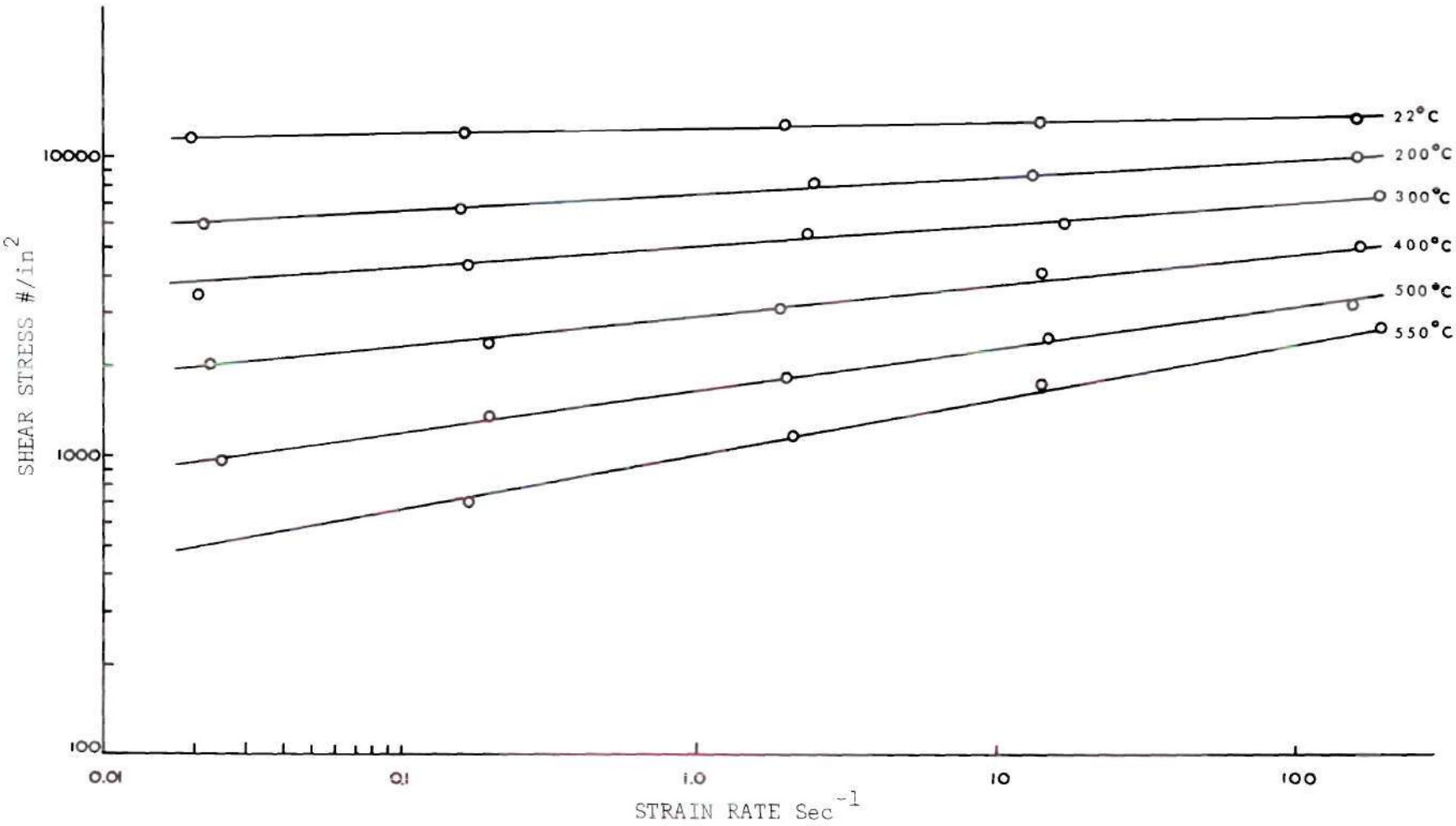

Figure 27. Shear Stress vs. Strain Rate for 1100-0 Aluminum at γ = 2.0

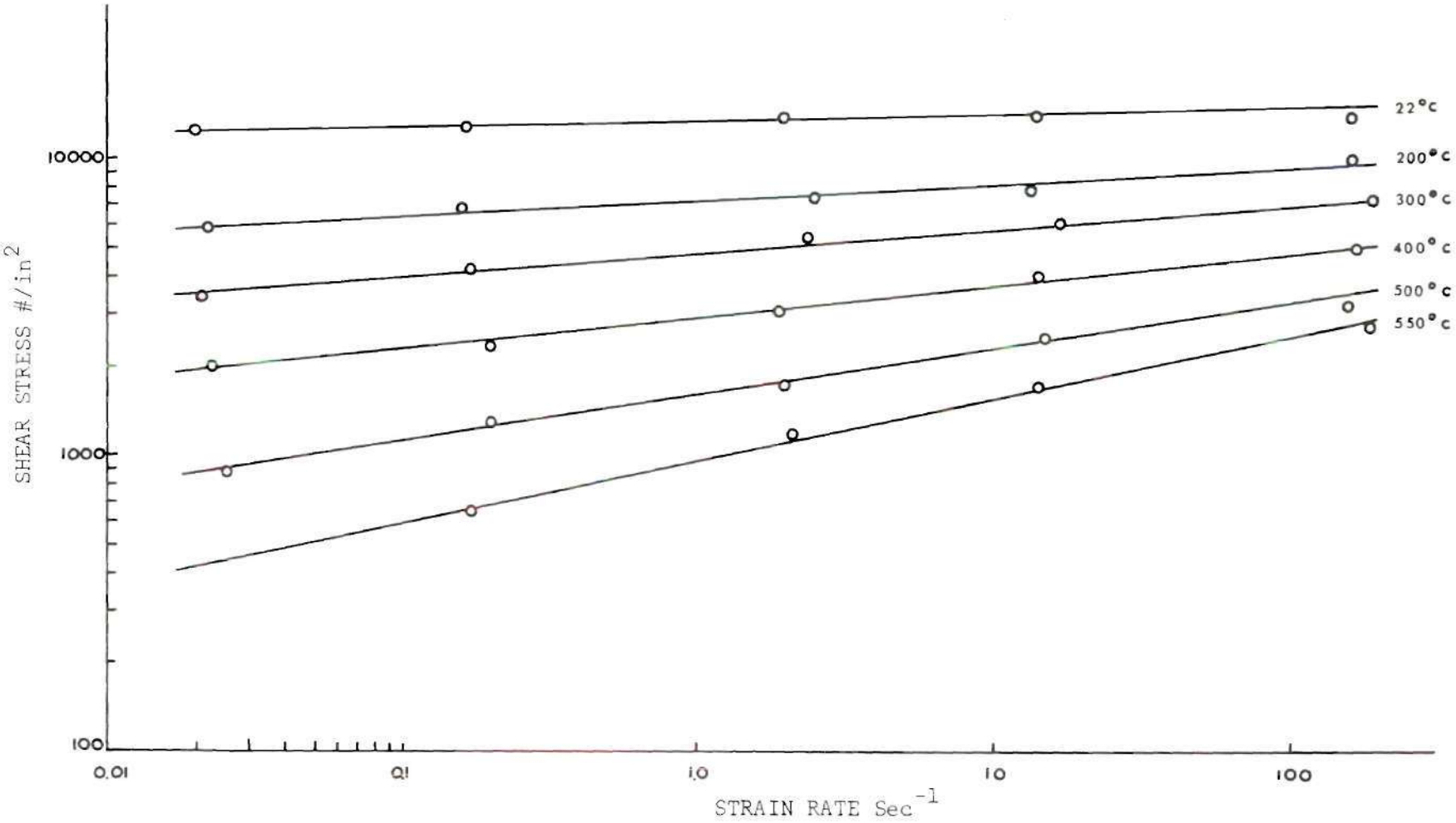

Figure 28. Shear Stress vs. Strain Rate for 1100-0 Aluminum at γ = 3.0

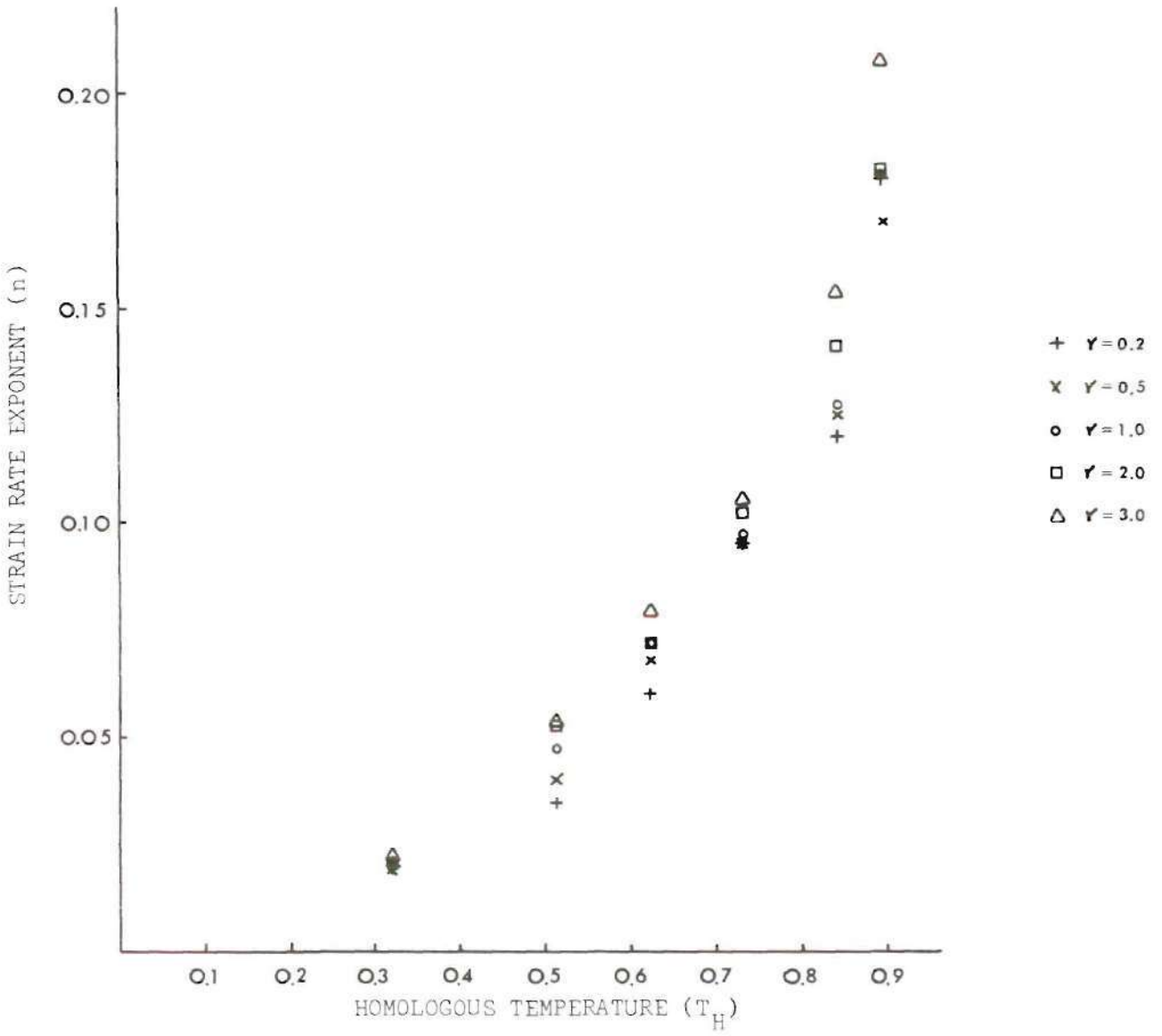

Figure 29. Relationship Between the Homologous Temperature and the Strain Rate Sensitivity

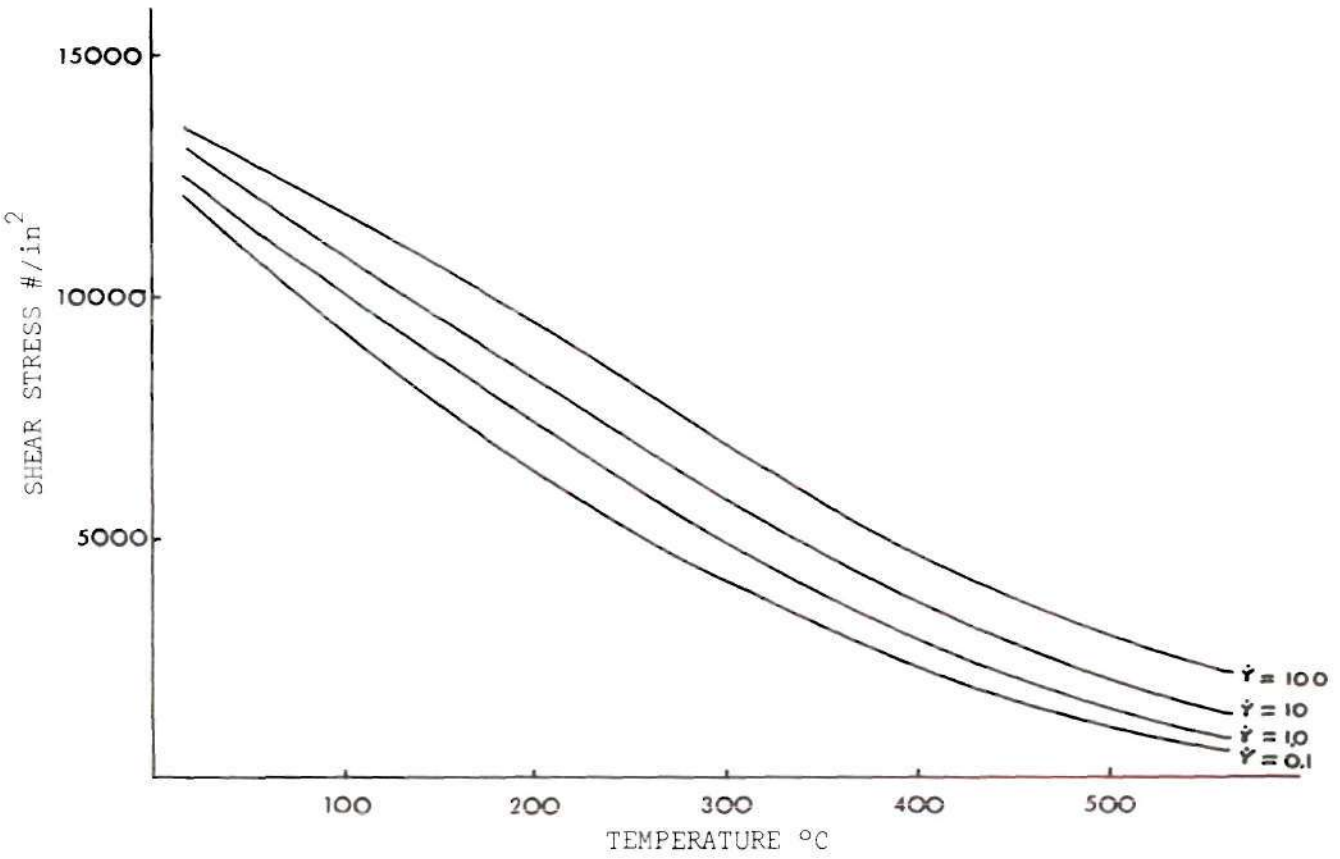

Figure 30. Effect of Temperature on the Shearing Stress for 1100-0 Aluminum

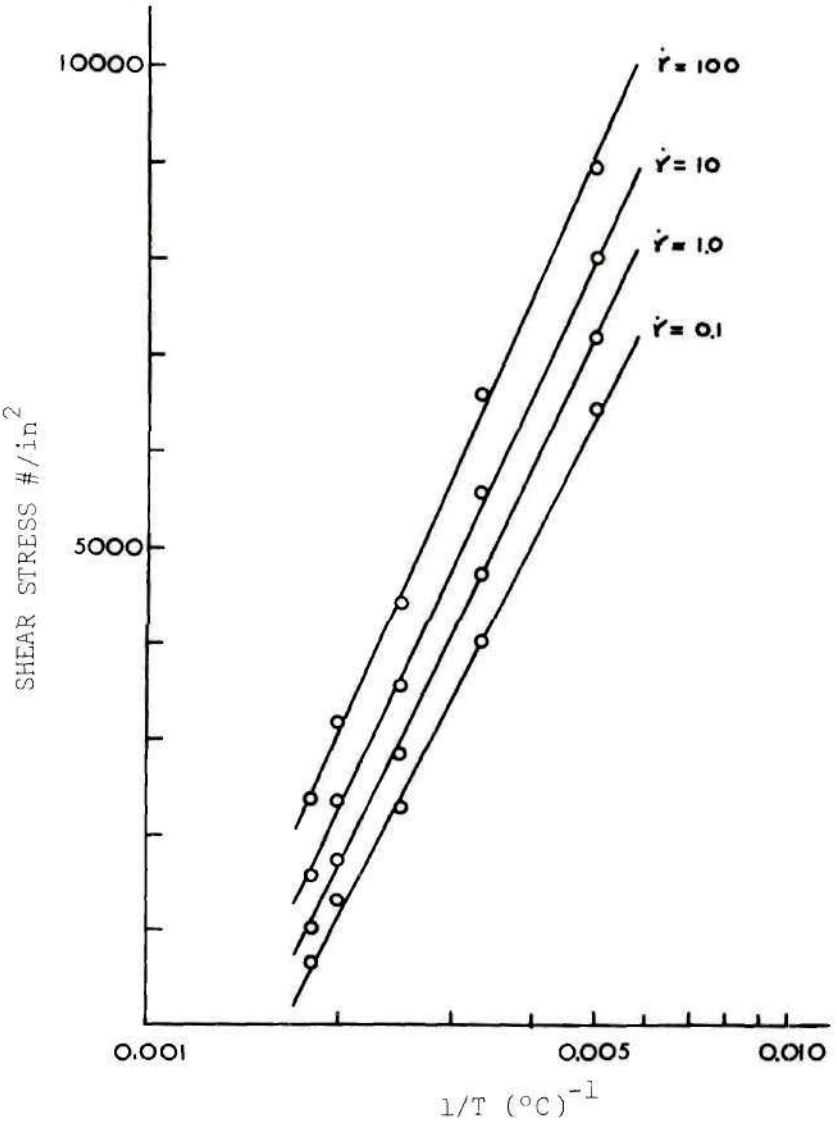

Figure 31. τ vs. ℓn 1/T for 1100-0 Aluminum at γ = 1.0

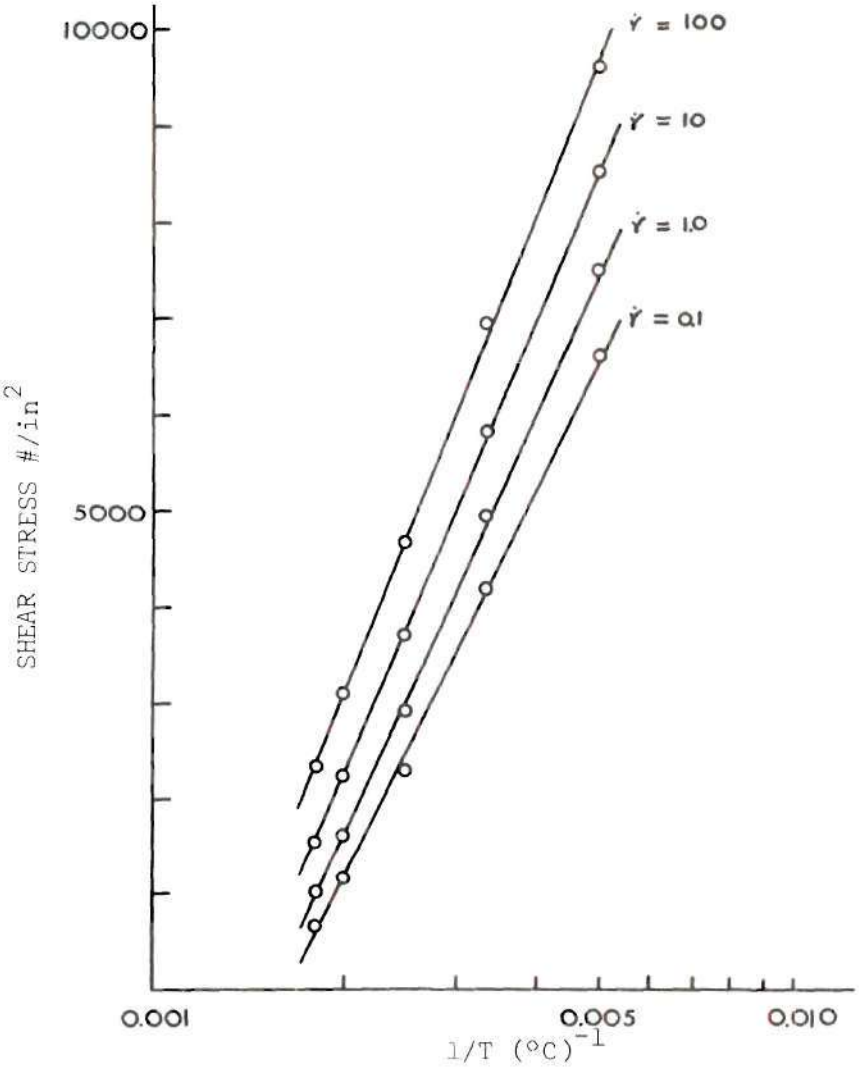

Figure 32. τ vs. ℓn 1/T for 1100-0 Aluminum at γ = 2.0

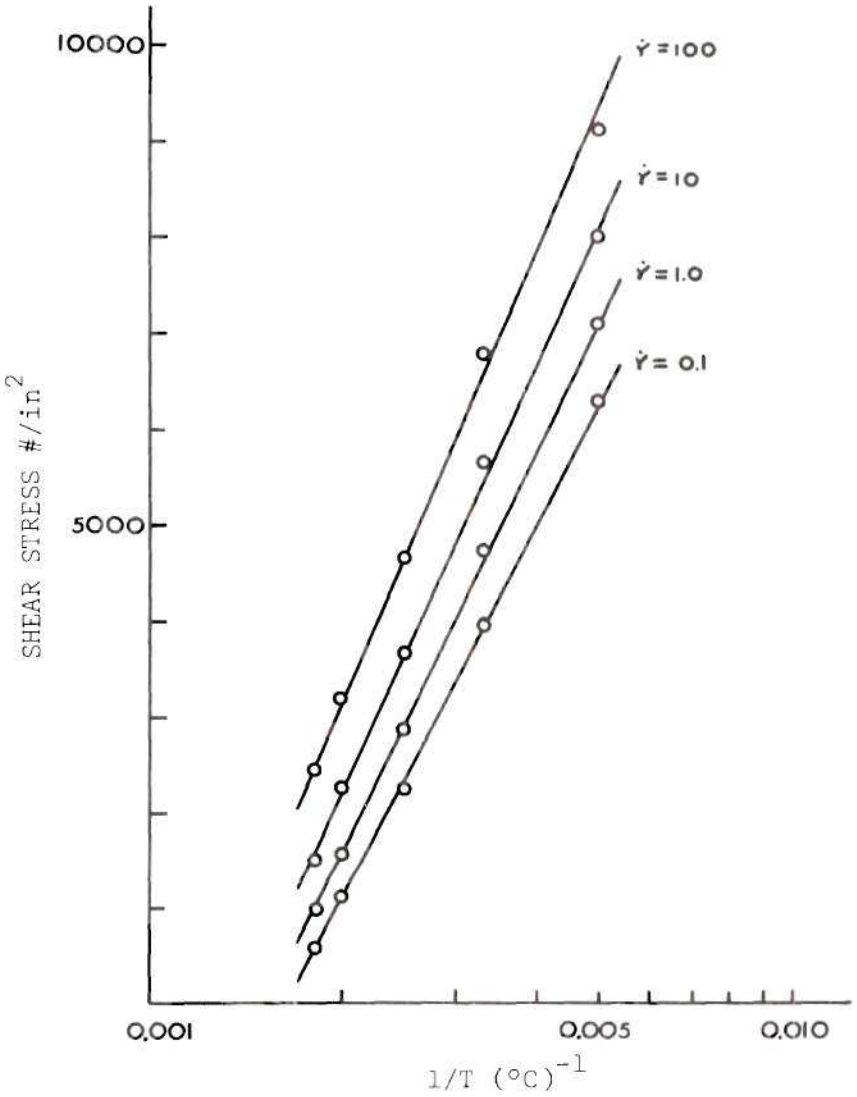

Figure 33. τ vs. ℓn 1/T for Aluminum at γ = 3.0

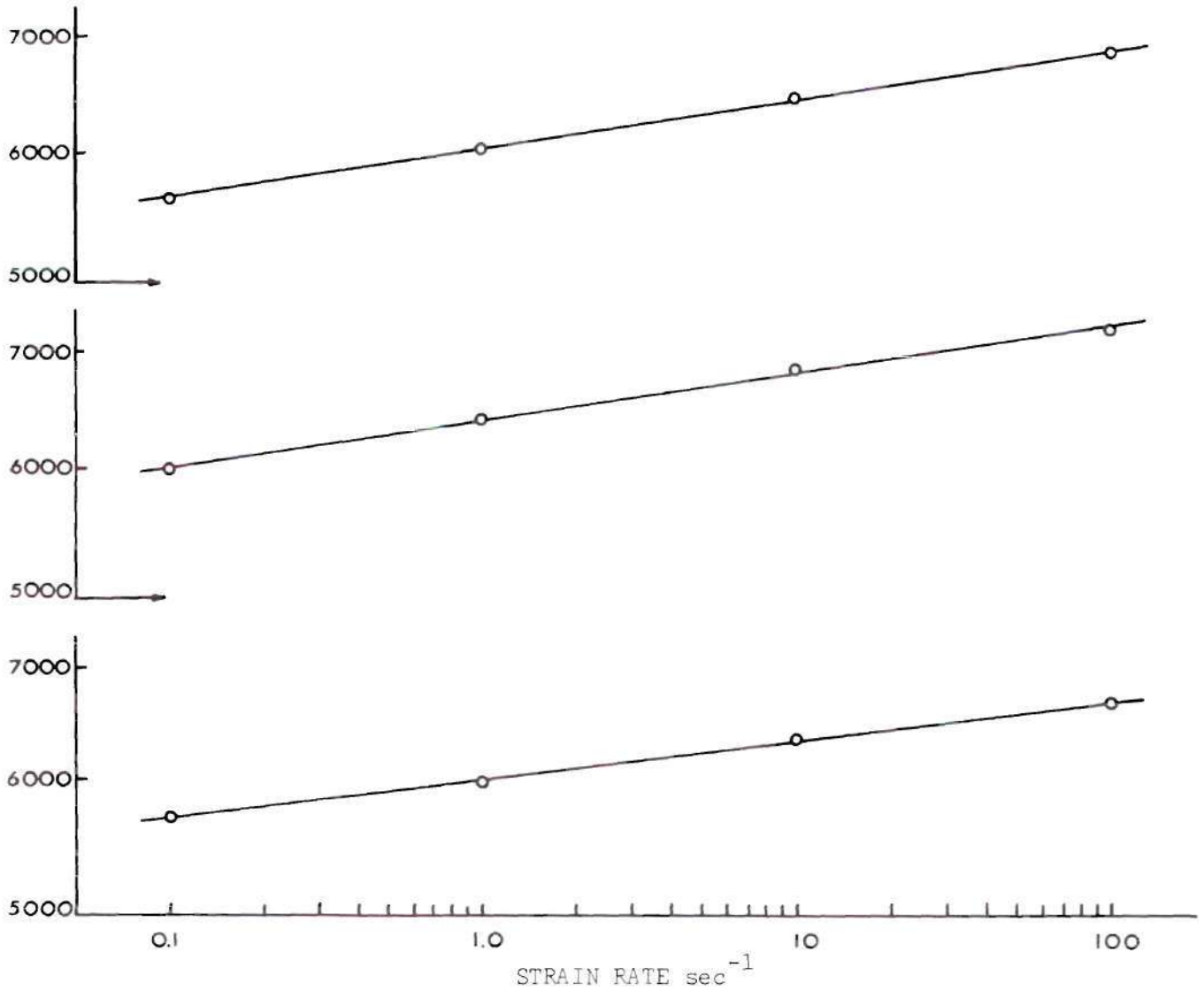

Figure 34. Variation of C_1 with Strain Rate

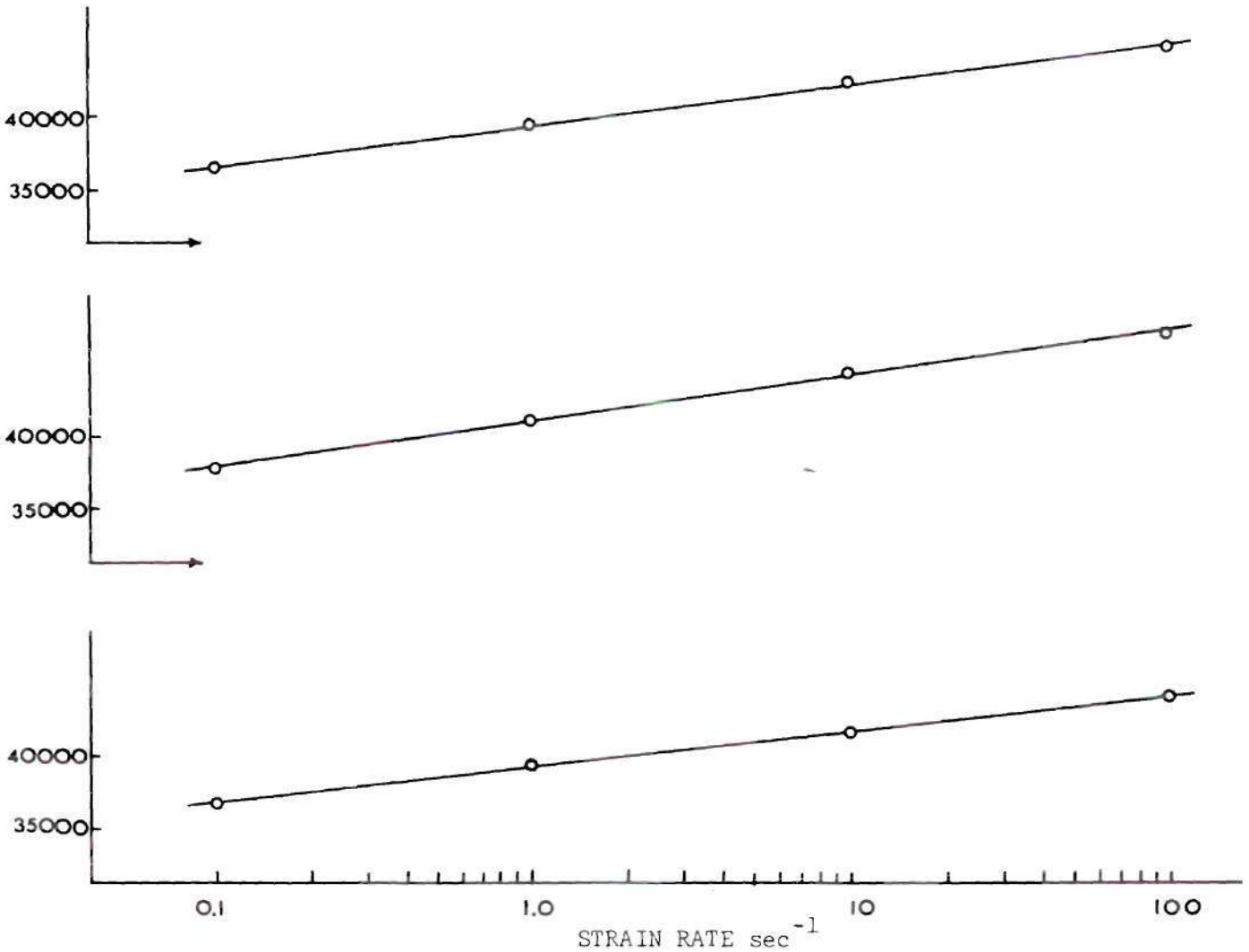

Figure 35. Variation of C_2 with Steam Rate

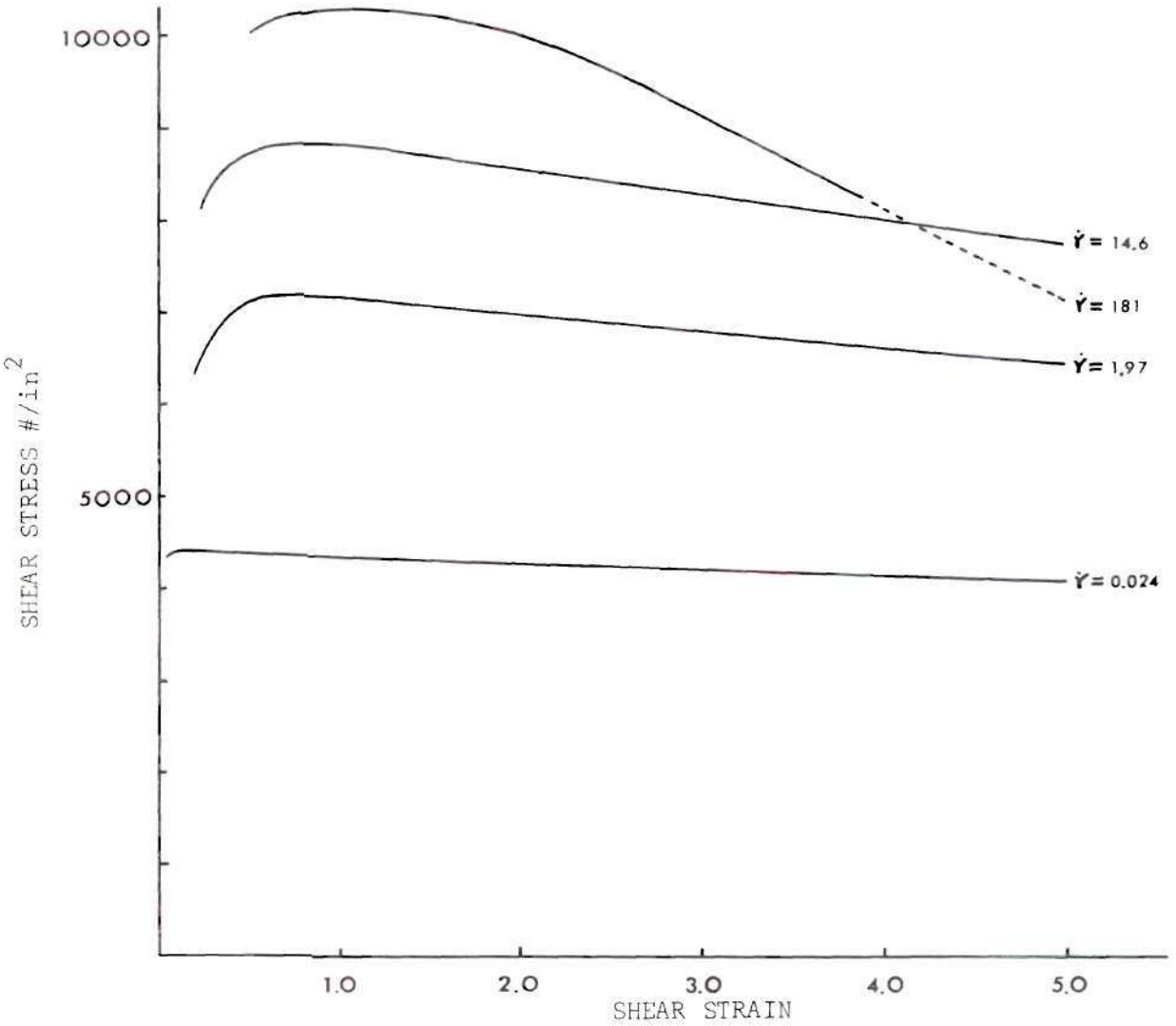

Figure 36. Shear Stress vs. Shear Strain for the 2017-0 Alloy at T = 350°C

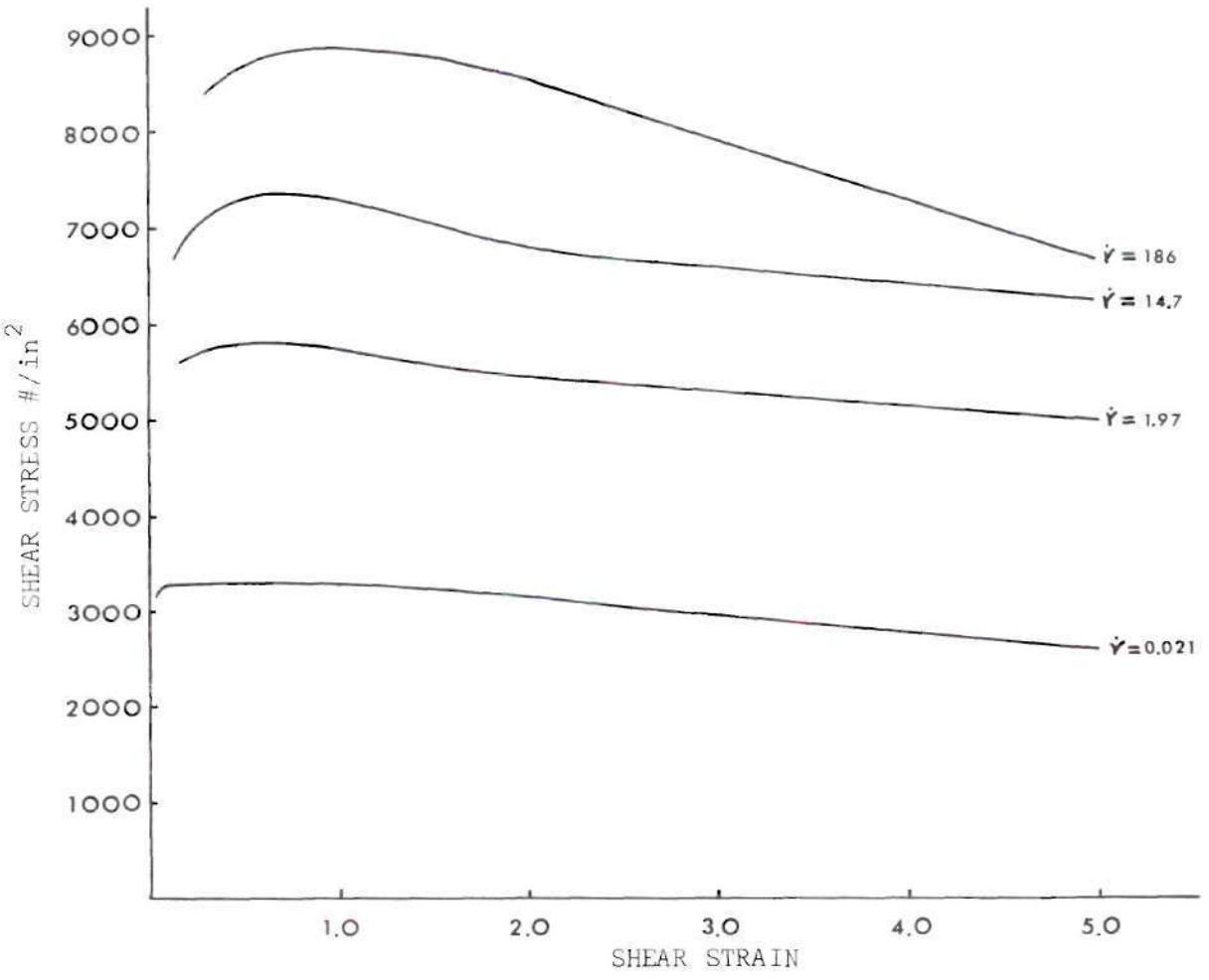

Figure 37. Shear Stress vs. Shear Strain for the 2017-0 Alloy at T = 400°C

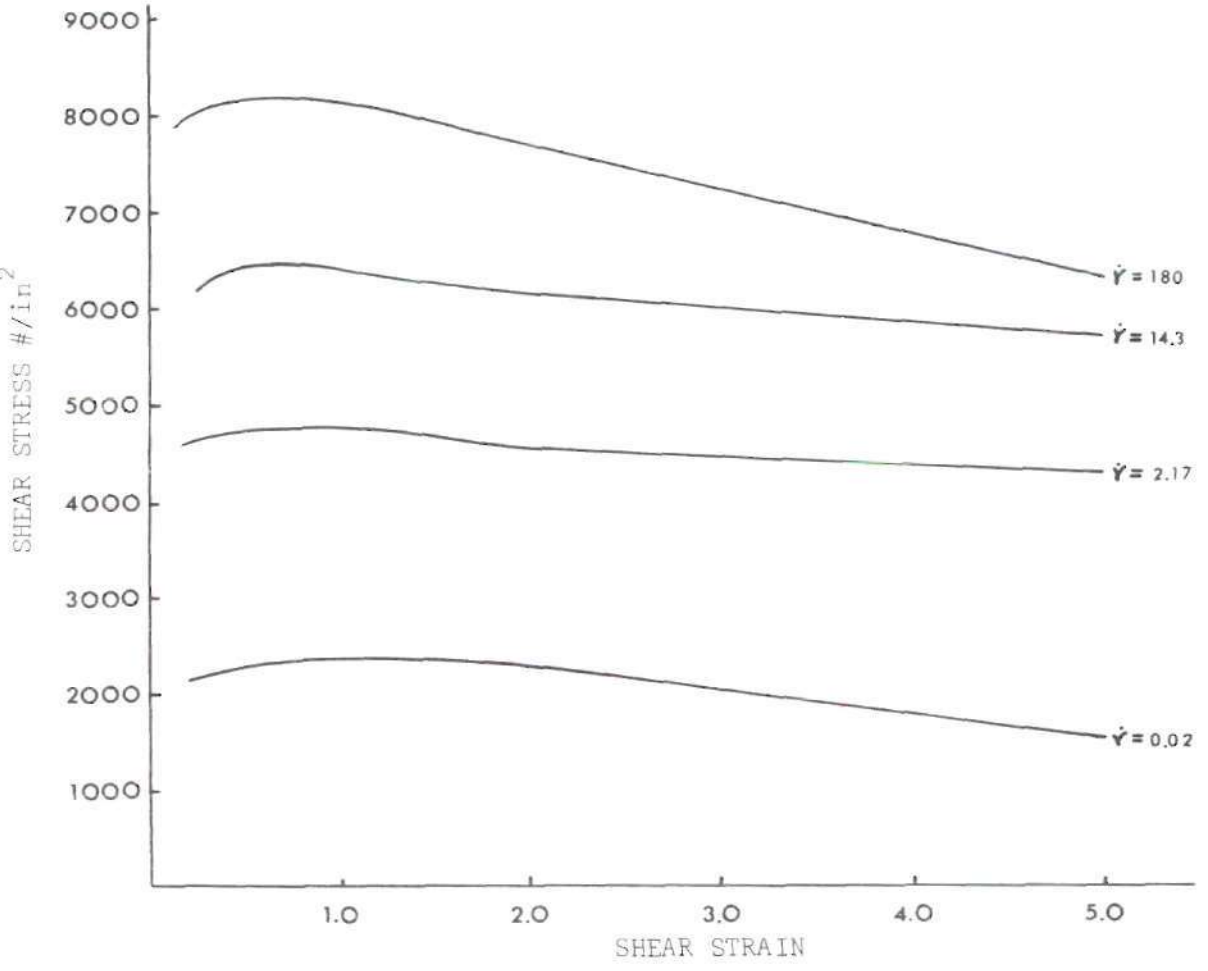

Figure 38. Shear Stress vs. Shear Strain for the 2017-0 Alloy at T = 450°C

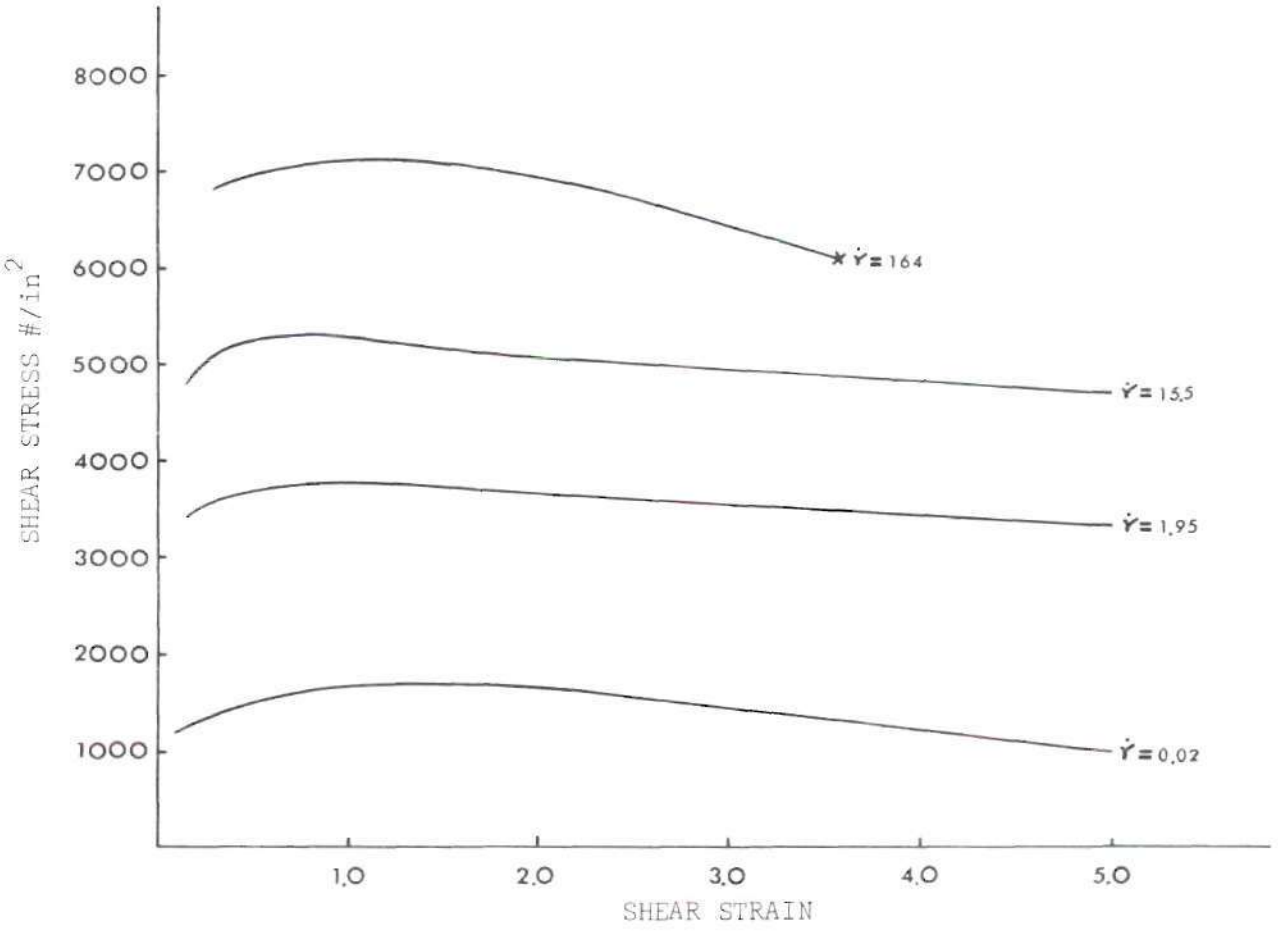

Figure 39. Shear Stress vs. Shear Strain for the 2017-0 Alloy at T = 500°C

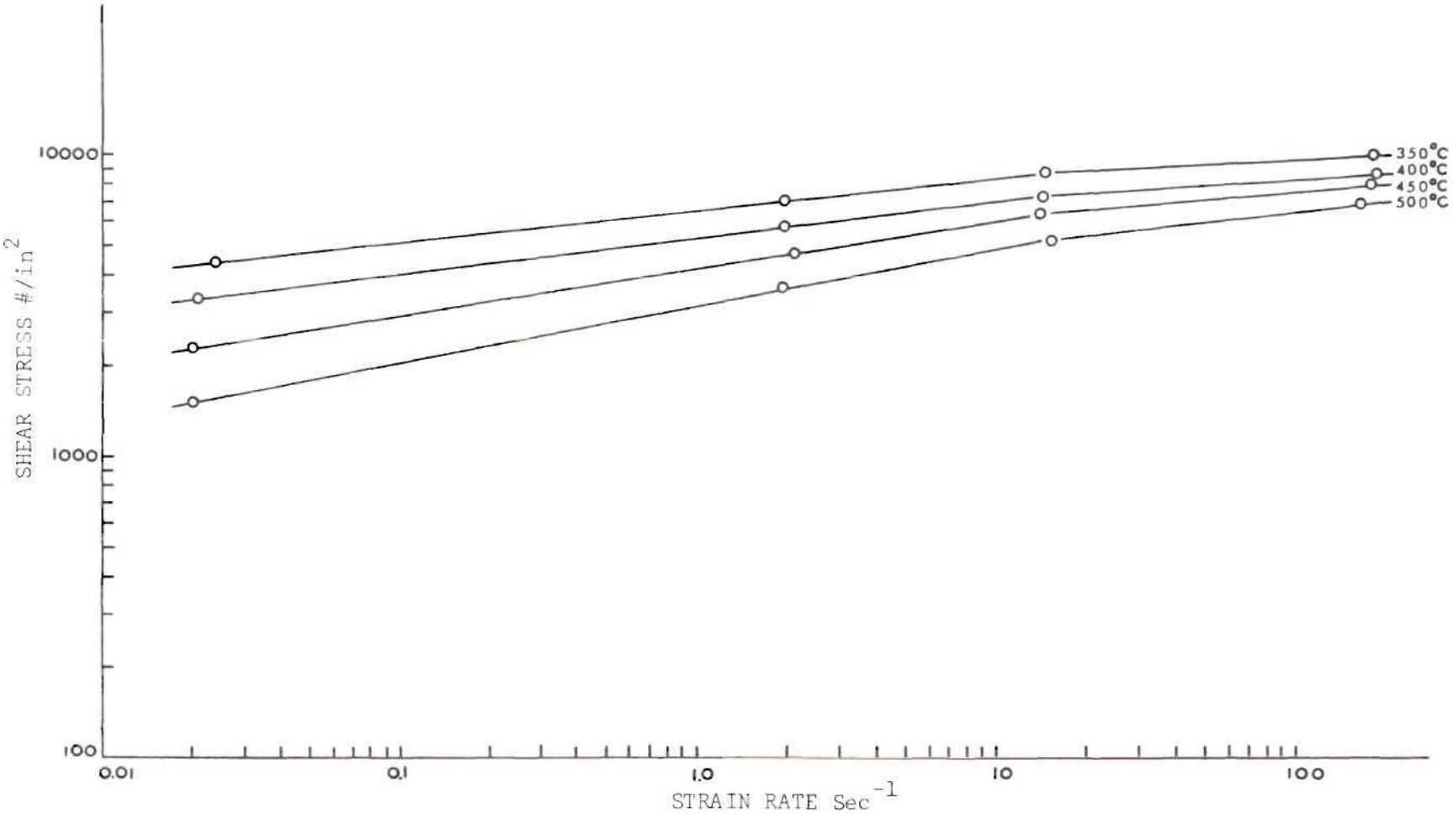

Figure 40. Shear Stress vs. Strain Rate for the 2017-0 Alloy at γ = 0.5.

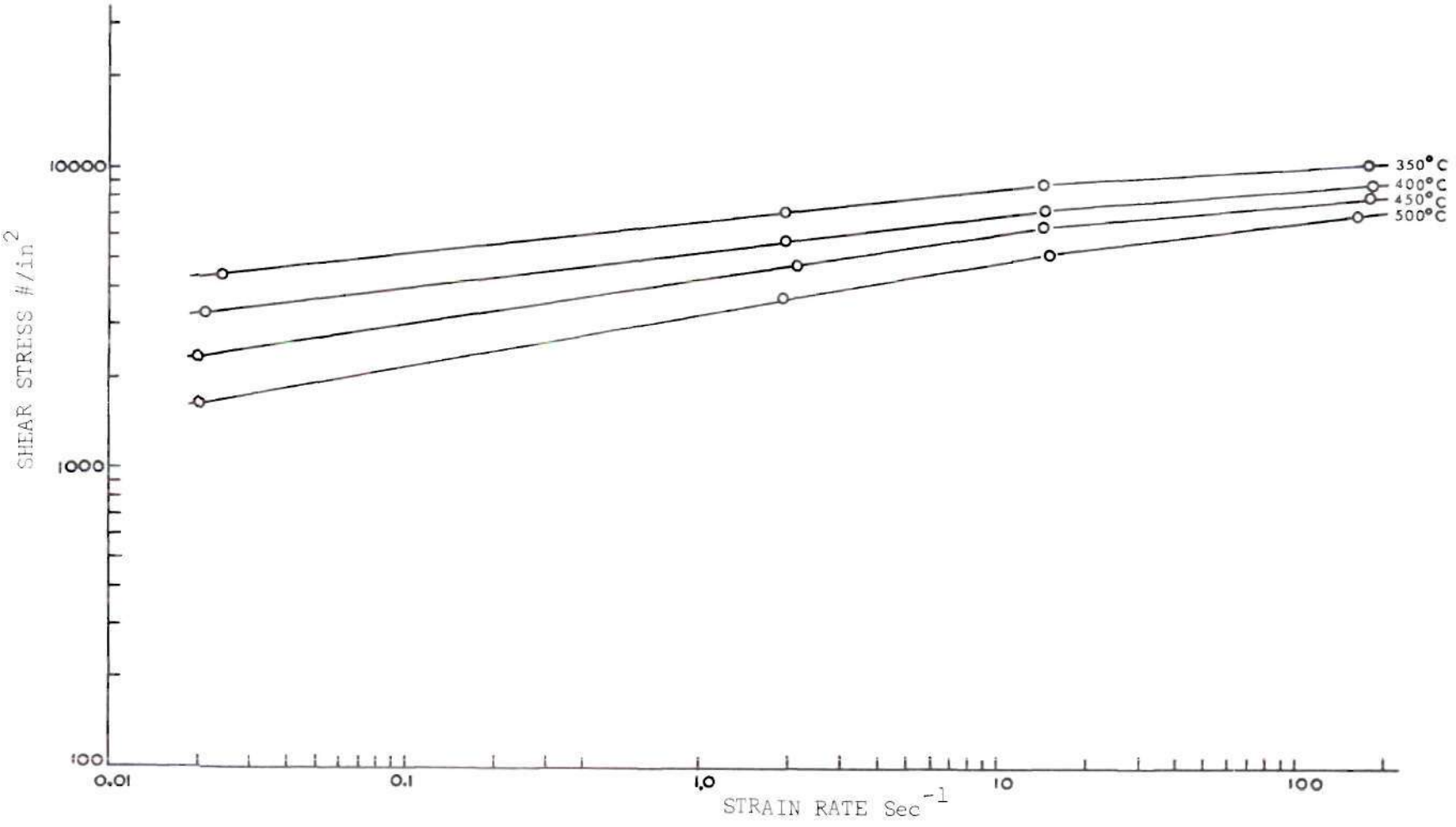

Figure 41. Shear Stress vs. Strain Rate for the 2017-0 Alloy at γ = 1.0

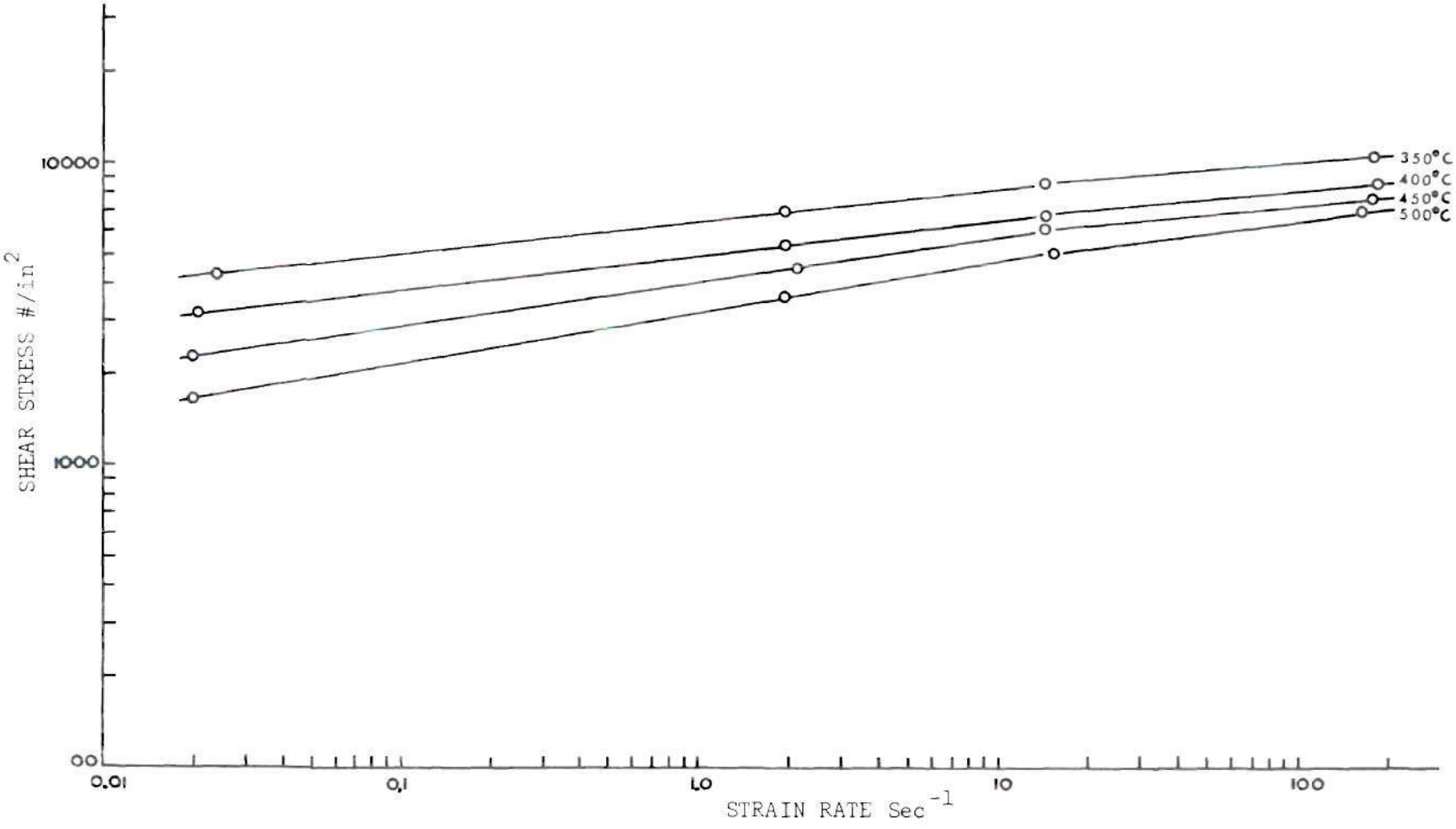

Figure 42. Shear Stress vs. Strain Rate for the 2017-0 Alloy at γ = 2.0

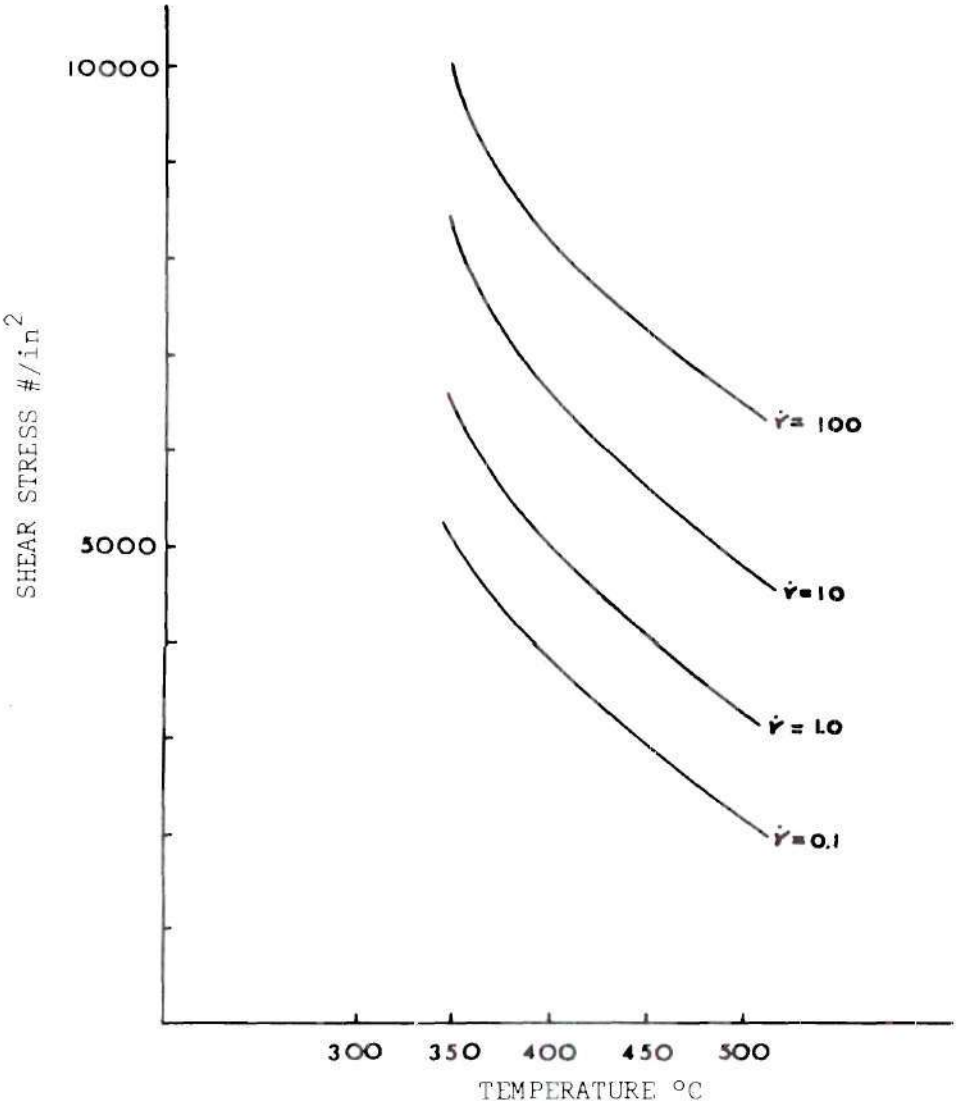

Figure 43. Effect of Temperature on the Shearing Stress for 2017-0

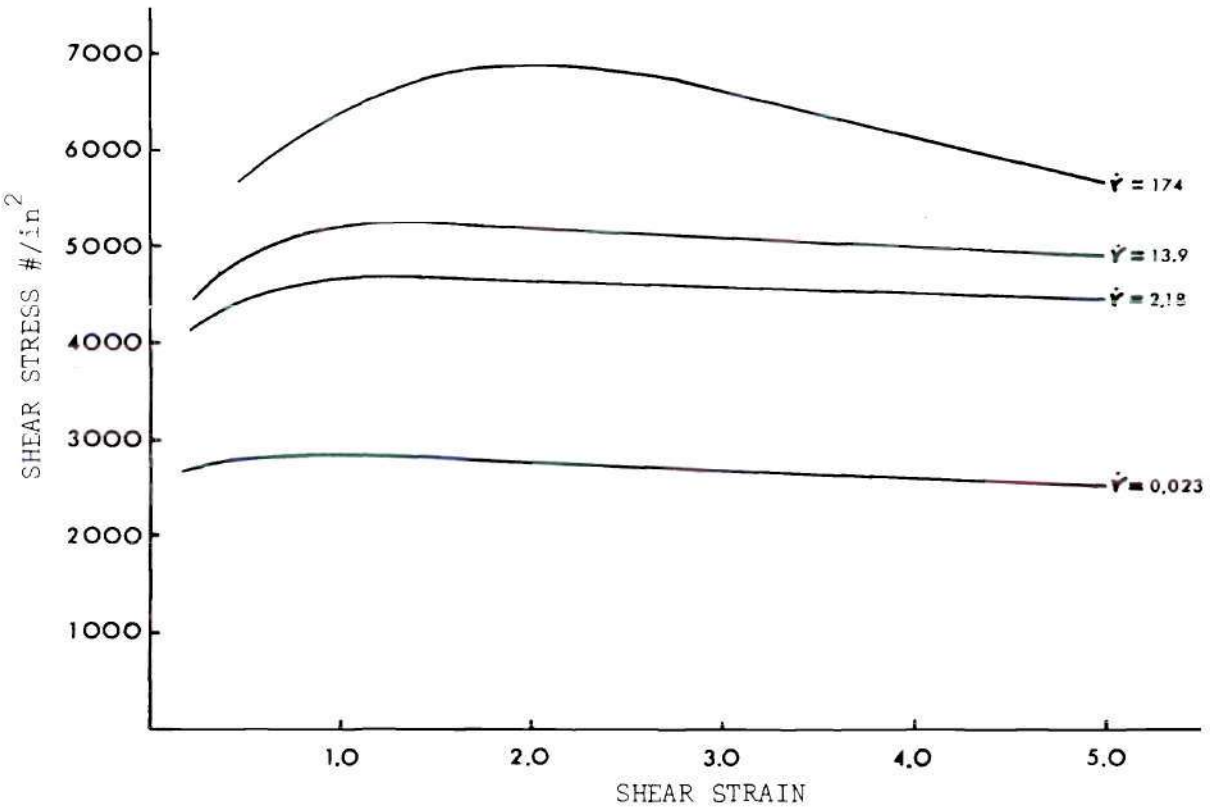

Figure 44. Shear Stress vs. Shear Strain for the 6061-0 Alloy at T = 350°C

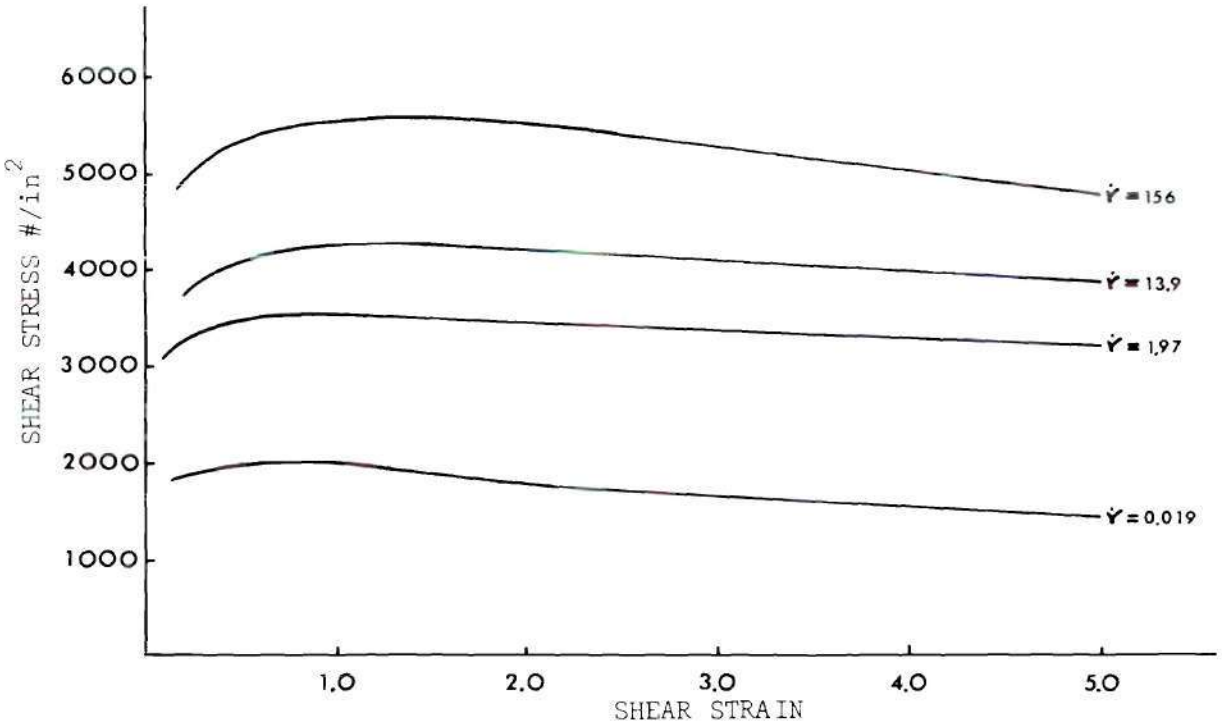

Figure 45. Shear Stress vs. Shear Strain for the 6061-0 Alloy at T = 400°C

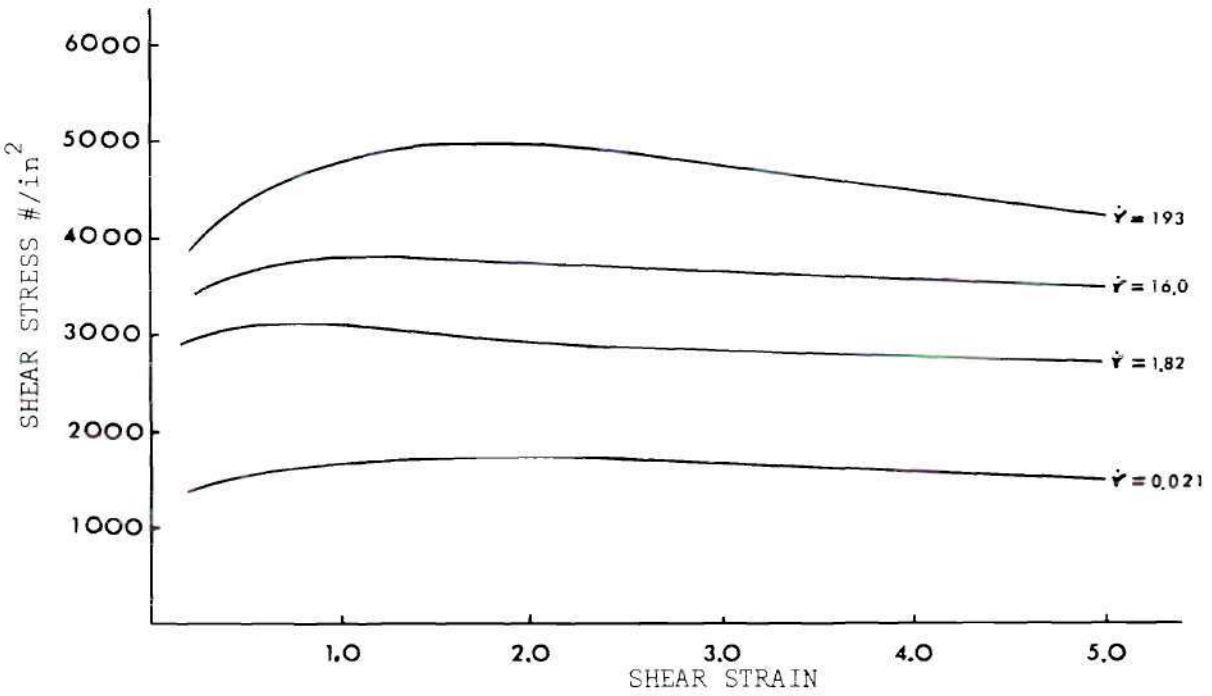

Figure 46. Shear Stress vs. Shear Strain for the 6061-0 Alloy at T = 450°C

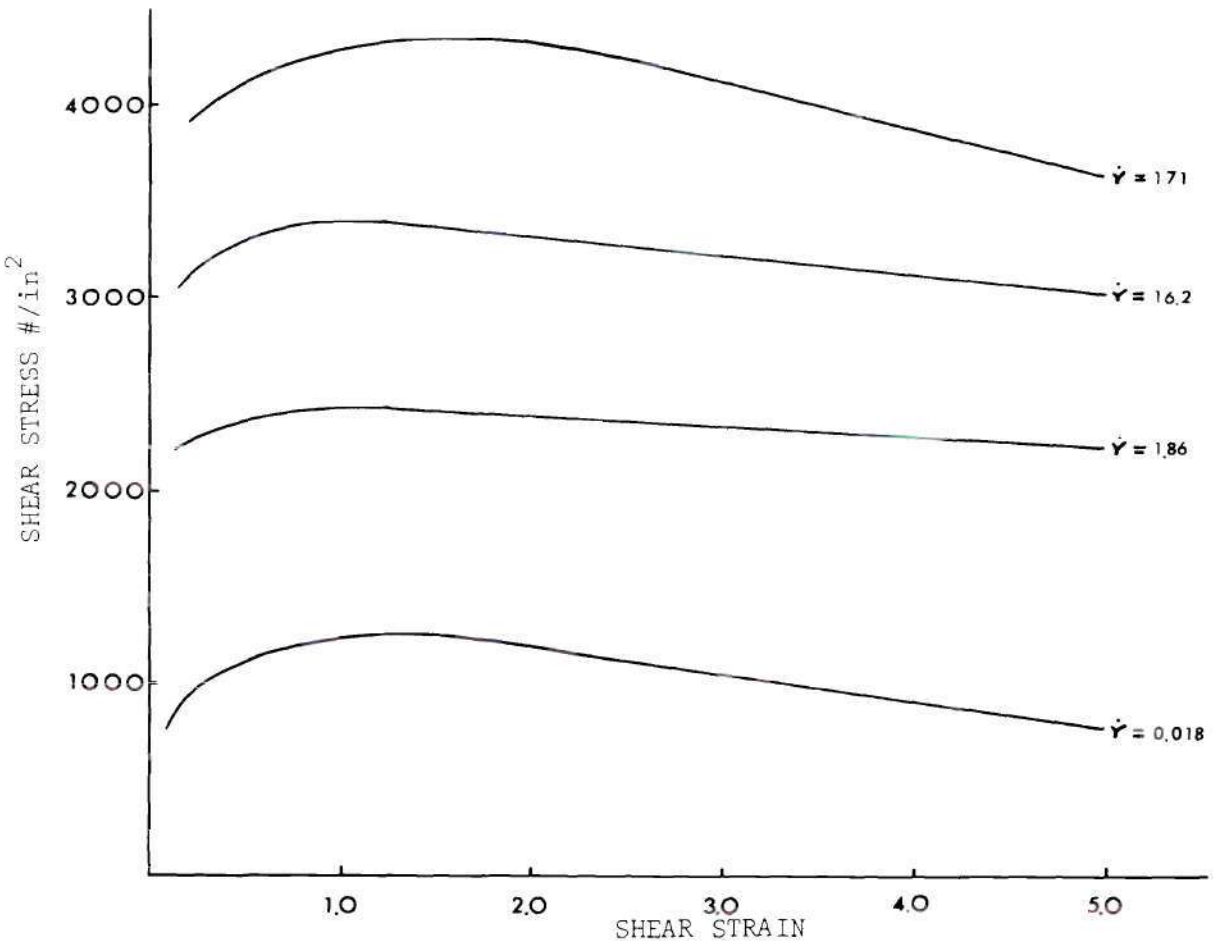

Figure 47. Shear Stress vs. Shear Strain for the 6061-0 Alloy at T = 500°C

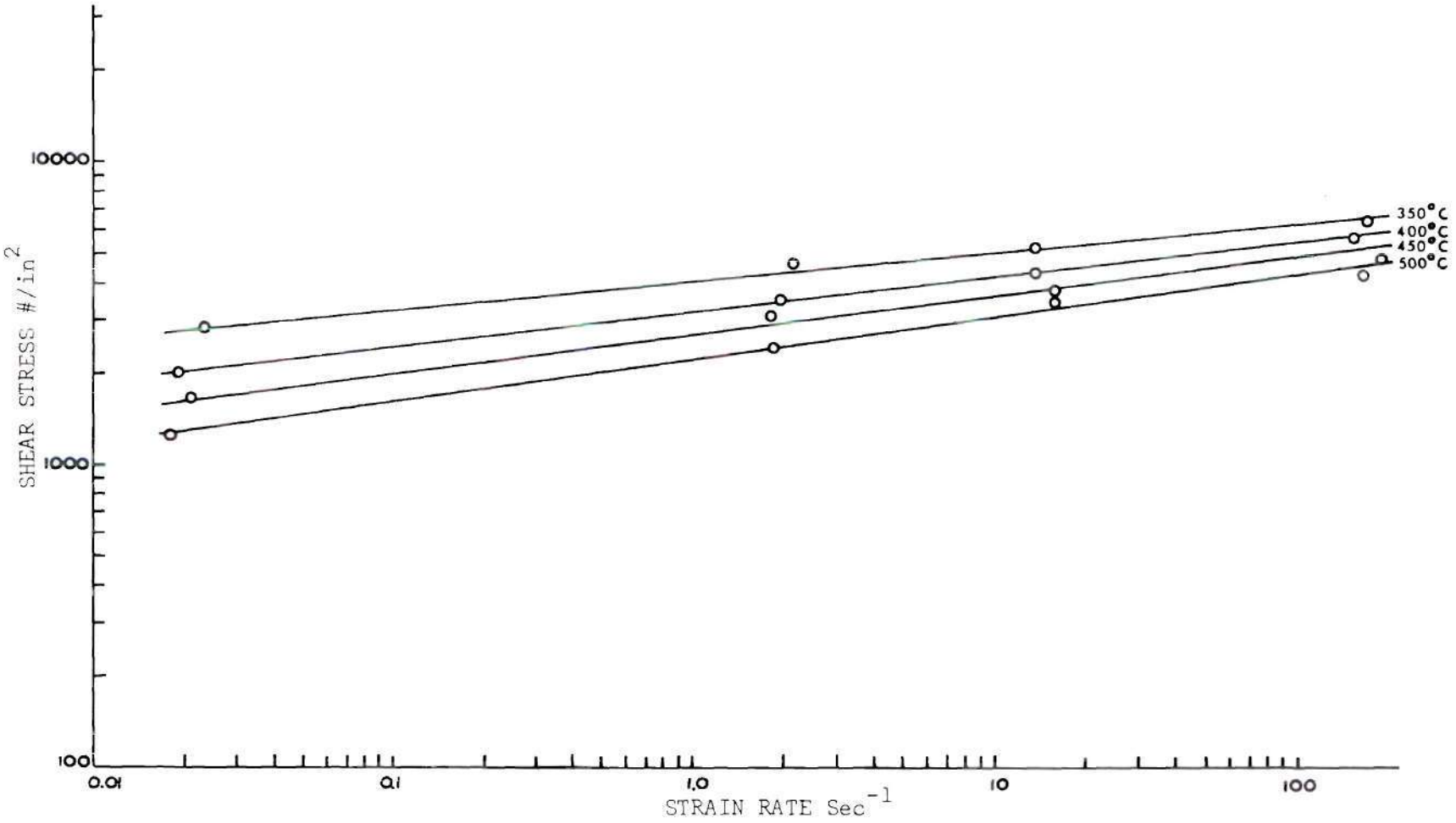

Figure 48. Shear Stress vs. Strain Rate for the 6061-0 Alloy at γ = 1.0

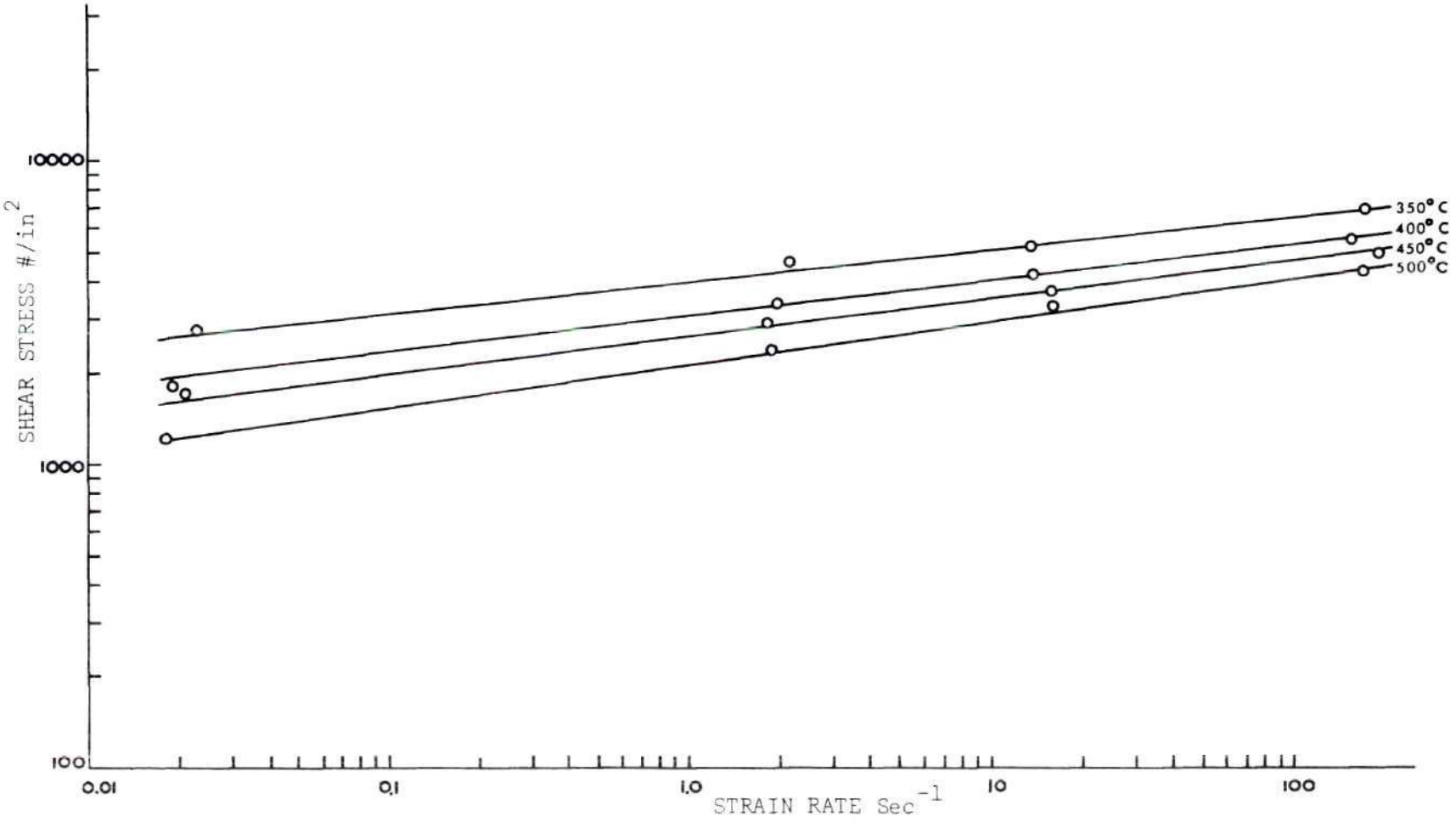

Figure 49. Shear Stress vs. Strain Rate for the 6061-0 Alloy at γ = 2.0

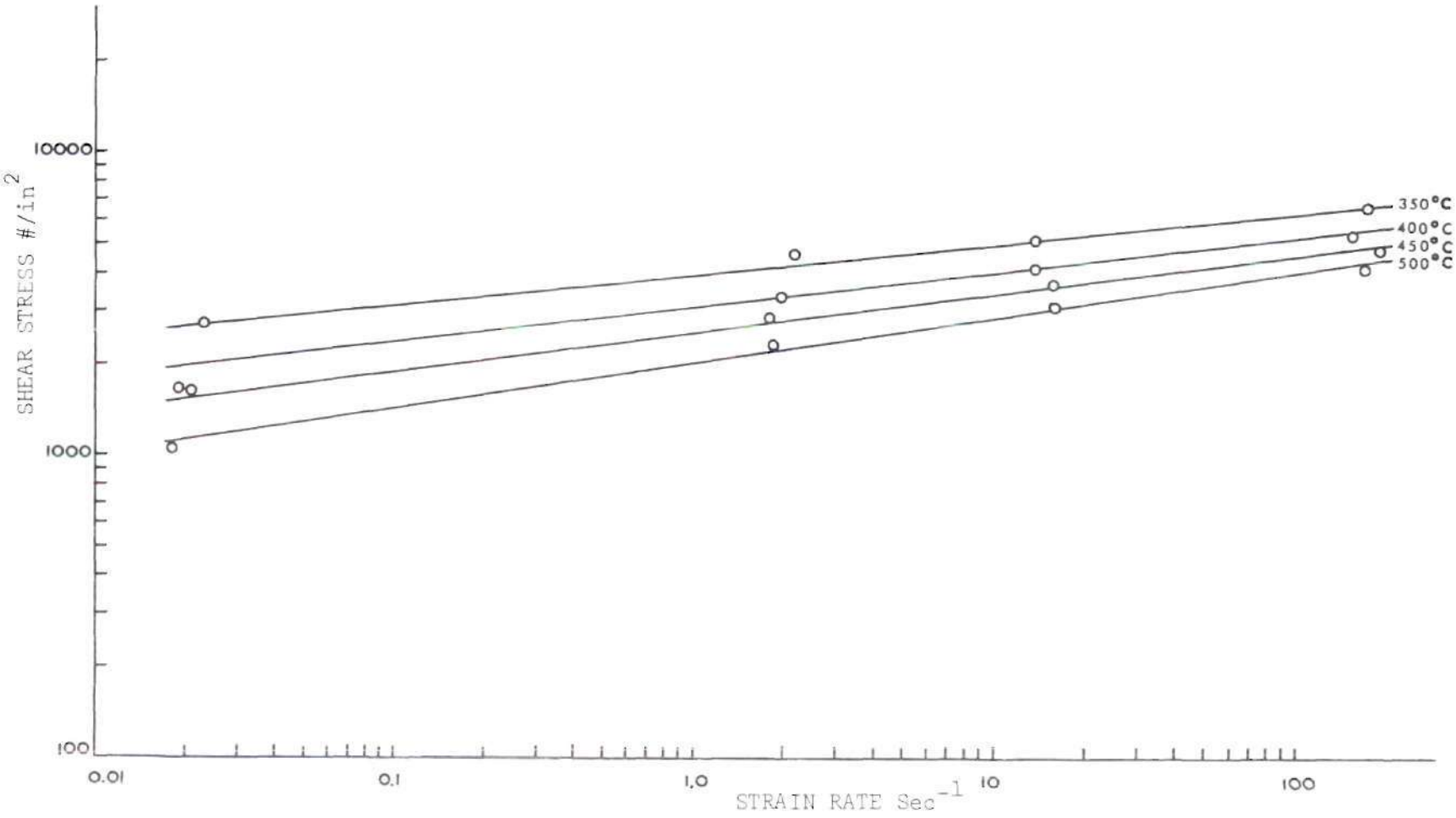

Figure 50. Shear Stress vs. Strain Rate for the 6061-0 Alloy at γ = 3.0

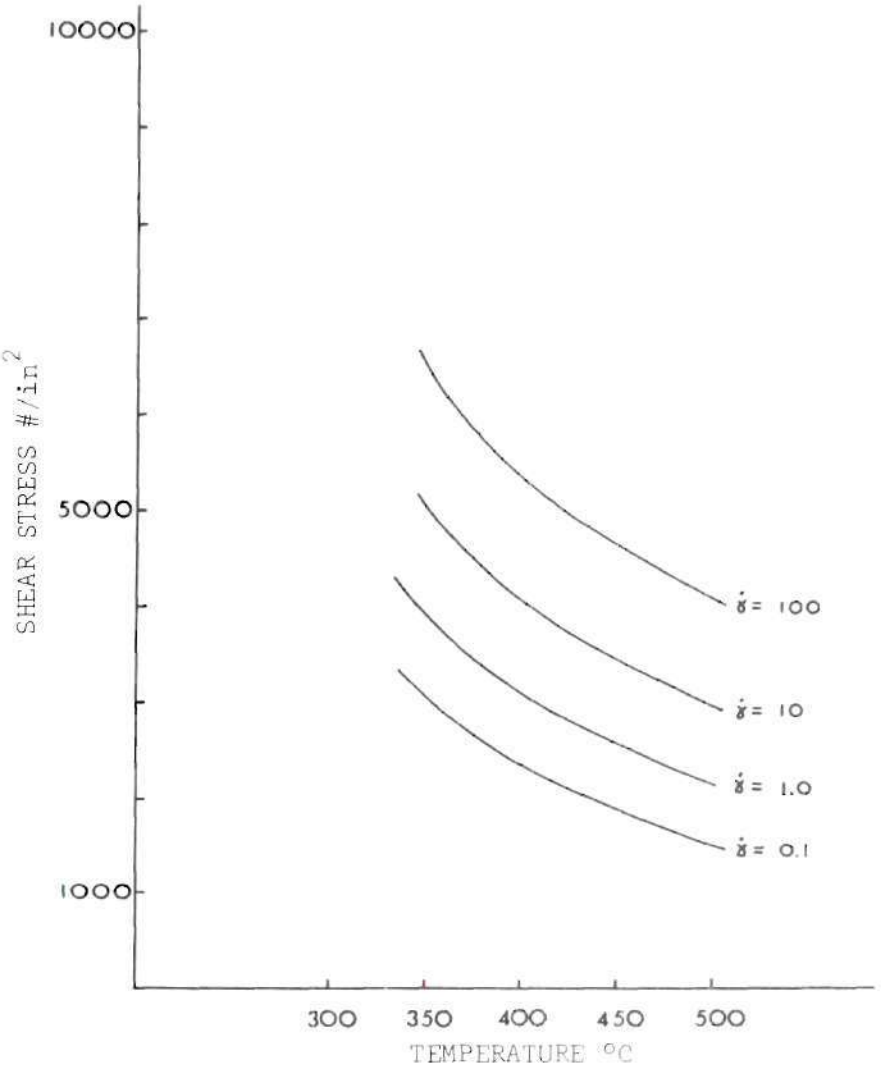

Figure 51. Effect of Temperature on the Shearing Stress for 6061-0 Aluminum

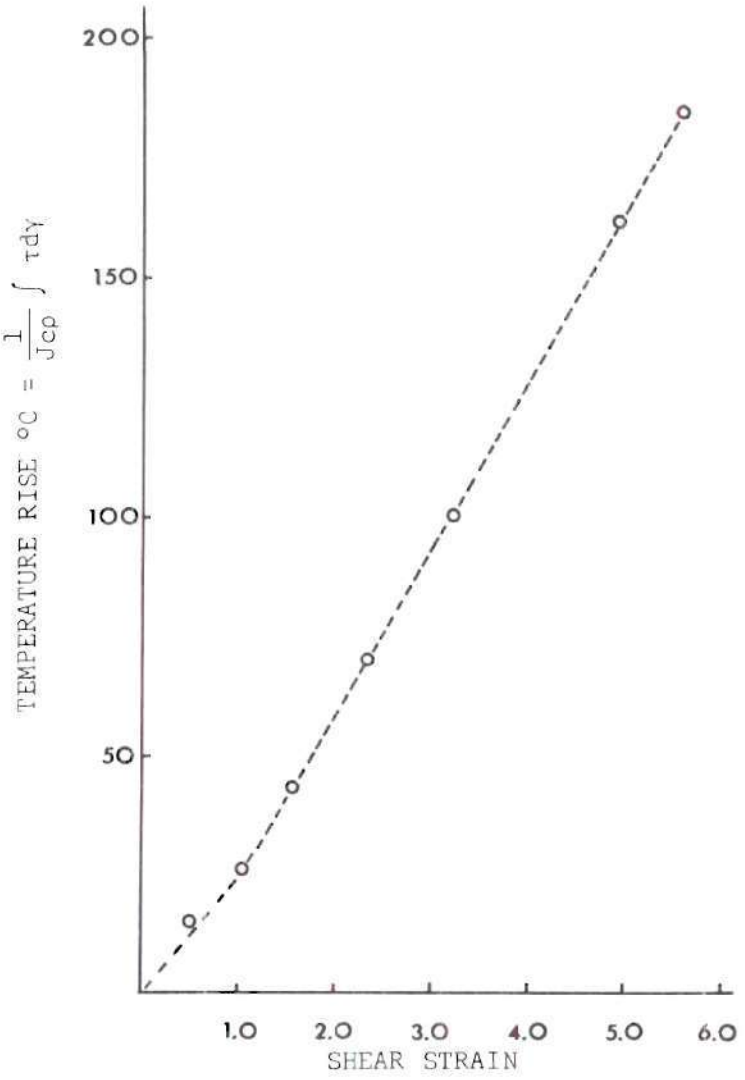

Figure 52. Calculated Temperature Rise vs. Shear Strain for an 1100-0 Aluminum Specimen

APPENDIX B

COMPUTER PROGRAM

```
COMMENT     ANISOTROPIC TORSION PROBLEM   S L HAAS
FILE OUT    SLH 16(2,15)
INTEGER     J
REAL        K,PSI,GAMMA,SINPHI,COSPHI,DPHI,GH,FH,N,BETA,TANPSI,
            TANA,TANBETA
ARRAY       PHI[0:100]
FORMAT      FMT1(X3,"GAMMA",X3,"PHI",X4,"DPHI/DGAMMA",X3,"BETA",X4,

            "2(G+2H)×T*2",X2,"2(F+2H)×T*2",X3,"2N×T*2"/),
            FMT2(X2,F5.1,X1,F9.5,X1,F10.7,X1,F10.7,X2,F10.7,X2,F10.7,
            X2,F10.7)
            WRITE (SLH,FMT1)

            K←-0.070
            J←1
            FOR GAMMA←0.1 STEP 0.1 UNTIL 10.0 DO
  BEGIN
            PSI←ARCTAN(2/GAMMA)
            TANPSI←SIN(PSI)/COS(PSI)
            SINPHI←SIN(PSI/2)/SQRT(1+((2×(1/TANPSI)×SIN(PSI/2))*2)
            -(2×COS(PSI)))
            COSPHI  ←SQRT(1-((SINPHI)*2))
            PHI[J]←ARCTAN(SINPHI/COSPHI)
            TANA ←SIN(2×PHI[J])/COS(2×PHI[J])
            DPHI←-(2/((GAMMA*2)+4))×(1/SQRT(1-(SINPHI*2)))
            ×(((0.5)×((SQRT(1+((2×(SIN(PSI/2)/TANPSI))*2)-2×COS(PSI))
            ×COS(PSI/2))-(SIN(PSI/2)×(1/SQRT(1+((2×(SIN(PSI/2)/TANPSI))
            *2)-2×COS(PSI)))×(4×(SIN(PSI/2)/TANPSI)×(((TANPSI
            ×COS(PSI/2))-(2×SIN(PSI/2)/(COS(PSI)*2)))/(TANPSI*2))
            +2×SIN(PSI)))))/(1+((2×SIN(PSI/2)/TANPSI)*2)
            -2×COS(PSI)))
            BETA←ARCTAN(-1/( 9×K×(COS(PHI[J]×2)*2)×SIN(PHI[J]×2)×DPHI))
            TANBETA←SIN(BETA)/COS(BETA)
            GH←1+((1/TANA)×(1/TANBETA))  +(3×K×(COS(2×PHI[J])
            *2)×DPHI)
            FH←1+((1/TANA)×(1/TANBETA))  -(3×K×(COS(2×PHI[J])
            *2)×DPHI)
            N← 1.0 - ((TANA × COS(BETA))/SIN(BETA))
            PHI[J]←PHI[J]×57.29578
            WRITE (SLH,FMT2,GAMMA,PHI[J],DPHI,BETA,GH,FH,N)
            J←J+1
  END
  END.
```

GAMMA	PHI	DPHI/DGAMMA	BETA	2(G+2H)×T*2	2(F+2H)×T*2	2N×T*2
0.1	46.43120	0.2493766	1.5704050	0.9998498	1.0001110	1.0078260
0.2	47.85530	0.2475248	1.5692600	0.9993317	1.0003610	1.0153630
0.3	49.26538	0.2444988	1.5674443	0.9983674	1.0006270	1.0223467
0.4	50.65497	0.2403846	1.5650848	0.9969161	1.0007992	1.0285580
0.5	52.01812	0.2352941	1.5623372	0.9949786	1.0007917	1.0338375
0.6	53.34962	0.2293578	1.5593692	0.9925948	1.0005486	1.0380922
0.7	54.64502	0.2227171	1.5563446	0.9898374	1.0000457	1.0412936
0.8	55.90071	0.2155172	1.5534098	0.9868021	0.9992873	1.0434706
0.9	57.11387	0.2079002	1.5506853	0.9835967	0.9983010	1.0446972
1.0	58.28253	0.2000000	1.5482606	0.9803302	0.9971302	1.0450791
1.1	59.40540	0.1919386	1.5461941	0.9771049	0.9958272	1.0447403
1.2	60.48188	0.1838235	1.5445157	0.9740096	0.9944464	1.0438111
1.3	61.51193	0.1757469	1.5432308	0.9711161	0.9930396	1.0424193
1.4	62.49601	0.1677852	1.5423259	0.9684780	0.9916526	1.0406830
1.5	63.43495	0.1600000	1.5417741	0.9661312	0.9903232	1.0387072
1.6	64.32990	0.1524390	1.5415395	0.9640953	0.9890804	1.0365815
1.7	65.18227	0.1451379	1.5415819	0.9623764	0.9879451	1.0343796
1.8	65.99361	0.1381215	1.5418597	0.9609694	0.9869301	1.0321608
1.9	66.76560	0.1314060	1.5423321	0.9598612	0.9860422	1.0299704
2.0	67.50000	0.1250000	1.5429612	0.9590327	0.9852827	1.0278423
2.1	68.19859	0.1189061	1.5437123	0.9584610	0.9846486	1.0258006
2.2	68.86316	0.1131222	1.5445550	0.9581214	0.9841344	1.0238612
2.3	69.49546	0.1076426	1.5454629	0.9579884	0.9837322	1.0220338
2.4	70.09722	0.1024590	1.5464136	0.9580367	0.9834331	1.0203230
2.5	70.67010	0.0975610	1.5473885	0.9582423	0.9832274	1.0187297
2.6	71.21570	0.0929368	1.5483723	0.9585824	0.9831053	1.0172521
2.7	71.73557	0.0885740	1.5493528	0.9590363	0.9830572	1.0158865
2.8	72.23116	0.0844595	1.5503203	0.9595851	0.9830739	1.0146278
2.9	72.70386	0.0805802	1.5512672	0.9602116	0.9831468	1.0134700
3.0	73.15497	0.0769231	1.5521881	0.9609010	0.9832679	1.0124069
3.1	73.58573	0.0734754	1.5530788	0.9616400	0.9834299	1.0114319
3.2	73.99731	0.0702247	1.5539365	0.9624169	0.9836264	1.0105384
3.3	74.39080	0.0671592	1.5547593	0.9632219	0.9838513	1.0097203
3.4	74.76723	0.0642674	1.5555463	0.9640462	0.9840996	1.0089713
3.5	75.12756	0.0615385	1.5562972	0.9648827	0.9843667	1.0082858
3.6	75.47270	0.0589623	1.5570121	0.9657250	0.9846485	1.0076584
3.7	75.80349	0.0565291	1.5576916	0.9665679	0.9849416	1.0070841
3.8	76.12073	0.0542299	1.5583365	0.9674071	0.9852430	1.0065582
3.9	76.42516	0.0520562	1.5589479	0.9682389	0.9855500	1.0060764
4.0	76.71748	0.0500000	1.5595270	0.9690604	0.9858604	1.0056349
4.1	76.99833	0.0480538	1.5600752	0.9698692	0.9861724	1.0052300
4.2	77.26833	0.0462107	1.5605937	0.9706633	0.9864843	1.0048586
4.3	77.52805	0.0444642	1.5610841	0.9714412	0.9867947	1.0045175
4.4	77.77802	0.0428082	1.5615476	0.9722019	0.9871026	1.0042041
4.5	78.01876	0.0412371	1.5619857	0.9729443	0.9874070	1.0039159
4.6	78.25072	0.0397456	1.5623998	0.9736679	0.9877072	1.0036507
4.7	78.47435	0.0383289	1.5627911	0.9743724	0.9880024	1.0034065
4.8	78.69007	0.0369822	1.5631610	0.9750574	0.9882923	1.0031814
4.9	78.89826	0.0357015	1.5635106	0.9757230	0.9885763	1.0029738
5.0	79.09930	0.0344828	1.5638411	0.9763692	0.9888543	1.0027821
5.1	79.29352	0.0333222	1.5641537	0.9769961	0.9891260	1.0026050
5.2	79.48125	0.0322165	1.5644493	0.9776040	0.9893913	1.0024412
5.3	79.66279	0.0311624	1.5647291	0.9781932	0.9896499	1.0022896
5.4	79.83843	0.0301568	1.5649938	0.9787640	0.9899020	1.0021491
5.5	80.00845	0.0291971	1.5652444	0.9793169	0.9901475	1.0020189
5.6	80.17309	0.0282805	1.5654818	0.9798522	0.9903864	1.0018981
5.7	80.33260	0.0274048	1.5657067	0.9803704	0.9906187	1.0017858
5.8	80.48720	0.0265675	1.5659199	0.9808721	0.9908446	1.0016815
5.9	80.63711	0.0257666	1.5661221	0.9813576	0.9910641	1.0015845
6.0	80.78253	0.0250000	1.5663138	0.9818274	0.9912774	1.0014942

6.1	80.92365	0.0242660	1.5664958	0.9822821	0.9914846	1.0014100
6.2	81.06065	0.0235627	1.5666686	0.9827221	0.9916857	1.0013315
6.3	81.19371	0.0228885	1.5668327	0.9831479	0.9918810	1.0012583
6.4	81.32299	0.0222420	1.5669886	0.9835600	0.9920706	1.0011899
6.5	81.44864	0.0216216	1.5671369	0.9839589	0.9922546	1.0011260
6.6	81.57080	0.0210261	1.5672779	0.9843449	0.9924332	1.0010662
6.7	81.68962	0.0204541	1.5674120	0.9847186	0.9926065	1.0010102
6.8	81.80523	0.0199045	1.5675397	0.9850804	0.9927747	1.0009578
6.9	81.91775	0.0193761	1.5676614	0.9854307	0.9929380	1.0009087
7.0	82.02730	0.0188679	1.5677772	0.9857699	0.9930964	1.0008626
7.1	82.13400	0.0183790	1.5678877	0.9860985	0.9932502	1.0008193
7.2	82.23795	0.0179083	1.5679930	0.9864167	0.9933994	1.0007787
7.3	82.33925	0.0174551	1.5680935	0.9867250	0.9935443	1.0007405
7.4	82.43800	0.0170184	1.5681894	0.9870238	0.9936849	1.0007046
7.5	82.53429	0.0165975	1.5682810	0.9873133	0.9938215	1.0006708
7.6	82.62822	0.0161917	1.5683684	0.9875940	0.9939540	1.0006389
7.7	82.71986	0.0158003	1.5684520	0.9878661	0.9940828	1.0006089
7.8	82.80930	0.0154226	1.5685319	0.9881299	0.9942078	1.0005806
7.9	82.89662	0.0150580	1.5686084	0.9883858	0.9943292	1.0005539
8.0	82.98188	0.0147059	1.5686815	0.9886341	0.9944472	1.0005287
8.1	83.06516	0.0143658	1.5687515	0.9888749	0.9945618	1.0005049
8.2	83.14652	0.0140371	1.5688185	0.9891086	0.9946732	1.0004824
8.3	83.22603	0.0137193	1.5688827	0.9893355	0.9947814	1.0004611
8.4	83.30375	0.0134120	1.5689442	0.9895558	0.9948866	1.0004410
8.5	83.37974	0.0131148	1.5690032	0.9897696	0.9949889	1.0004219
8.6	83.45405	0.0128271	1.5690598	0.9899773	0.9950883	1.0004038
8.7	83.52675	0.0125486	1.5691140	0.9901791	0.9951850	1.0003867
8.8	83.59787	0.0122790	1.5691661	0.9903752	0.9952790	1.0003705
8.9	83.66747	0.0120178	1.5692161	0.9905657	0.9953705	1.0003551
9.0	83.73560	0.0117647	1.5692642	0.9907509	0.9954595	1.0003405
9.1	83.80230	0.0115194	1.5693103	0.9909309	0.9955462	1.0003266
9.2	83.86761	0.0112816	1.5693546	0.9911060	0.9956304	1.0003134
9.3	83.93159	0.0110509	1.5693973	0.9912763	0.9957125	1.0003009
9.4	83.99426	0.0108272	1.5694383	0.9914419	0.9957924	1.0002889
9.5	84.05567	0.0106101	1.5694777	0.9916031	0.9958702	1.0002776
9.6	84.11586	0.0103993	1.5695157	0.9917599	0.9959459	1.0002668
9.7	84.17485	0.0101947	1.5695522	0.9919126	0.9960197	1.0002565
9.8	84.23269	0.0099960	1.5695874	0.9920612	0.9960916	1.0002467
9.9	84.28941	0.0098030	1.5696213	0.9922059	0.9961617	1.0002374
10.0	84.34503	0.0096154	1.5696540	0.9923468	0.9962300	1.0002285

BIBLIOGRAPHY

BIBLIOGRAPHY

1. P. Ludwik, *Elements der Technologischm Mechanik*, J. Springer, Berlin, 1909, p. 44.

2. L. A. Prandtl, *Zeitschrift für Angewandte Mathematik und Mechanik*, 1928, p. 85.

3. E. Meyer, "Der Verlauf des Zugversuches bei raschem Zerreissen," *Forschungsarbeiten, des Vereines deutscher Ingenieure*, No. 295 (Carl von Bach commemorative volume), 1927, pp. 62-73.

4. J. Weerts, "Dynamische und Statische Zugversuche an Aluminum Einzelkrystalen," Dissertation, Berlin, 1928.

5. F. Voeber, and H. Storp, "Über den Kraftverlauf bei der Schlagprüfung," *Mitteilungen des Kaiser Wilhelm Instituts für Eisenforschung*, Düsseldorf, Vol. 7, 1925, pp. 81-97.

6. J. L. M. Morrison, "The Influence of Rate of Strain in Tension Tests," *The Engineer*, August 24, 1934, Vol. 158, pp. 183-185.

7. C. F. Elam, "The Influence of Rate of Deformation on the Tensile Test with Special Reference to the Yield Point in Iron and Steel," *Proceedings of the Royal Society*, Vol. 165, 1938, pp. 568-591.

8. E. A. Davis, "The Effect of the Speed of Stretching and the Rate of Loading on the Yielding of Mild Steel," *Transactions, ASME*, Vol. 60, 1938, pp. A137-A140.

9. D. S. Clark, and G. Dätwyler, "Stress-Strain Relations under Tension Impact Loading," *Proceedings, ASTM*, 1938, Vol. 38, Part II, p. 98.

10. E. Honegger, "Schlagzerreissversuche an Aluminum und Kupfer," *Bericht 95, Eidgenössische Materialprufungsanstalt an der E.T.H.*, Zurich, April, 1935, pp. 1-11.

11. D. W. Ginns, "The Mechanical Properties of Some Metals and Alloys Broken at Ultra-High Speeds," *Journal of the Institute of Metals*, Vol. 61, 1937, pp. 61-78.

12. H. C. Mann, "High Velocity Tension-Impact Tests," *Proceedings, ASTM*, 1936, Vol. 36, Part II, p. 85.

13. Clark and Wood, "Tensile Impact Properties of Some Metals and Alloys," *Proceedings of the Western Metals Congress*, Los Angeles, California, 1949.

14. Abbe, "Determination of Yield Strengths of Engineering Materials at High Loading Rates," *Proceedings of the Conference on Dynamic Behavior of Materials and Structures*, Springfield Armory, 1962, U.S. Army Research Office, Durham, N. C.

15. Hammer and Cadle, "The Effect of High Rate Loading on Mechanical Properties," *Proceedings of the Conference on Dynamic Behavior of Materials and Structures*, Springfield Armory, 1962, U.S. Army Research Office, Durham, N.C.

16. P. P. Gillis, "Dislocation Dynamics and Strain Rate Effects," paper presented at 5th Intern. Symp. High Speed Testing, 1965.

17. K. G. Hoge, "The Effect of Strain Rate on Mechanical Properties of Some Widely-Used Engineering Materials," UCRL-14599, Livermore, California.

18. Campbell, "The Dynamic Yielding of Mild Steel," *Acta Metallurgica*, Vol. 1, November, 1953, pp. 706-710.

19. D. P. Kendall, and T. E. Davidson, "The Effect of Strain Rate on Yielding in High Strength Steels," ASME Paper No. 65-WA/Met-8.

20. D. S. Holt, S. G. Babcock, S. J. Green, and C. J. Maiden, "The Strain Rate Dependence of the Flow Stress in Some Aluminum Alloys," *Transactions of the ASM*, June, 1967, Vol. 60, No. 2, pp. 152-159.

21. M. Itihara, "Impact Torsion Test," *Technology Reports of the Tohoku Imperial University*, Reviewed in *Metallurgist*, Vol. 10, June, 1936, pp. 141-143.

22. A. Nadai, and M. J. Manjoine, "High Speed Tension Tests at Elevated Temperatures--Part I," *Proceedings, ASTM*, Vol. 40, 1940, pp. 822-837.

23. A. Nadai, and M. J. Manjoine, "High Speed Tension Tests at Elevated Temperatures--Parts II and III," *Journal of Applied Mechanics*, June, 1941, pp. A77-A85.

24. C. L. Clark, and J. Russ, "A Laboratory Evaluation of the Hot Working Characteristics of Metals," *Metals Technology*, Vol. 12, 1945, Technical Publication No. 1839.

25. H. K. Ihrig, "The Effect of Various Elements on the Hot Workability of Steel," *Metals Technology*, Vol. 12, 1945, Technical Publication, 1932.

26. F. K. Bloom, W. C. Clarke, Jr., and P. A. Jennings, "Relation of Structure of Stainless Steel to Hot Ductility," *Metal Progress*, Vol. 59, 1951, pp. 250-256.

27. D. E. R. Hughes, "The Hot Torsion Test for Assessing Hot-Working Properties of Steels," *Journal of the Iron and Steel Institute*, March, 1952, pp. 214-220.

28. C. Zener, and J. H. Hollomon, "Effect of Strain Rate on the Plastic Flow of Steel," *Journal of Applied Physics*, Vol. 15, 1944, pp. 22-32.

29. J. H. Bechtold, "Effects of Temperature on the Flow and Fracture Characteristics of Molybdenum," *Transactions of the AIME*, November, 1953, Vol. 197, pp. 1469-1475.

30. T. A. Trozera, O. D. Sherby, and J. E. Dorn, "Effect of Strain Rate and Temperature on the Plastic Deformation of High Purity Aluminum," *Transactions of the ASM*, 1957, Vol. 49, pp. 173-188.

31. D. S. Fields and W. A. Backofen, "Temperature and Rate Dependence of Strain Hardening in the Aluminum Alloy 2024-0," *Transactions of the ASM*, Vol. 51, 1959.

32. C. W. MacGregor, and J. C. Fisher, "A Velocity Modified Temperature for the Plastic Flow of Metals," *Journal of Applied Mechanics*, Vol. 13, 1946, pp. 11-16.

33. J. E. Dorn, A. Goldberg, and T. E. Tietz, "The Effect of Thermal Mechanical History on the Strain Hardening of Metals," *Metals Technology*, Vol. 15, September, 1948.

34. T. E. Tietz, and J. E. Dorn, "Cold Working of Metals," American Society for Metals, Metals Park, Ohio, 1949, pp. 163-179.

35. G. V. Smith, "Stress-Strain-Time-Temperature Relations in Metallic Materials," *Symposium on Stress-Strain-Time-Temperature Relationships in Materials*, ASTM Special Publication No. 325.

36. J. D. Lubahn, "Derivation of Stress, Strain, Temperature, Strain-Rate Relation for Plastic Deformation," *Journal of Applied Mechanics*, Vol. 14, 1947, pp. 229-230.

37. H. I. Fusfeld, "New Interpretation of the n-Power Law in Plastic Deformation," *Journal of Applied Physics*, Vol. 20, 1949, pp. 1052-1055.

38. J. R. Low, and F. Garofalo, "Precision Determination of Stress-Strain Curves in the Plastic Range," *Proceedings of the Society of Experimental Stress Analysis*, Vol. 4, No. 2A, 1947, pp. 16-24.

39. J. E. Dorn, P. Pietrokowsky, and T. E. Tietz, "The Effect of Alloying Elements on the Plastic Properties of Aluminum Alloys," *Transactions of the American Institute of Mining and Metallurgical Engineers*, Vol. 188, 1950, pp. 933-943.

40. O. D. Sherby, R. A. Anderson, and J. E. Dorn, "Effect of Alloying Elements on the Elevated Temperature Plastic Properties of Alpha Solid Solutions of Aluminum," *Transactions of the American Institute of Mining and Metallurgical Engineers*, Vol. 191, 1951, pp. 643.

41. J. F. Alder, and V. A. Phillips, "The Effect of Strain Rate and Temperature on the Resistance of Aluminum, Copper, and Steel to Compression," *Journal of the Institute of Metals*, Vol. 83, 1954-55, pp. 80-86.

42. L. D. Sokolov, *Zhur. Tekhn. Fiziki*, Vol. 16, 1946, p. 437.

43. L. D. Sokolov, *Zhur. Tekhn. Fiziki*, Vol. 17, 1947, p. 543.

44. L. D. Sokolov, *Zhur. Tekhn. Fiziki*, Vol. 18, 1948, p. 93.

45. L. D. Sokolov, *Doklady. Akad. Nauk. S.S.S.R.*, Vol. 70, 1950, p. 839.

46. C. E. Work, and T. J. Dolan, "The Influence of Temperature and Rate on the Properties of Metals in Torsion," *Bulletin Series 420*, Engineering Experiment Station, University of Illinois, November, 1953.

47. K. Fenk, W. Lueg, and G. Bürger, *1955 Archiv. für das Eisenhüttenweisen*, November, p. 655.

48. E. Orowan, *B.I.S.R.A. Restricted Report (MW/F/22/50)*, 1950.

49. J. A. Bailey, and A. E. Singer, "A Plane Strain Cam Plastometer for Use in Metal Working Studies," *Journal of the Institute of Metals*, Vol. 92, 1963-64, p. 288.

50. J. E. Hockett, "Compression Testing at Constant True Strain Rates," *Proceedings of the ASTM*, Vol. 59, 1959, pp. 1309-1319.

51. N. Loizou, and R. B. Sims, "The Yield Stress of Pure Lead in Compression," *Journal of the Mechanics and Physics of Solids*, Vol. 1, 1952, pp. 234-243.

52. L. D. Sokolov, *Doklady Akad. Nauk. S.S.S.R.*, Vol. 67, 1949, p. 459.

53. P. M. Cook, "True Stress-Strain Curves for Steel in Compression at High Temperatures and Strain Rates, for Application to the Calculation of Load and Torque in Hot Rolling," *Conference on the*

Properties of Materials at High Rates of Strain, Proceedings of the Institute of Mechanical Engineers, 1957, pp. 86-97.

54. A. J. Griest, A. M. Sabroff, and P. D. Frost, "Effect of Strain Rate and Temperature on the Compressive Flow Stresses of Three Titanium Alloys," *Transactions, ASM*, Vol. 51, 1958, pp. 935-945.

55. R. R. Arnold, and R. J. Parker, "Resistance to Deformation of Aluminum and Some Aluminum Alloys," *Journal of the Institute of Metals*, Vol. 88, 1959-60, pp. 255-259.

56. C. Rossard, and P. Blain, *Publ. Institut de Recherches de la Sidérugie*, Vol. 174, Part II.

57. C. Rossard, and P. Blain, "A Method of Simulation by Torsion for Determining the Influence of Hot Rolling Conditions on the Structure of Steel," *Flat Rolled Products III*, John Wiley & Sons, Inc., New York, pp. 3-28.

58. H. Ormerod, and W. J. McG. Tegart, "Resistance to Deformation of Super Pure Aluminum at High Temperatures and Strain Rates," *Journal of the Institute of Metals*, Vol. 89, 1960-61, pp. 94-96.

59. D. S. Fields, and W. A. Backofen, "Determination of Strain Hardening Characteristics by Torsion Testing," *Proceedings of the ASTM*, Vol. 57, 1957, pp. 1259-1272.

60. F. A. Hodierne, "A Torsion Test for Use in Metal Working Studies," *Journal of the Institute of Metals*, Vol. 91, 1962-63, pp. 267-273.

61. D. Hardwick, and W. J. McG. Tegart, "Structural Changes During the Deformation of Copper, Aluminum and Nickel at High Temperatures and High Strain Rates," *Journal of the Institute of Metals*, Vol. 90, 1961-62, pp. 17-21.

62. J. A. Bailey, *The Effect of Temperature and Strain Rate on the Resistance to Deformation of Some Metals and Alloys*, Ph.D. Thesis, University of Wales, 1963.

63. J. A. Bailey, "Some Strain Rate Effects Observed During Deformation in Plane Compression," ASME Publication 67-Met-11.

64. J. A. Bailey, and A. R. E. Singer, "The Effect of Strain Rate and Temperature on the Resistance to Deformation of Aluminum, Two Aluminum Alloys, and Lead," *Journal of The Institute of Metals*, Vol. 92, 1963-64, p. 404.

65. J. A. Bailey, and A. R. E. Singer, "The Determination of the Coefficient of Friction at Elevated Temperatures Using a Plane Strain Compression Test," *Journal of the Institute of Metals*, Vol. 92, 1963-64, p. 34.

66. R. A. Reynolds, and W. J. McG. Tegart, "The Deformation of Some Pure Irons by High Speed Torsion over the Temperature Range 700-1250°C," *Journal of the Iron and Steel Institute*, December, 1962, pp. 1044-1057.

67. J. L. Robbins, H. Wagenaar, O. C. Shepard, and O. D. Sherby, "Torsion Testing on a Means of Assessing Ductility at High Temperatures," *Journal of Materials*, Vol. 2, No. 2, June, 1967, pp. 271-299.

68. J. L. Robbins, O. C. Shepard, and O. D. Sherby, "Torsional Ductility and Strength of Iron-Carbon Alloys at Elevated Temperature," *Transactions of the ASM*, June, 1967, Vol. 60, No. 2, pp. 205-216.

69. N. H. Cook, "A Differential Torsion Testing Machine," *Proceedings of the Society for Experimental Stress Analysis*, Vol. 14, No. 2, 1957, p. 155-158.

70. J. Marin, *Mechanical Behavior of Engineering Materials*, Prentice-Hall, Inc., Englewood Cliffs, N.J., 1962, pp. 72-76.

71. C. W. Richards, *Engineering Materials Science*, Wadsworth, Inc., Belmont, California, 1961, pp. 212-213.

72. J. H. Poynting, "On Pressure Perpendicular to the Shear Planes in Finite Pure Shears, and on the Lengthening of Loaded Wires when Twisted," *Proceedings of the Royal Society*, Vol. A82, 1909, pp. 546-559.

73. J. H. Poynting, "On the Changes in the Dimensions of a Steel Wire when Twisted and on the Pressure of Distortional Waves in Steel," *Proceedings of the Royal Society*, Vol. A86, 1912, pp. 534-561.

74. M. Reiner, "The Complete Elasticity Law for Some Metals According to Poyntings Observations," Applied Scientific Research, Section A, Vol. 5, 1955, pp. 281-295.

75. H. W. Swift, "Length Changes in Metals under Torsional Overstrain," *Engineering*, April 4, 1947, pp. 253-257.

76. M. Cook, "Directional Properties in Rolled Brass Strip," *Journal of the Institute of Metals*, Vol. 60, 1937, pp. 159-185.

77. N. L. Svennson, "Some Observations on the Anisotropy of Yield Strength in Cold-Rolled and Annealed Metals," *Journal of the Institute of Metals*, Vol. 94, 1966, pp. 284-291.

78. T. H. Hazlett, A. T. Robinson, and J. E. Dorn, "An Evaluation of a Theory for Plastic Flow in Anisotropic Sheet Metals," *Transactions A.S.M.*, Vol. 42, pp. 1326-1356.

79. J. E. Dorn, "Stress-Strain Rate Relations for Anisotropic Plastic Flow," *Journal of Applied Physics*, Vol. 20, January, 1949, pp. 15-20.

80. L. J. Klinger, and G. Sachs, "Plastic Flow Characteristics of an Aluminum-Alloy Plate," *Journal of the Aeronautical Sciences*, October, 1948, pp. 599-604.

81. D. V. Wilson, "Plastic Anisotropy in Sheet Metals," *Journal of the Institute of Metals*, Vol. 94, 1966, pp. 84-93.

82. M. Grumbach, and G. Pomey, "Method of Measuring the Coefficients of Anisotropy and Work Hardening," *Sheet Metal Industries*, July, 1966, pp. 515-529.

83. R. Hill, "A Theory of Yielding and Plastic Flow of Anisotropic Metals," *Proceedings of the Royal Society*, Series A, Vol. 193, 1948, pp. 281-297.

84. R. Hill, *The Mathematical Theory of Plasticity*, Oxford University Press, London, 1950.

85. L. W. Hu, "Studies on Plastic Flow of Anisotropic Metals," *Journal of Applied Mechanics*, September, 1956, pp. 444-450.

86. E. G. Thomsen, C. T. Yang, S. Kobayashi, *Mechanics of Plastic Deformation in Metal Processing*, The Macmillan Company, New York, 1965, p. 132.

87. *The Aluminum Data Book*, Reynolds Metals Company, Richmond, Virginia, 1961.

88. *Aluminum Heat Treating*, Reynolds Metals Company, Richmond, Virginia, 1958.

VITA

Steven L. Haas was born in Brooklyn, New York, on July 1, 1938, the son of Albert and Gertrude Haas. In 1956, he graduated from Palm Beach High School in West Palm Beach, Florida, and entered the Georgia Institute of Technology.

He received his BME degree in 1960, and was commissioned a second lieutenant in the U.S. Army. He served two years in the U.S. Army Ordnance Corps, 16 months of which were spent with the 7th Infantry Division, 707th Ordnance Battalion in Korea.

After his discharge in 1962, he worked as a manufacturing engineer with the Western Electric Company in Baltimore, Maryland. In 1964, he entered the Graduate Division of the Georgia Institute of Technology, and received his MSME in 1966.

Mr. Haas was married in 1963 to the former Helen Joy Grace. They have a son, David Patrick.